Analysis of Short-Term and Long-Term Outcomes of Living Donor Liver Transplantation for Patients with a High Model for End-Stage Liver Disease Score

Daijiro Matoba, Takehiro Noda, Shogo Kobayashi*, Kazuki Sasaki, Yoshifumi Iwagami, Daisaku Yamada, Yoshito Tomimaru, Hidenori Takahashi, Yuichiro Doki, and Hidetoshi Eguchi

Department of Gastroenterological Surgery, Graduate School of Medicine, Osaka University, Suita, Osaka, Japan

ABSTRACT

Background. The Model of End-Stage Liver Disease (MELD) scoring system can predict short-term survival among patients awaiting liver transplantation and is used to allocate organs prioritizing liver transplantation. Patients with high MELD scores have been reported to have worse early graft dysfunction and survival. However, recent studies have shown that patients with high MELD scores had satisfactory graft survival, although they showed more postoperative complications. In this study, we examined the effect of the MELD score on the short-term and long-term prognosis of living donor liver transplantation (LDLT).

Methods. This study included 102 patients who underwent LDLT in our institution between 2005 and 2020. The patients were divided into 3 groups according to MELD score (low MELD group: ≤20, moderate MELD group: 21−30, and high MELD group: ≥31). Perioperative factors were compared among the 3 groups, and cumulative overall survival rates were calculated using the Kaplan-Meier method.

Results. The patients' characteristics were comparable, and the median age was 54 years. Hepatitis C virus cirrhosis was the most common primary disease (n = 40), followed by hepatitis B virus (n = 11). The low MELD group consisted of 68 patients (median score: 16, 10−20); the moderate MELD group, 24 patients (median score: 24, 21−30); and the high MELD group, 10 patients (median score: 35, 31−40). The mean operative time (1241 min versus 1278 min versus 1158 min, $P = .19$) and mean blood loss (7517 mL vs 11162 mL vs 8808 mL, $P = .71$) were not significantly different among the 3 groups. The vascular and biliary complication rates were similar. The periods of intensive care unit and hospital stay tended to be longer in the high MELD group, but the difference was insignificant. The 1-year postoperative survival rate (85.3 % vs 87.5 % vs 90.0 %, $P = .90$) and overall survival rate were also not significantly different among the 3 groups.

Conclusions. Our study showed that LDLT patients with high MELD scores do not have a worse prognosis than those with low scores.

THE Model of End-Stage Liver Disease (MELD) score is a scoring system using blood biochemical test data (total bilirubin level, creatinine level, and international normalized ratio for prothrombin time) and the presence of dialysis treatment to evaluate liver functional reserve in cirrhosis and liver transplant registrants aged ≥12 years [1]. The MELD scoring system has been shown to accurately predict short-term survival among patients awaiting liver transplantation. It is used to allocate organs, prioritizing liver transplantation to patients with a higher risk of death [1].

*Address correspondence to Shogo Kobayashi, Department of Gastroenterological Surgery, Graduate School of Medicine, Osaka University, 2-2-E2, Yamadaoka, Suita, Osaka 565-0871, Japan. E-mail: skobayashi@gesurg.med.osaka-u.ac.jp

0041-1345/20
https://doi.org/10.1016/j.transproceed.2023.03.011

Previous studies have shown that the MELD system might also predict graft outcomes after deceased donor liver transplantation (DDLT) and living donor liver transplantation (LDLT) [2,3]. Our group investigated the risk factors of 39 cases of graft dysfunction after adult-to-adult LDLT between 1999 and 2004 and reported that a high preoperative MELD score (≥31) was associated with postoperative graft failure in 2006 [4]. Moreover, Ishigami et al reported that the graft outcomes in patients with high MELD scores (≥25) combined with the presence of hepatitis C virus (HCV) between 1997 and 2004 were significantly poor in LDLT [5]. In 2004, treatment with peginterferon-alpha2a and ribavirin for HCV was developed. Direct-acting antivirals such as daclatasvir plus asunaprevir or ledipasvir and sofosbuvir produced dramatic outcomes (a sustained virological response) in many patients with HCV, including recipients of liver transplantation [6,7]. Due to these developments in HCV treatment and perioperative management, recent studies have shown that the high MELD score group had satisfactory rates of graft survival and patient overall survival. However, they showed significantly more frequent postoperative complications and longer intensive care unit (ICU) stays [8−10].

Therefore, the aim of this study was to evaluate the effect of the MELD score on LDLT patients' short-term and long-term prognosis, especially after 2005, in the era of the establishment of HCV treatment.

MATERIAL AND METHODS

Between 2005 and 2020, 104 patients who underwent adult-to-adult LDLT in our hospital were retrospectively reviewed. Re-transplantation cases (n = 2) were excluded. The primary diagnoses in these 102 cases were HCV cirrhosis (n = 40), hepatitis B virus cirrhosis (n = 11), alcoholic liver cirrhosis (n = 9), fulminant hepatitis (n = 8), primary biliary cholangitis (n = 7), hepatocellular carcinoma (n = 6), primary sclerosing cholangitis (n = 5), biliary atresia (n = 5), nonalcoholic steatohepatitis (n = 5), Budd-Chiari syndrome (n = 2), cryptogenic cirrhosis (n = 2), autoimmune hepatitis (n = 1), and Wilson disease (n = 1). The eligible criteria for graft size in our institute were a graft volume (GV)/standard liver volume (SLV) ratio >40% and a remnant liver volume >35% of the whole liver volume, as previously reported [2]. The recipients' preoperative performance status (PS) was judged by a modified version of the Eastern Cooperative Oncology Group, and the candidate for LDLT for chronic liver failure needed to have a PS of under 2 [11].

The MELD score was calculated using the UNOS formula based on data obtained within 3 days of LDLT [1]. Patients were divided into 3 groups: low MELD group (≤20), moderate MELD group (21−30), and high MELD group (≥31). The groups were compared based on the following perioperative factors: age, sex, primary disease, MELD score, incompatibility of blood type, GV, GV/SLV ratio, operation time, blood loss, presence of vascular complication, presence of biliary complication, length of ICU stay, periods of hospital stay after transplantation, and postoperative survival rate (1-year and overall survival [OS] rates).

This research was conducted in accordance with the 2000 Declaration of Helsinki and the Declaration of Istanbul 2008. The patients provided written informed consent of their own free will. No prisoners were used, and donors were neither paid nor coerced.

The values are expressed as the mean ± SD. In statistical analysis, 3-group comparisons were performed using the Wilcoxon rank-sum test. Cumulative OS rates were calculated using Kaplan-Meier methods, and differences between curves were evaluated using the log-rank test. A P value of $< .05$ was considered significant. The JMP Pro version16 (SAS Institute, Cary, NC, United States) statistics package was used for analysis.

RESULTS

The patients' characteristics and postoperative outcomes are summarized in Table 1. The median age was 54 years, ranging from 19 years to 69 years. Fifty patients were male, and 52 were female. The median MELD score was 17. An ABO-identical transplantation was the most common, seen in 62 cases. An ABO-incompatible transplantation was conducted in 19 cases. The mean GV was 518 g, and the mean GV/SLV ratio was 43.2%. The mean operation time was 1176 min, and the mean intraoperative blood loss was 8555 mL. The vascular and biliary complication rates were 18.6% and 14.7%, respectively. The 1-year postoperative survival rate was 86.2% in all cases. Out of 40 recipients with HCV cirrhosis, 27 patients (67.5%) received anti-viral treatment such as peginterferon-alpha2a and ribavirin and a direct acting-antiviral. Twenty-four patients achieved a sustained virological response.

In Fig 1, the distribution of the MELD score is shown. Patients with 15 to 20 points were the most common (35%). Sixty-eight patients were classified as the low MELD group, 24 patients as the moderate MELD group, and 10 patients as the high MELD group. A comparative analysis of the characteristics and the perioperative outcomes among the 3 groups is demonstrated in Table 2. There were no significant differences in patient age, sex, primary disease, or ratio of ABO-compatible, identical, or incompatible transplantation. The mean GV in each group was not significantly different (521 g, 524 g, and 487 g in the low, moderate, and high MELD groups, respectively; $P = .73$). The mean operation times were not significantly different (1241 min, 1278 min, and 1158 min, respectively; $P = .19$). The mean blood loss was also similar among the 3 groups. The incidence of vascular and biliary complications was 19.1% and 14.7% in the low MELD group, respectively; 20.8% and 12.5% in the moderate MELD group, respectively; and 10.0% and 20.0% in the high MELD group, respectively. The morbidity rates were not significantly different ($P = .74$ and $P = .85$,

Table 1. Patient Characteristics and Perioperative Outcome

Parameters	n = 102
Median Age (Range) (y)	54 (19−69)
Sex (male/female)	50/52
Primary Disease (HCV/HBV/PBC/Alcoholism/Others)	40/11/7/9/35
Median MELD Score (Range)	17 (10−40)
Compatible/Identical/Incompatible (n[%])	21/62/19
Mean Graft Volume (g) ± SD	518 ± 12
Mean Graft Volume/Standard Liver Volume (%) ± SD	43.2 ± 096
Mean Operation Time (min) ± SD	1176 ± 38
Mean Blood Loss (mL) ± SD	8555 ± 832
Vascular Complication (n[%])	19 (18.6)
Biliary Complication (n[%])	15 (14.7)
Mean ICU Stay (d) ± SD	21 ± 35
Mean Hospital Stay After Transplantation (y) ± SD	106 ± 75
1-Year Postoperative Survival Rate (%)	86.2

HCV, hepatitis C virus; HBV, hepatitis B virus; ICU, intensive care unit; MELD; Model for End-Stage Liver Disease; PBC, primary biliary cholangitis.

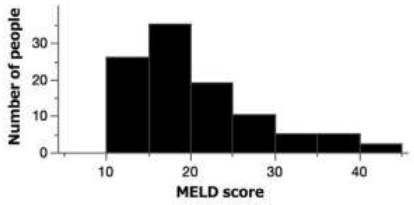

Fig 1. Distribution of Model for End-Stage Liver Disease scores in all patients. MELD, Model for End-Stage Liver Disease.

respectively). The ICU stay periods after transplantation were 22.0 days, 16.5 days, and 30.1 days, respectively (P = .32). The postoperative hospital stay periods were 102 days, 102 days, and 145 days, respectively; the stay periods tended to be longer in the high MELD group, but the difference was not significant (P = .37).

As for the long-term clinical outcome, the OS curve in all cases is shown in Fig 2. The 10-year survival rate was about 80%. The OS rates were not significantly different among the 3 groups, and the 1-year postoperative survival rates were 85.3 %, 87.5 %, and 90.0 %, respectively (P = .25), as shown in Fig 3.

DISCUSSION

The MELD system has improved organ allocation, and it is well-established in the literature as an excellent predictor of the risk of death on the waiting list [12]. A previous study by our group showed that the MELD score was significantly higher in the subgroup with graft dysfunction after LDLT, and a high preoperative MELD score (>30) was identified as a risk factor for graft failure [4]. Wang et al also reported that the MELD score was superior for predicting postoperative short-term survival after LDLT [13]. In a multi-institutional retrospective study, Ishigami et al demonstrated that the MELD score was useful for predicting 1-year survival in cirrhosis patients and that a MELD score of 15 had a discriminatory value for LDLT indication [5]. On the other hand, Hayashi et al reported that the MELD score did not predict post-LDLT patient survival or graft survival at

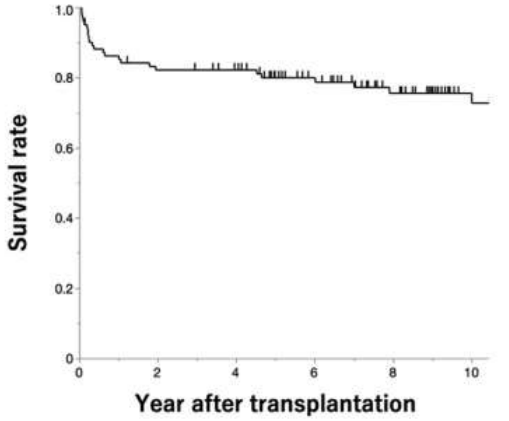

Fig 2. Overall survival rate in all patients. The 10-year survival rate was approximately 80%.

1 year. However, they reported that a higher MELD score (>18) was associated with a longer hospital stay [14]. Another report by Ikegami et al showed that a high MELD score (>25) combined with the presence of HCV was associated with a worse 5-year graft survival rate in LDLT [15]. However, a recent large cohort study showed that a high pretransplant MELD score did not affect clinical outcomes after LDLT, and Yadav et al concluded that LDLT could be a good option for high MELD score recipients [16]. Recently, Roll et al systematically reviewed recipient factors influencing clinical outcomes after LDLT and demonstrated that recipients with a high MELD score could be expected to require longer stays in the ICU and hospital after transplantation because of the higher incidence of postoperative complications [17]. In this study, our data showed that the OS rates in the high MELD group were not inferior to those in the low and moderate MELD groups. The postoperative ICU and hospital stays tended to be slightly longer in the high MELD group, but no significant differences existed.

Table 2. Comparative Analysis of the Patient Characteristics and Perioperative Outcome

	Low MELD (n = 68)	Moderate MELD (n = 24)	High MELD (n = 10)	*P* value
Median Age (y)	52	52	54	.89
Sex (male/female)	31/37	14/10	7/3	.25
Primary Disease (HCV/HBV/PBC/Alcoholism/Others) (n[%])	33/5/4/5/21	6/4/2/3/9	1/2/1/1/5	.15
Median MELD Score (Range)	16 (10–20)	24 (21–30)	35 (31–40)	< .0001
Compatible/Identical/Incompatible (n[%])	15/40/13	5/15/4	1/7/2	.92
Mean Graft Volume (g) ± SD	521 ± 130	524 ± 88	487 ± 147	.73
Mean Graft Volume/Standard Liver Volume (%) ± SD	42.58 ± 9.7	45.09 ± 5.7	42.55 ± 13.9	.42
Mean Operation Time (min) ± SD	1241 ± 304	1278 ± 210	1158 ± 435	.19
Mean Blood Loss (mL) ± SD	7517 ± 5769	11162 ± 12727	8808 ± 8394	.71
Vascular Complication (n[%])	13 (19.1)	5 (20.8)	1 (10.0)	.74
Biliary Complication (n[%])	10 (14.7)	3 (12.5)	2 (20.0)	.85
Mean ICU Stay (d) ± SD	22.0 ± 39.0	16.5 ± 18.3	30.1 ± 38.5	.32
Mean Hospital Stay After Transplantation (y) ± SD	102 ± 69.2	102 ± 71.1	145 ± 122.9	.37
1-Year Postoperative Survival (%)	85.3	87.5	90.0	.90

HCV, hepatitis C virus; HBV, hepatitis B virus; ICU, intensive care unit; MELD; Model for End-Stage Liver Disease; PBC, primary biliary cholangitis.

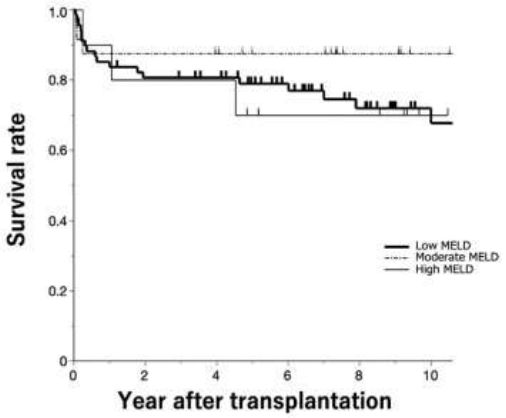

Fig. 3. Overall survival rate of the 3 groups. There were no significant differences among the 3 groups (P = .25, log-rank test). MELD, Model for End-Stage Liver Disease.

The cut-off values for the high MELD score group varied in previous reports. Most studies defined the high MELD group as the cohort with a MELD score of >25 or >30 [10,14,18]. The review by Roll et al suggested that MELD scores of >25 alone are not a contraindication to LDLT and that the transplantation team needs to consider the presence of comorbidities and donor factors that influence the immediate graft function, such as donor age, graft size, the presence of steatosis, and venous drainage of the graft. Moreover, patients with a high MELD score (>35) should receive an optimal graft [17].

Hepatitis C virus infection is a common cause of liver cirrhosis in both Eastern and Western countries, and numerous liver transplantations for HCV cirrhosis have been performed. However, most recipients with HCV developed recurrent hepatitis C with progressive fibrosis. Some patients developed fibrosing cholestatic hepatitis with marked jaundice, cholestatic hepatic dysfunction, and high viremia titers, leading to graft loss [19]. Around 2000, the combination of interferon-alfa with ribavirin was established as a treatment for chronic HCV infection [20,21]. Subsequently, this combination of treatments was applied for HCV-positive recipients with liver transplantation, and recurrent HCV infections in transplanted liver recipients were well controlled. Several authors reported that therapy with pegylated interferon and ribavirin achieved a good response, with a sustained virological response observed in liver transplant recipients [22,23]. After the development of direct acting-antivirals, a multicenter retrospective study in Japan showed that treatment with asunaprevir and daclatasvir for recurrent HCV infection after liver transplantation achieved a high rate of sustained viral response (>80%) [24]. It was hypothesized that the development of HCV treatment contributed to improved survival in patients with high MELD scores. In this study, only 1 of 40 patients with HCV-related cirrhosis had a high MELD score. This may be due to the development of HCV treatment; the number of patients with severe cirrhosis due to HCV infection and a high MELD score has decreased. Advances in HCV treatment that enable patients to receive anti-viral therapy before and after liver transplantation have improved OS in LDLT recipients.

Progress in the perioperative management of LDLT recipients is also hypothesized to improve the prognosis of high MELD score patients. Another factor is the selection of appropriate patients for LDLT. Our group has decided that the preoperative PS score of the recipient needs to be under 2. The PS scores were stratified into 3 groups: PS 1 (normal or minimally restricted level of activity), PS 2 (able to self-care), and PS 3 (confined to bed or chair or completely reliant on medical care). The PS score is closely related to sarcopenia, and it is reported that sarcopenia before LDLT is a significant prognostic factor for patient survival [25,26]. An appropriate patient selection might contribute to the improvement in OS after LDLT for high MELD score patients.

CONCLUSIONS

In the era of advanced HCV treatment and perioperative management, our study found that with appropriate patient selection in LDLT, patients with high MELD scores had non-inferior short- and long-term outcomes compared to those with low scores. In the high MELD group, the ICU and hospital stay periods might be longer. From the perspective of organ shortage, especially in regions such as Japan, where brain-dead liver transplantation is limited, LDLT may be a useful option for patients with a high MELD score.

DISCLOSURES

The authors declare that they have no known competing financial interests or personal relationships that could have appeared to influence the work reported in this paper.

DATA AVAILABILITY

Data will be made available on request.

REFERENCES

[1] Kamath PS, Wiesner RH, Malinchoc M, et al. A model to predict survival in patients with end-stage liver disease. Hepatology 2001;33:464–70.

[2] Jacob M, Copley LP, Lewsey JD, et al. Pretransplant MELD score and post liver transplantation survival in the UK and Ireland. Liver Transpl 2004;10:903–7.

[3] Onaca NN, Levy MF, Netto GJ, et al. Pretransplant MELD score as a predictor of outcome after liver transplantation for chronic hepatitis C. Am J Transplant 2003;3:626–30.

[4] Marubashi S, Dono K, Asaoka T, et al. Risk factors for graft dysfunction after adult-to-adult living donor liver transplantation. Transplant Proc 2006;38:1407–10.

[5] Ishigami M, Honda T, Okumura A, et al. Use of the Model for End-Stage Liver Disease (MELD) score to predict 1-year survival of Japanese patients with cirrhosis and to determine who will benefit from living donor liver transplantation. J Gastroenterol 2008;43:363–8.

[6] Stephanos J, Hadziyannis HS, Morgan Timothy R, et al. Peginterferon-α2a and ribavirin combination therapy in chronic hepatitis C. Ann Intern Med 2004;140:346–55.

[7] Belli LS, Berenguer M, Cortesi PA, et al. Delisting of liver transplant candidates with chronic hepatitis C after viral eradication: a European study. J Hepatol 2016;65:524–31.

[8] Chok K, Chan SC, Fung JY, et al. Survival outcomes of right-lobe living donor liver transplantation for patients with high Model for End-stage Liver Disease scores. Hepatobiliary Pancreat Dis Int 2013;12:256–62.

[9] Li C, Wen T, Yan L, et al. Does model for end-stage liver disease score predict the short-term outcome of living donor liver transplantation? Transplant Proc 2010;42:3620–3.

[10] Ferraz-Neto BH, Zurstrassen MP, Hidalgo R, et al. Analysis of liver transplantation outcome in patients with MELD Score >or = 30. Transplant Proc 2008;40:797–9.

[11] Oken MM, Creech RH, Tormey DC, et al. Toxicity and response criteria of the Eastern Cooperative Oncology Group. Am J Clin Oncol 1982;5:649–55.

[12] Wiesner R, Edwards E, Freeman R, et al. Model for end-stage liver disease (MELD) and allocation of donor livers. Gastroenterology 2003;124:91–6.

[13] Wang ZX, Yan LN, Wang WT, Xu MQ, Yang JY. Impact of pretransplant MELD score on posttransplant outcome in orthotopic liver transplantation for patients with acute-on-chronic hepatitis B liver failure. Transplant Proc 2007;39:1501–4.

[14] Hayashi PH, Forman L, Steinberg T, et al. Model for End-Stage Liver Disease score does not predict patient or graft survival in living donor liver transplant recipients. Liver Transpl 2003;9:737–40.

[15] Ikegami T, Shirabe K, Yoshiya S, et al. A high MELD score, combined with the presence of hepatitis C, is associated with a poor prognosis in living donor liver transplantation. Surg Today 2014;44:233–40.

[16] Yadav SK, Saraf N, Saigal S, et al. High MELD score does not adversely affect outcome of living donor liver transplantation: experience in 1000 recipients. Clin Transplant 2017;31(8).

[17] Roll GR, Spiro M, Raptis DA, et al. Which recipient pretransplant factors, such as MELD, renal function, sarcopenia, and recent sepsis influence suitability for and outcome after living donor liver transplantation? A systematic review of the literature and expert panel recommendations. Clin Transplant 2022;36:e14656.

[18] Poon KS, Chen TH, Jeng LB, et al. A high model for end-stage liver disease score should not be considered a contraindication to living donor liver transplantation. Transplant Proc 2012;44:316–9.

[19] Hori T, Onishi Y, Kamei H, et al. Fibrosing cholestatic hepatitis C in post-transplant adult recipients of liver transplantation. Ann Gastroenterol 2016;29:454–9.

[20] McHutchison JG, Gordon SC, Schiff ER, et al. Interferon Alfa-2b alone or in combination with ribavirin as initial treatment for chronic hepatitis C. N Engl J Med 1998;339:1485–92.

[21] Poynard T, Marcellin P, Lee SS, et al. Randomised trial of interferon alpha2b plus ribavirin for 48 weeks or for 24 weeks versus interferon alpha2b plus placebo for 48 weeks for treatment of chronic infection with hepatitis C virus. Lancet 1998;352:1426–32.

[22] Moreno A, Bárcena R, García-Garzón S, et al. HCV clearance and treatment outcome in genotype 1 HCV-monoinfected, HIV-coinfected and liver transplanted patients on peg-IFN-alpha-2b/ribavirin. J Hepatol 2005;43:783–90.

[23] Fernandez I, Meneu JC, Colina F, et al. Clinical and histological efficacy of pegylated interferon and ribavirin therapy of recurrent hepatitis C after liver transplantation. Liver Transpl 2006;12:1805–12.

[24] Ikegami T, Ueda Y, Akamatsu N, et al. Asunaprevir and daclatasvir for recurrent hepatitis C after liver transplantation: a Japanese multicenter experience. Clin Transplant 2017;31(11).

[25] Kaido T, Ogawa K, Fujimoto Y, et al. Impact of sarcopenia on survival in patients undergoing living donor liver transplantation. Am J Transplant 2013;13:1549–56.

[26] Sim JH, Kwon HM, Kim KW, et al. Associations of sarcopenia with graft failure and mortality in patients undergoing living donor liver transplantation. Liver Transpl 2022;28:1345–55.

Efficacy of Autologous Skeletal Myoblast Cell Sheet Transplantation for Liver Regeneration in Liver Failure

Keisuke Toya, MD,[1] Yoshito Tomimaru, MD, PhD,[1] Shogo Kobayashi, MD, PhD,[1] Akima Harada, BS,[2] Kazuki Sasaki, MD, PhD,[1] Yoshifumi Iwagami, MD, PhD,[1] Daisaku Yamada, MD, PhD,[1] Takehiro Noda, MD, PhD,[1] Hidenori Takahashi, MD, PhD,[1] Takeshi Kado, MD,[1] Hiroki Imamura, MD,[1] Shohei Takaichi, MD, PhD,[1] Ryota Chijimatsu, PhD,[3] Tadafumi Asaoka, MD, PhD,[1] Masahiro Tanemura, MD, PhD,[1] Shigeru Miyagawa, MD, PhD,[2] Yuichiro Doki, MD, PhD,[1] and Hidetoshi Eguchi, MD, PhD[1]

Background. No effective therapies have yet been established for liver regeneration in liver failure. Autologous skeletal myoblast cell sheet transplantation has been proven to improve cardiac function in patients with heart failure, and one of the mechanisms has been reported to be a paracrine effect by various growth factors associated with liver regeneration. Therefore, the present study focused on the effect of myoblast cells on liver regeneration in vitro and in vivo. **Methods.** We assessed the effect of myoblast cells on the cells comprising the liver in vitro in association with liver regeneration. In addition, we examined in vivo effect of skeletal myoblast cell sheet transplantation in C57/BL/6 mouse models of liver failure, such as liver fibrosis induced by thioacetamide and hepatectomy. **Results.** In vitro, the myoblast cells exhibited a capacity to promote the proliferation of hepatic epithelial cells and the angiogenesis of liver sinusoidal endothelial cells, and suppress the activation of hepatic stellate cells. In vivo, sheet transplantation significantly suppressed liver fibrosis in the induced liver fibrosis model and accelerated liver regeneration in the hepatectomy model. **Conclusions.** Autologous skeletal myoblast cell sheet transplantation significantly improved the liver failure in the in vitro and in vivo models. Sheet transplantation is expected to have the potential to be a clinically therapeutic option for liver regeneration in liver failure.

(*Transplantation* 2023;107: e190–e200).

INTRODUCTION

Liver diseases, such as hepatitis virus infection and alcoholic and nonalcoholic steatohepatitis, can lead to severe liver cirrhosis, resulting in liver failure, an irreversible and life-threatening state.[1-3] The only treatment for severe liver failure is currently liver transplantation, but donors for liver transplantation are lacking,[4] and there are many problems with transplantation, including technical difficulties and highly invasive surgery, the risk of life-threatening postoperative complications, requirement for immunosuppression after the transplantation, and declining quality of the posttransplant life because of the immunosuppressive status. Thus, liver transplantation is not indicated for all cases with liver failure, suggesting a need to develop novel new therapeutic interventions for liver failure.

On such a background, liver regenerative medicine is rapidly expanding as an intervention for liver failure.[5] This approach is considered theoretically eligible for liver regeneration based on the concept that the liver originally exhibited regenerative ability and some signaling pathways promoting liver regeneration.[6-8] The approaches proposed for liver regeneration include the use of bone marrow cell transplantation[9-11] and clinical application of induced pluripotent stem cells (iPSCs).[12,13] However, no regenerative medicines have been clinically established for liver failure, which indicates unsolved problems in the approaches. For example, a large number of cells are required for treatment with bone marrow cell transplantation, implying infeasibility due to the invasiveness associated with

Received 9 June 2022. Revision received 4 November 2022.

Accepted 14 December 2022.

[1] Department of Gastroenterological Surgery, Graduate School of Medicine, Osaka University, Osaka, Japan.

[2] Department of Cardiovascular Surgery, Graduate School of Medicine, Osaka University, Osaka, Japan.

[3] Center for Comprehensive Genomic Medicine, Okayama University Hospital, Okayama, Japan.

The authors declare no funding or conflicts of interest.

K.T., Y.T., S.K., S.M., and H.E. designed this study. K.T., Y.T. A.H., K.S., T.K., H.I., and S.T. acquired the data. K.T., Y.T., R.C., and A.H. interpreted the data. K.T., Y.T., S.K., and H.E. drafted this article. Y.I., D.Y., T.N., H.T., T.A., and M.T. supported the interpretation. S.M. and Y.D. supervised the study.

Supplemental digital content (SDC) is available for this article. Direct URL citations appear in the printed text, and links to the digital files are provided in the HTML text of this article on the journal's Web site (www.transplantjournal.com).

Correspondence: Shogo Kobayashi, MD, PhD, Department of Gastroenterological Surgery, Graduate School of Medicine, Osaka University, 2-2-E2, Yamadaoka, Suita, Osaka, 565-0871, Japan. (skobayashi@gesurg.med.osaka-u.ac.jp).

ISSN: 0041-1337/20/1078-e190

DOI: 10.1097/TP.0000000000004567

harvesting the cells. Treatment with iPSCs is also promising, but its safety and difficulty in preparation remains to be solved. Thus, there remains a necessity to develop a new approach for liver regeneration in liver failure.

Myoblasts are cells that promote repair when skeletal muscle is injured. Skeletal myoblast sheets have been studied in several fields of regeneration, including pancreatic fistula, gastric perforation, and duodenal perforation.[14-16] Recently, an autologous skeletal myoblast cell sheet was demonstrated to functionally prevent deterioration of the impaired myocardium in an animal infarction model.[17,18] Furthermore, the effect of sheet transplantation on impaired cardiac function was confirmed in humans.[19] As a result, treatment of cardiac failure by a skeletal myoblast cell sheet has been covered by health insurance in Japan. One of the mechanisms underlying the effect of the skeletal myoblast sheet on cardiac regeneration is a paracrine effect associated with growth factors, including vascular endothelial growth factor (VEGF), hepatocyte growth factor (HGF), and stromal derived factor-1.[17,20,21] Interestingly, these growth factors have been independently reported to promote liver regeneration.[6,22-25] These previous studies let us consider the possibility that the myoblast cell sheet exhibits the potential to promote liver regeneration, leading to a new therapeutic option for liver failure. If transplantation of the myoblast cell sheet is shown to be useful for liver failure, it may be helpful in overcoming the problems described earlier. This potential therapeutic option also has advantages over liver transplantation, which is currently the only option: it does not require liver donors, is less invasive than liver transplantation, and does not require posttransplant immunosuppression.

In the present study, we focused on the transplantation of an autologous skeletal myoblast cell sheet as a new therapeutic option for liver regeneration in liver failure. Therefore, in this study, we investigated the efficiency of autologous skeletal myoblast cell sheet transplantation for liver regeneration in liver failure in in vitro and in vivo models.

MATERIALS AND METHODS

Cytokine Secretion Capacity of Myoblast Cells

Human skeletal muscle myoblasts (HSMMs; Lonza Japan, Ltd, Tokyo, Japan) were examined for their capacity to secrete myoblast cytokines. The cells were seeded on a dish without any serum, and the supernatant was collected after 3 and 7 d. The levels of VEGF and HGF were measured using the Human VEGF and HGF ELISA Kit (Abcam, Cambridge, UK).

Coculture of Hepatic Epithelial Cells With Skeletal Myoblast Cells

The capacity of myoblast cells to induce proliferation of hepatic cells was assessed by a CCK-8 assay (Dojindo, Kumamoto, Japan) as described previously.[26] Immortalized human liver epithelial THLE-2 cells (American Type Culture Collection, Manassas, VA) were seeded with or without HSMMs using a 24-well 0.4-μm pore polyester membrane insert. The CCK-8 solution was added to each well 0, 24, 48, and 72 h after seeding and the absorbance measured by a microplate reader. The results were expressed as the absorbance relative to 0 h of CCK-8 exposure. Immunocytochemical staining analysis was performed with anti-Ki-67 antibody (Abcam), Hoechst 33342 (Dojindo), and Alexa Fluor 488-conjugated phalloidin (Thermo Fisher Scientific, MA).

Tube Formation Assay

Immortalized human liver sinusoidal endothelial TMNK-1 cells (Japanese Collection of Research Bioresources Cell Bank, Osaka, Japan)[27] were used for the tube formation assay. TMNK-1 cells were seeded on Matrigel in DMEM with or without HSMMs using 12-well 0.4-μm pore polyester membrane inserts (Corning Inc., Armonk, NY). The length of the tube and the number of capillary branches were quantified by microscopy in 10 randomly chosen optical fields after 24 h.

Coculture of Hepatic Stellate Cells With Skeletal Myoblast Cells

To examine the influence of skeletal myoblast cells on hepatic stellate cells (HSCs), which play an important role in liver fibrosis, LX-2 cells (Millipore, Billerica, MA) were cultured with or without HSMMs. The human LX-2 HSCs were plated in DMEM and treated with 10 ng/mL recombinant human transforming growth factor-β1 (TGF-β1; R&D Systems, Minneapolis, MN) and with or without the same number of HSMMs using 12-well 0.4-μm pore polyester membrane inserts. To assess the conversion from quiescent HSCs to myofibroblast-like cells (activated HSCs), the total RNA was extracted from LX-2 cells after 24 h, and real-time quantitative reverse-transcription polymerase chain reaction (RT-PCR) was performed.

Isolation of Myoblast Cells and Construction of Myoblast Sheet

Myoblast cells were isolated from the skeletal muscle in the legs (thigh and gluteus muscles) of 4-wk-old female C57BL/6 mice and cultured as described previously.[28] They were dissociated from the culture dishes with trypsin-ethylenediaminetetraacetic acid and reincubated on 24-well temperature-responsive culture dishes (UpCell; Cellseed, Tokyo, Japan) at 37 °C. The cell number was adjusted to 3.0×10^6 per dish. After 24 h, the dishes were incubated at 20 °C for 30 min. During that time, the skeletal myoblast cell sheet detached spontaneously to generate free-floating, monolayer cell sheets.

Animal Models of Liver Failure

Male 7-wk-old C57BL/6 mice were purchased from Clea Japan (Tokyo, Japan). All mice were acclimatized for 1 wk before experiments and housed in a 12-h dark/light cycle.

To induce liver fibrosis, the mice were injected intraperitoneally with thioacetamide (TAA) twice a week. After 1 or 6 wk, the mice underwent a surgical procedure. In the myoblast sheet group, the myoblast sheet was sutured onto the liver using 6-0 nylon. In the control group, the mice only underwent the laparotomy and suturing procedures without the sheet transplantation. After the operation, the TAA injection was continued until death. The mice were

euthanized under isoflurane anesthesia, and the liver and serum were collected and assessed at several time points (n = 5 for each group and time point).

Mice with partial hepatectomy were also used in this study. At the same time as the hepatectomy, a sheet was transplanted onto the remnant liver. In the control group, hepatectomy was performed without the sheet transplantation. The mice in both the groups were euthanized under isoflurane anesthesia, and the liver and serum were assessed at various time points (n = 5 for each group and time point). A 70% partial hepatectomy was performed as the standard hepatectomy model as described previously,[29] and a 90% partial hepatectomy was performed as a fatal hepatic failure model.[30] After the surgical procedures were completed without problems, whether the mice were alive was noted every 6 h (n > 15 for each group).

These animal studies were approved by the Animal Experiments Committee, Osaka University (approval number 02-022-008).

Blood Test

To measure the serum level of total protein, albumin, total bilirubin, aspartate aminotransferase, and alanine aminotransferase, blood was collected from the inferior vena cava of mice and centrifuged at 10 000*g* at room temperature for 15 min. Serum status was measured using a standard method at the Oriental Kobo Life Science Laboratory (Nagahama, Japan).

Real-time RT-PCR

Total RNA was isolated from the liver tissues using the RNeasy Mini Kit (Qiagen, Hilden, Germany). The RNA was reverse-transcribed and subjected to real-time RT-PCR as described previously.[31] For quantitative PCR, complementary DNA was synthesized using the Reverse Transcription System (Promega, Madison, WI). Applications were performed in triplicate with the VilA7 Software (Thermo Fisher Scientific) based on the Thunderbird SYBR qPCR Mix (Toyobo Co, Ltd, Osaka, Japan). The relative expression was calculated as the ratio of specific mRNA to endogenous GAPDH mRNA. The following primers were used: Human ACTA2: forward 5′-GTGTTGCCCCTGAAGAGCAT-3′, reverse 5′-GCTGGGACATTGAAAGTCTCA-3′; Human COL1α1: forward 5′-ACGAAGACATCCCACCAATC-3′, reverse 5′-AGATCACGTCATCGCACAAC-3′; Human MMP-2: forward 5′-GACAGGTGATCTTGACCAGAAT-3′, reverse 5′-GTGTGTAGCCAATGATCCTGTA-3′; Human GAPDH: forward 5′-CGAGATCCCTCCAAAATCAA-3′, reverse 5′-TTCACACCCATGACGAACAT-3′; Mouse Acta2: forward 5′-GTCCCAGACATCAGGGAGTAA-3′, reverse 5′-TCGGATACTTCAGCGTCAGGA-3′; Mouse Col1α1: forward 5′-GCTCCTCTTAGGGGCCACT-3′, reverse 5′-CCACGTCTCACCATTGGGG-3′; Mouse Gapdh: forward 5′-TGTGTCCGTCGTGGATCTGA-3′, reverse 5′-TTGCTGTTGAAGTCGCAGGAG-3′.

Western Blot Analysis

Total proteins were extracted from liver tissue using RIPA buffer (Thermo Fisher Scientific) containing protease and phosphatase inhibitor. The homogenates were purified by centrifugation at 1000*g* at 4 °C for 15 min. The protein concentrations were determined by a bicinchoninic acid protein assay (Thermo Fisher Scientific). Equal amounts of protein extract were separated by sodium dodecyl sulfate polyacrylamide gel electrophoresis on 12% Tris-HCL gels (Bio-Rad Laboratories Inc, Hercules, CA). The separated proteins were transferred to polyvinylidene difluoride membranes (Bio-Rad Laboratories Inc) and incubated with primary antibodies for 1 h: anti-CD31 (Abcam), anti-Akt, phosphorylated Akt, Erk1/2, phosphorylated Erk1/2 (Cell Signaling Technology Inc, MA), and anti-β actin antibody (Sigma–Aldrich, Tokyo, Japan). Next, the membranes were incubated with HRP-linked anti-rabbit IgG (GE Healthcare, Amersham, Buckinghamshire, UK) at room temperature for 1 h, and the antigen–antibody complex was detected using the ECL Prime Western Blotting Detection kit (GE Healthcare). The expression relative to actin expression was depicted as a column and measured using ImageJ software (rsb.info.nih.gov/ij).

Histological Analysis

The liver tissues were formalin-fixed and paraffin-embedded and cut into 5-μm sections using a microtome. Briefly, the tissues were removed, immersed in fixative for 1 h in 4% paraformaldehyde, rinsed several times with PBS, infiltrated with 30% sucrose, frozen in OCT compound, and processed for immunohistochemistry. The paraffin-embedded sections were stained with hematoxylin and eosin (H&E) and visualized using standard light microscopy. The sections were also stained with Sirius red or Masson trichrome. The images were examined by optical microscopy (Keyence, Osaka, Japan), and quantitative morphometric analysis was performed for each sample using MetaMorph (Molecular Devices, San Jose, CA). The sections were labeled immunohistologically with polyclonal anti-Ki-67 antibody (Abcam) and visualized using the LSABTM kit (DAKO, Glostrup, Denmark), which is an automated immunostaining system based on the labeled streptavidin biotinylated antibody method. Next, the sections were labeled immunohistologically with antidesmin antibody (Abcam) and anti-VEGFA antibody (Abcam) and visualized using the corresponding secondary antibodies (Alexafluor 488 or Alexafluor 555, Molecular Probes, Eugene, OR). Counterstaining was performed with Hoechst 33342 (Dojindo) and assessed by confocal microscopy (Olympus, Tokyo, Japan).

Spatial Transcriptomics Analysis

After 70% hepatectomy with sheet transplantation, the mouse was euthanized 2 d after transplantation. The liver tissues were collected and consequently trimmed on ice for spatial transcriptomics analysis by Visium (10x Genomics, Pleasanton, CA) according to the protocol reported previously,[32] utilizing Visium Spatial Gene Expression Reagent Kits (Chemistry v1). Visium sequencing libraries were loaded on an Illumina NovaSeq 6000 with sequencing settings recommended by 10X Genomics. The trimmed data were processed by 10x Genomics Space Ranger (version 1.2.1). All data

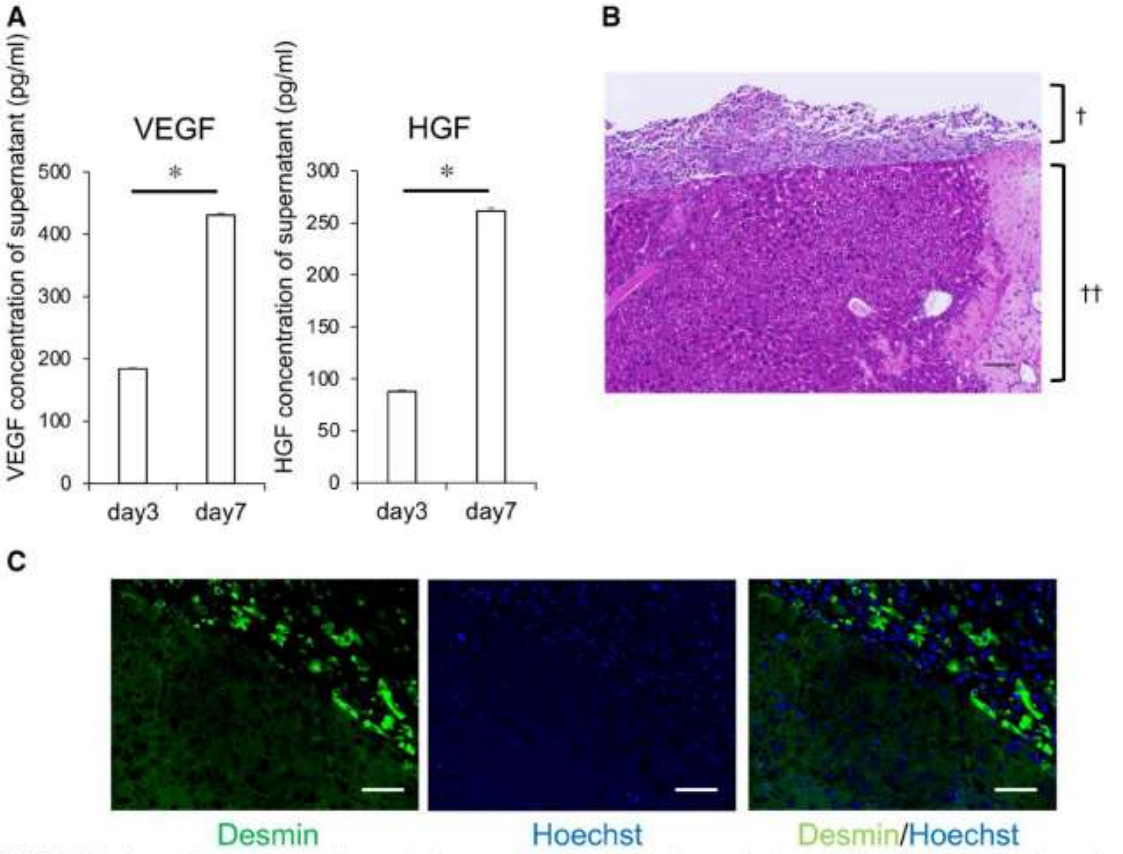

FIGURE 1. Myoblast cells secreted cytokines and sheets produced with the cells remained on the liver after sheet transplantation. A, The concentrations of vascular endothelial growth factor (VEGF) and hepatocyte growth factor (HGF) were significantly higher after 7 d than after 3 d. *$P < 0.05$. B, Hematoxylin-eosin staining of the liver confirmed that the sheet remained on the liver 2 d after transplantation. † = myoblast sheet, †† = liver. Scale bar = 100 μm. C, Immunohistology for desmin and Hoechst 33342 confirmed the viability of the myoblast cells on the surface of the liver tissue 2 d after transplantation. Scale bar = 50 μm.

from the sequence were analyzed using Seurat R package (version 4.0).

Statistical Analysis

All data are presented as means ± SDs unless otherwise noted. The means of continuous numerical variables were compared using the analysis of variance followed by Tukey's post hoc test. $P < 0.05$ was considered significant. JMP Pro 15.0 (SAS Institute Inc, Cary, NC) was used for statistical analysis.

RESULTS

Secretion Capacity of Myoblast Cells

Prior to the experiments, the myoblast cells were confirmed to continuously secrete VEGF and HGF by ELISA of the supernatant (Figure 1A). After confirming secretion, the skeletal myoblast cell sheet was produced for transplantation onto the livers of mice. H&E staining and immunohistochemical staining for desmin as a marker of myoblast cells confirmed that the myoblast sheet cells remained viable on the surface of the liver tissue 2 d after transplantation (Figure 1B and C).

In Vitro Effect of Myoblast Cells on Cells Associated With Liver Regeneration

The in vitro effect of the myoblast cells on liver regeneration was investigated. First, we investigated whether the myoblast cells play a role in the acceleration of hepatic cell proliferation using THLE-2 cells. The proliferative capacity of THLE-2 cells 24 h after seeding was significantly accelerated in the presence of HSMMs (Figure 2A). The percentage of Ki-67–positive cells was significantly higher in the coculture 24 h after seeding than in the cells without HSMMs (Figure 2B). In contrast, the proliferation 48 and 72 h after seeding was not significantly different between THLE-2 cells cocultured with or without HSMMs. These results suggest that, although the proliferative capacity of THLE-2 cells was enhanced by coculture with HSMMs, the difference in the proliferative capacity was modest. Next, we evaluated the effect of the myoblast cells on liver sinusoidal endothelial cells (LSECs) in a tube formation assay. In this assay, we used TMNK-1 cells cocultured with or without HSMMs. The assay revealed that the length of the tube and the number of capillaries were significantly increased in coculture with HSMMs and that the increase was dependent on the number of HSMMs (Figure 2C and D). Furthermore,

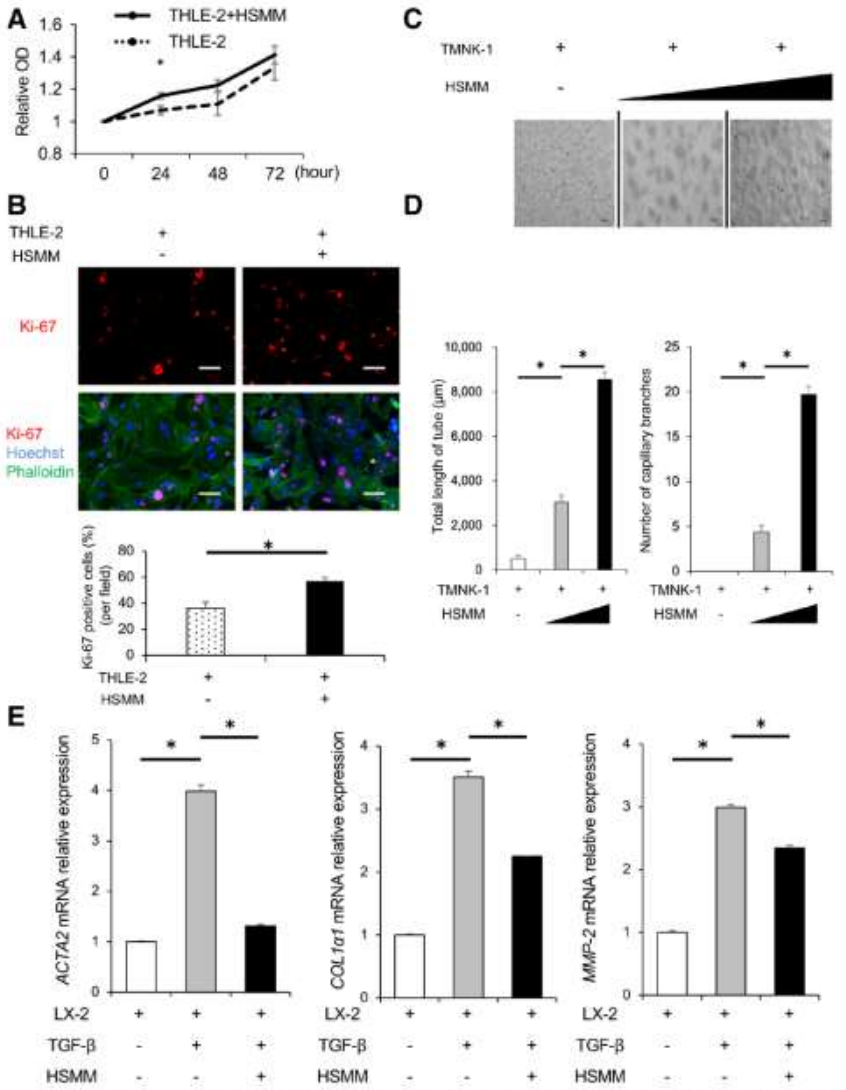

FIGURE 2. Myoblast cells affected cells associated with liver regeneration. A, The proliferative capacity of THLE-2 with and without human skeletal muscle myoblasts (HSMMs) was assessed. The group with HSMMs was more accelerated than the group without HSMMs 24 h after seeding. *$P < 0.05$. B, The percentage of Ki-67–positive cells was higher in the group with HSMMs (right panels) than the group without HSMMs (left panels) 24 h after seeding. *$P < 0.05$. C, TMNK-1 (1.0×10^5/well) was cocultured with HSMMs (1.0×10^5 or 5.0×10^5/well) for 24 h. Micrographs of the cells are shown. Scale bar = 100 μm. D, The total length of the tube and number of capillary branches were quantified. Both parameters were significantly increased in the groups with HSMMs, and the increase was dependent on HSMM dose. *$P < 0.05$. E, The mRNA levels of *ACTA2*, *COL1α1*, and *MMP-2* were examined. All mRNA levels in LX-2 were increased by transforming growth factor-β1 (TGF-β1) treatment and suppressed in the group with HSMMs 24 h after TGF-β1 treatment. *$P < 0.05$.

we assessed the influence of myoblast cells on HSCs, which play an important role in liver fibrosis. TGF-β1 converts HSCs into their activated form as a myofibroblast-like cell, expressing actin alpha 2 (ACTA2), collagen 1α-1 (COL1α-1), and matrix metalloproteases 2.[33-35] LX-2 cells were used as human HSCs in this experiment, which comprised 3 groups: LX-2 without TGF-β1 treatment, LX-2 with TGF-β1 treatment (10 ng/mL), and LX-2 with TGF-β1 treatment (10 ng/mL) in coculture with HSMMs. Twenty-four hours after TGF-β1 treatment, the total RNA was extracted from LX-2 cells and analyzed for the mRNA expression of ACTA2, COL1α-1, and matrix metalloproteases 2. The mRNA expression was significantly increased by TGF-β1, and the increase was significantly weakened by coculture with HSMMs (Figure 2E). These results indicate that the myoblast cells promote hepatic cell proliferation and angiogenesis and inhibit HSC activation in the liver. Considering that these phenomena induced by the myoblast cells were closely associated with liver fibrosis, the possibility was raised that the myoblast cells promote liver regeneration in liver fibrosis.

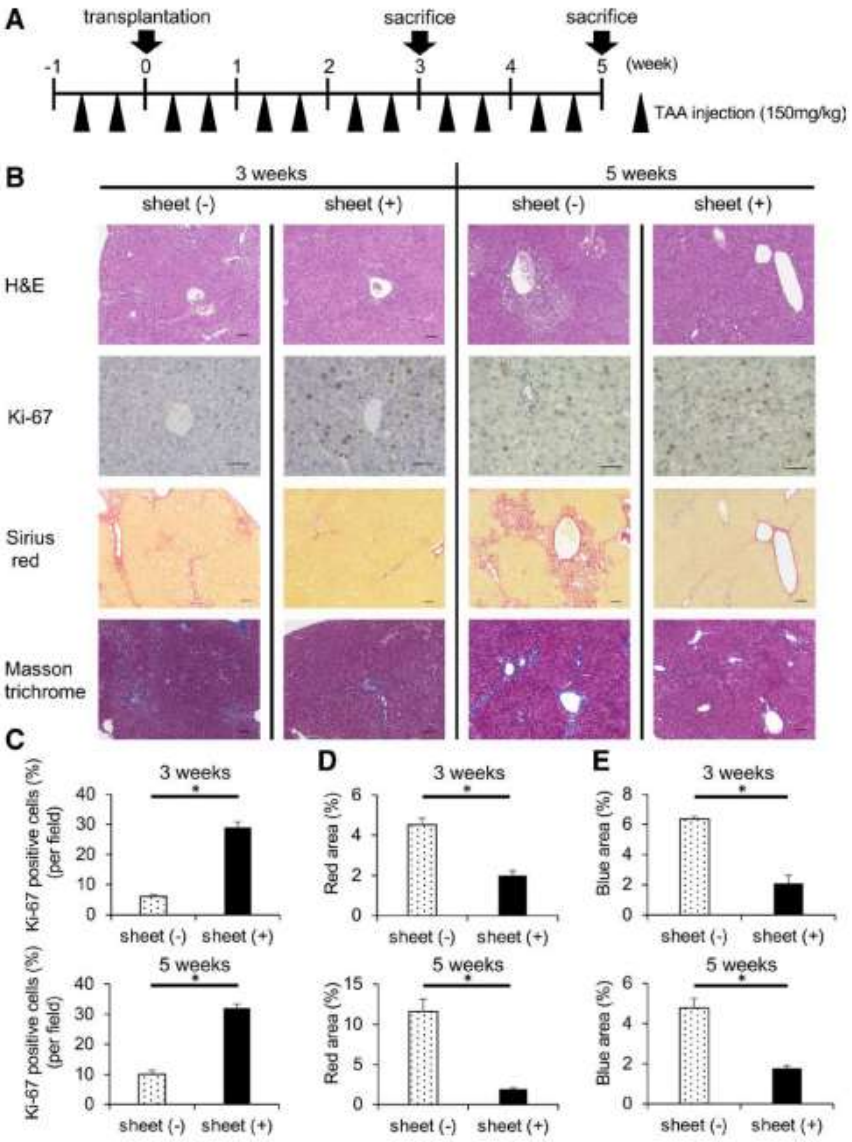

FIGURE 3. Myoblast cell sheets suppressed thioacetamide (TAA)-induced liver fibrosis. A, The assay schedule. TAA (150 mg/kg) was intraperitoneally injected twice a week. Mice were euthanized and analyzed 3 wk and 5 wk after sheet transplantation. B, Histological analysis (hematoxylin-eosin [H&E] staining, Ki-67 staining, Sirius red staining, and Masson trichrome staining) showed that sheet transplantation had the capacity to promote liver proliferation and improve liver fibrosis. Scale bar = 100 μm. C, The percentage of Ki-67–positive cells was significantly higher in the myoblast sheet group (sheet [+]) than the control group (sheet [-]). $^*P < 0.05$, n = 5 each group and each time. D and E, Liver fibrosis was evaluated by Sirius red staining (D) and Masson trichrome staining (E). The fibrotic area was significantly smaller in the sheet (+) group than in the control group. $^*P < 0.05$, n = 5 each group and each time.

Suppression of Liver Fibrosis by the Skeletal Myoblast Cell Sheet in Mice

The above results suggest that the skeletal myoblast cell sheet affects liver regeneration in liver failure, letting us investigate the effect of sheet transplantation in in vivo models. First, the effect was examined in a mouse model with liver fibrosis produced by intraperitoneal injection of TAA. One week after TAA injection, myoblast cell sheet transplantation was performed. Three weeks or 5 wk after transplantation, liver tissues were excised from the mouse model and analyzed. The schedule is shown in Figure 3A. H&E staining of the excised liver tissue indicated liver damage by TAA in both groups, and the liver damage was less severe in the myoblast sheet group than in the control group at both 3 wk and 5 wk (Figure 3B). Next, to assess the proliferation of hepatocytes for liver regeneration, the liver tissues were immunohistochemically stained for Ki-67, one of the principal markers of DNA replication. The percentage of Ki-67–positive cells was significantly higher in the myoblast sheet group than in the control group at both 3 wk and 5 wk (Figure 3B and C). Next, to evaluate the degree of liver fibrosis, Sirius red staining

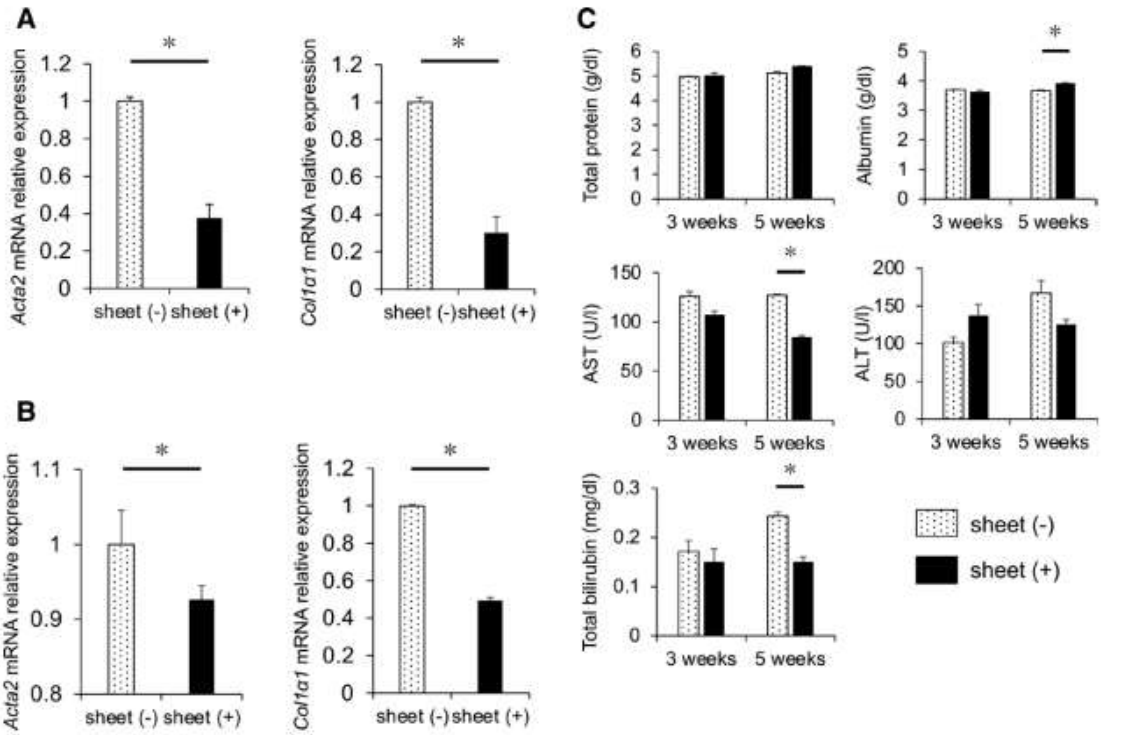

FIGURE 4. Suppression of liver fibrosis by the myoblast cell sheet was verified by real-time reverse-transcription PCR and blood test. A and B, *Acta2* and *Col1α1* mRNA levels in the liver were determined by real-time reverse-transcription PCR 3 wk (A) and 5 wk (B) after sheet transplantation. Expression was significantly lower in groups transplanted with the myoblast sheet (sheet [+]) than in control groups (sheet [–]). *$P < 0.05$, n = 5 each group. C, Serum levels of factors associated with liver function were assessed. Aspartate aminotransferase (AST) and total bilirubin levels were significantly lower and albumin level significantly higher in the sheet (+) group than in the control group 5 wk after sheet transplantation. *$P < 0.05$, n = 5 each group. PCR, polymerase chain reaction.

and Masson trichrome staining were performed. The area of liver fibrosis, determined as the red area in Sirius red staining and blue area in Masson trichrome staining, was significantly smaller in the sheet group than in the control group. These differences between the 2 groups were particularly remarkable 5 wk after transplantation (Figure 3B–E).

Liver fibrosis was assessed by real-time RT-PCR, which demonstrated that the mRNA expression of ACTA2 and Col1α-1 was significantly decreased in the sheet group compared with the control group at both 3 and 5 wk (Figure 4A and B). The results of the blood test performed 5 wk after transplantation are shown in Figure 4C; aspartate aminotransferase and total bilirubin were significantly lower and albumin was significantly higher in the sheet group than in the control group. These results were verified in another mouse model with more severe liver fibrosis, which was produced by 6 wk of TAA injection before myoblast cell sheet transplantation (**Figure S1, SDC,** http://links.lww.com/TP/C721).

Acceleration of Liver Regeneration by the Myoblast Cell Sheet in a Hepatectomy Model

Next, we assessed the effect of myoblast cell sheet transplantation on liver regeneration after hepatectomy. The 70% hepatectomy model was used for this assessment, and histological examination included H&E staining and Ki-67 staining of the remnant liver. H&E staining showed no inflammatory cells or thrombosis in the sheet or control groups. However, the percentage of Ki-67–positive cells was significantly higher in the remnant livers of the sheet group than in the control group 48 h after 70% hepatectomy (Figure 5A). The remnant liver to body weight ratio rapidly recovered in the sheet group, and a significant difference was found in the ratio 2 d after the hepatectomy (Figure 5B). These results suggest that myoblast cell sheet transplantation may also promote liver regeneration after hepatectomy. To assess the underlying effect of the transplantation, molecules associated with liver regeneration were investigated in the remnant liver tissue 48 h after hepatectomy. The expression of CD31 in the remnant liver was significantly increased in the sheet group compared with the control group, implying that more angiogenesis was induced by sheet transplantation (Figure 5C). The Akt and Erk1/2 pathways, which initiate cell cycle progression after liver resection, were also examined. The phosphorylated form of both Akt and Erk1/2 was more strongly expressed in the remnant livers in the sheet group than in the control group, indicating more rapid cell cycle progression in the sheet group.

Furthermore, the effect of the skeletal cell sheet transplantation was investigated in regard to survival after

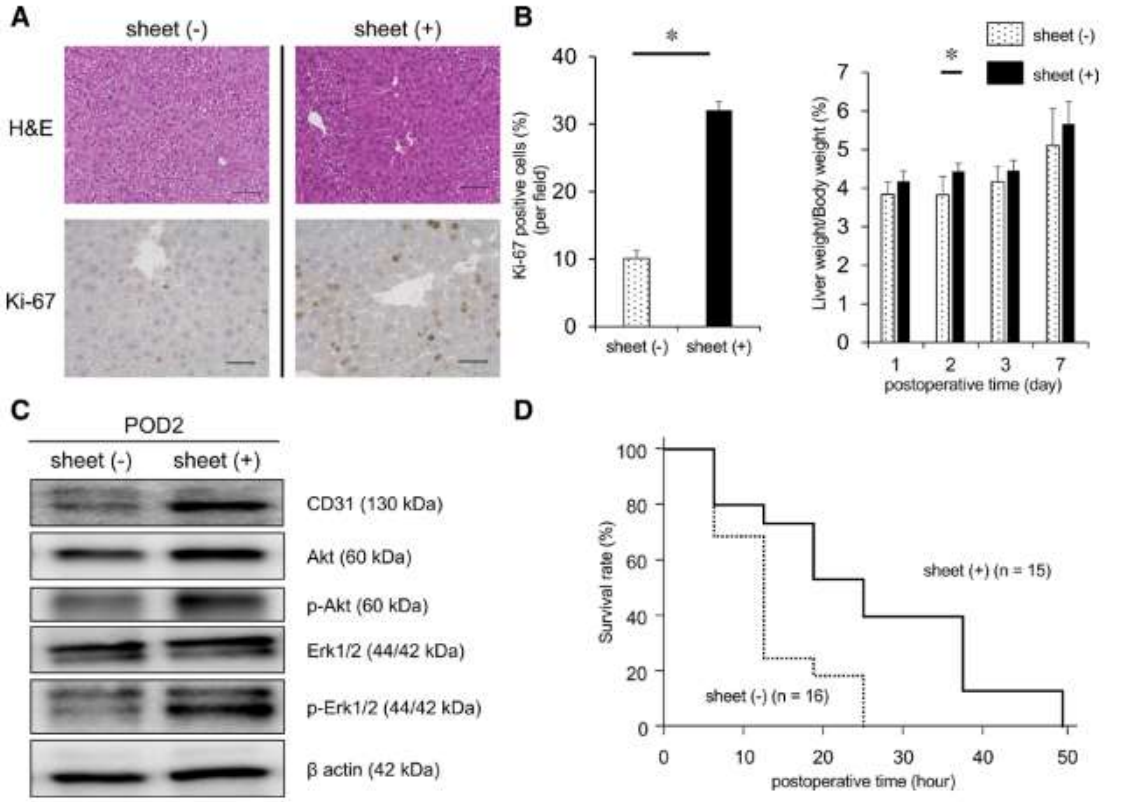

FIGURE 5. The myoblast cell sheet promoted liver regeneration after hepatectomy. A, Left, hematoxylin-eosin (H&E) staining (upper panels) and Ki-67 immunological staining (lower panels) of liver tissue 2 d after 70% hepatectomy. Scale bar = 100 μm (upper panels) or 50 μm (lower panels). Right, The percentage of Ki-67–positive cells was higher in the group with sheet transplantation (sheet [+]) than in the control group (sheet [–]). *$P < 0.05$, n = 5 each group. B, Liver weight/body weight ratios were measured 1, 2, 3, and 7 d after hepatectomy (n = 5 each group). The ratio was significantly higher in the sheet (+) group than in the control group. *$P < 0.05$. C, Western blot analysis of the expression of molecules associated with liver regeneration in the remnant liver tissue 2 d after hepatectomy. CD31 and phosphorylated forms of Akt and Erk1/2 were more strongly expressed in the sheet (+) group than in the control group. D, Kaplan-Meier survival curve demonstrating that the survival rate after 90% hepatectomy was higher in the sheet (+) group than in the control group. $P < 0.05$.

90% hepatectomy. Although all mice in the control group died within 24 h after 90% hepatectomy, half of the mice in the sheet group survived at least 24 h after hepatectomy. Using the Kaplan-Meier methods, the survival rate was significantly improved by cell sheet transplantation ($P < 0.05$; Figure 5D). These results suggest that myoblast cell sheet transplantation accelerates liver regeneration by promoting cell cycle progression and proliferation signals.

Investigation of the Mechanism of Liver Regeneration by the Myoblast Cell Sheet

To investigate the underlying mechanism of liver regeneration after skeletal myoblast cell sheet transplantation, we performed spatial transcriptomic analysis of the liver tissue collected from a mouse 2 d after 70% hepatectomy with sheet transplantation. Clustering roughly identified the remnant liver and the transplanted skeletal myoblast cells on the H&E-stained section (Figure 6A), and uniform manifold approximation and projection of these clusters indicated that the clusters were mainly divided into 2 groups: clusters 2 and 5 were myoblast cells, and the other clusters were cells that comprise the liver (Figure 6B). Cells in cluster 5, where the myoblast cells attached to the remnant liver, overexpressed Vegfa, which is one of the secretions by skeletal myoblast cells (Figure 6C). Furthermore, immunohistochemical analysis of the liver tissue obtained from mice 6 h after 70% hepatectomy with myoblast cell sheet transplantation showed that the VEGFA protein level was higher in the myoblast cells stained by desmin and the remnant liver near the cells than in the remaining area of the liver (Figure 6D). These findings suggest that the myoblast cell sheet secreted VEGFA since the early phase after sheet transplantation and that the secreted VEGFA penetrated into the remnant liver, which implies a possibility that the secretion of VEGFA by the myoblast cell sheet is one of the mechanisms of liver regeneration.

DISCUSSION

In this study, we demonstrated in vitro that myoblast cells significantly affect cells associated with liver regeneration, such as hepatic cells, LSECs, and HSCs, implying the possibility that skeletal myoblast cell sheet transplantation significantly affects liver regeneration. To verify this

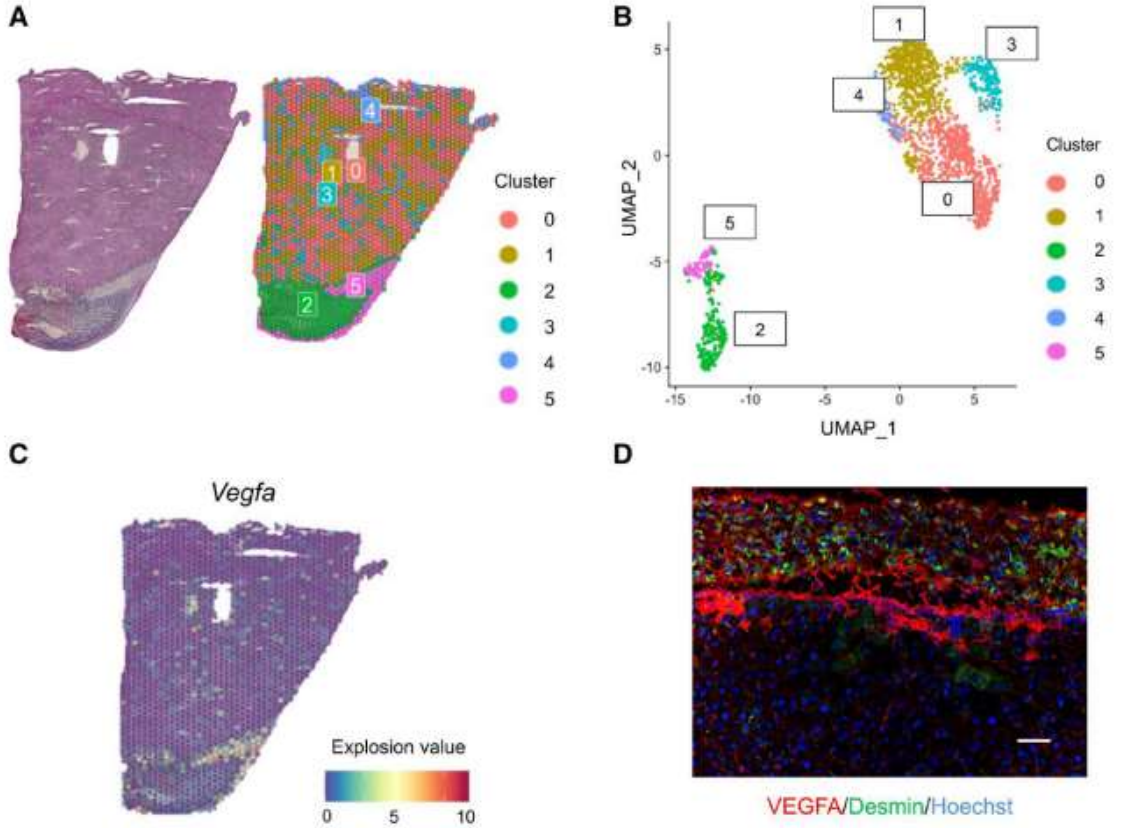

FIGURE 6. Vascular endothelial growth factor (VEGFA) contributed to liver regeneration after hepatectomy with myoblast cell sheet transplantation. A and B, Hematoxylin-eosin staining and unbiased clustering of spatial transcriptomic analysis of liver tissue 2 d after 70% hepatectomy with myoblast cell sheet transplantation. The data were visualized using Visium and summarized in the uniform manifold approximation and projection (UMAP). C, Spatial feature plots show *Vegfa* overexpression in the myoblast cells attached to the remnant liver. D, Representative immunohistochemistry for the tissue 6 h after 70% hepatectomy with sheet transplantation. VEGFA (red) was overexpressed at the myoblast cells stained with desmin (green) and the remnant liver near the cells. Scale bar = 50 μm.

possibility in vivo, experiments were performed in mouse models. The in vivo results revealed that myoblast cell sheet transplantation significantly suppressed liver fibrosis after induction of liver fibrosis by TAA and accelerated liver regeneration after hepatectomy. Taken together, the results suggest that skeletal myoblast cell sheet transplantation has the capacity for liver regeneration. This suggestion has not yet been addressed, indicating the clinical utility of sheet transplantation for liver regeneration in liver failure.

Myoblast cell sheets have been proven to improve cardiac failure, and the underlying mechanism for heart regeneration has been investigated.[19] In the field of heart regeneration, myoblast cells have been known to have the capacity to secrete several cytokines, including VEGF, HGF, and stromal derived factor-1.[22,24,36-38] In addition, the therapy using myoblast cells has been reported to have the ability to regulate inflammation via macrophage polarization mainly into the anti-inflammatory phenotype in peripheral artery disease.[39] Based on previous studies, these cytokines have been considered independently to have an important role in liver regeneration; VEGF is known to activate the HGF-Wnt2 pathway through VEGF2-Id1 activation in LSECs to stimulate liver regeneration.[6] Moreover, VEGF has been reported to improve the formation of LSECs at the time when the liver is injured.[40-42] In addition to the abovementioned HGF signaling pathway, HGF has other capacities in liver regeneration; when the liver is injured, HSCs transform into myofibroblast-like cells, which cause liver fibrosis,[43-45] but HGF promotes apoptosis of myofibroblast-like cells.[46] Considering these potential capacities of the cytokines in liver regeneration and our finding that the myoblast cell sheet overexpressed and secreted VEGFA in the in vivo model, the liver regenerative capacity shown in this study may be derived from the cytokines secreted by the myoblast cells. In particular, one of our results showing the HSMM dose-dependency in in vitro experiments may be the evidence that the cytokine secretion from skeletal cells is a mechanism for liver regeneration. Furthermore, the efficacy of the myoblast cell sheet transplantation was evident in our results, especially in the in vivo experiments, although the effect on hepatocyte growth itself in vitro was relatively modest compared with the effect to the other cells. This discrepancy may be explained by assuming that the liver regenerative capacity of the skeletal cells is derived not only from the direct effect on the hepatocytes but also from the comprehensive effects on various cells, including hepatocytes, LSECs, and HSCs. Thus, the possibility that these various cells may induce liver regeneration

may indicate that the liver regenerative capacity is derived from the cytokines secreted by the myoblast cells.

Thus far, several options for liver regeneration have been advocated, including treatments with bone marrow cells, adipose-derived stem cells, and iPSCs.[10,13] However, none of these approaches have been clinically established. On the contrary, our option for liver regeneration using skeletal myoblast cell sheet transplantation remains to develop similarly to the above options, but we consider that our option has some advantages. First, we utilized sheet technology that has been reported to be an efficient means of administration. This approach allows the administration of a larger number of cells than simple intravenous injection and retains cell–cell interactions inside the sheet, which then potentially exerts stronger effects than simple cell administration.[47] Furthermore, retaining the sheet directly on the liver surface may advantageously supply its effect, considering the nature of the paracrine effect when considering the mechanism compared to administration far from the subject site. Second, although some of the other methods utilize allogenic cells, autologous cells are used in this method, indicating an advantage in terms of avoiding potential immunogenicity. Finally, from another perspective, this therapeutic option for liver regeneration is based on an expanded adaptation of skeletal myoblast cell sheet transplantation, the clinical effect of which has already been confirmed, leading to coverage by the health insurance in Japan. In this context, the safety of this method is already proven, suggesting easier clinical application than other methods.

This study has several limitations. One limitation is in regard to the investigation of mechanisms underlying the effect of the skeletal myoblast cells on liver regeneration being limited in this study. Although the results of the transcriptomic analysis and immunohistochemical analysis of the sample after hepatectomy actually implied that the secretion of VEGFA by the myoblast cell sheet may be one of the key mechanisms, we have not comprehensively performed an investigation of the mechanisms. Clarification of the more detailed mechanism can lead to predicting the effect and enhancing the effect based on the mechanism. Another is that this study contains only data on the local administration of the skeletal cell sheet. The administration was effective for the liver transplantation in our experiments, but the efficacy was not compared to other administrative methods, such as the intravenous administration, suggesting that, although the skeletal cell may be clinically useful for liver regeneration, the optimal route of administration remains to be undetermined. Considering that intravenous administration has been introduced in some other regenerative therapies, such as bone marrow-derived stem cells and adipose-derived stem cells, the comparison to other methods should be performed. Therefore, we are currently analyzing the mechanism and determining the optimal administration route. In addition, we did not compare the effect of the skeletal cell sheet to other cell sources, such as other mesenchymal stem cells. However, to prioritize prompt announcement of our results in order to speed up the clinical application of this novel therapeutic option, we summarized the results without any comparative analyses in this report.

In conclusion, this study revealed that skeletal myoblast cell sheet transplantation significantly improved liver failure in the in vitro and in vivo models and that VEGF was one of the mechanisms responsible for improvements caused by the myoblast cell sheet, suggesting clinical utility of myoblast cell sheet transplantation for liver regeneration. This finding could help establish autologous skeletal myoblast cell sheet transplantation as an effective therapeutic option for liver failure.

REFERENCES

1. Friedman SL, Sheppard D, Duffield JS, et al. Therapy for fibrotic diseases: nearing the starting line. *Sci Transl Med*. 2013;5:167sr1.
2. Diehl AM. Neighborhood watch orchestrates liver regeneration. *Nat Med*. 2012;18:497–499.
3. Philip G, Hookey L, Richardson H, et al. Alcohol-associated liver disease is now the most common indication for liver transplant waitlisting among young American adults. *Transplantation*. 2022;106:2000–2005.
4. Hay DC. Cadaveric hepatocytes repopulate diseased livers: life after death. *Gastroenterology*. 2010;139:729–731.
5. Terai S, Tsuchiya A. Status of and candidates for cell therapy in liver cirrhosis: overcoming the "point of no return" in advanced liver cirrhosis. *J Gastroenterol*. 2017;52:129–140.
6. Ding BS, Nolan DJ, Butler JM, et al. Inductive angiocrine signals from sinusoidal endothelium are required for liver regeneration. *Nature*. 2010;468:310–315.
7. Wang L, Wang X, Xie G, et al. Liver sinusoidal endothelial cell progenitor cells promote liver regeneration in rats. *J Clin Invest*. 2012;122:1567–1573.
8. Russell JO, Monga SP. Wnt/β-catenin signaling in liver development, homeostasis, and pathobiology. *Ann Rev Pathol*. 2018;13:351–378.
9. Sakaida I, Terai S, Yamamoto N, et al. Transplantation of bone marrow cells reduces CCl4-induced liver fibrosis in mice. *Hepatology*. 2004;40:1304–1311.
10. Terai S, Sakaida I. Current status of autologous bone marrow cell infusion therapy for liver cirrhosis patients. *Hepatol Res*. 2008;38(Suppl 1):S72–S75.
11. Terai S, Tanimoto H, Maeda M, et al. Timeline for development of autologous bone marrow infusion (ABMi) therapy and perspective for future stem cell therapy. *J Gastroenterol*. 2012;47:491–497.
12. Tolosa L, Pareja E, Gómez-Lechón MJ. Clinical application of pluripotent stem cells: an alternative cell-based therapy for treating liver diseases? *Transplantation*. 2016;100:2548–2557.
13. Takebe T, Sekine K, Enomura M, et al. Vascularized and functional human liver from an iPSC-derived organ bud transplant. *Nature*. 2013;499:481–484.
14. Tanaka T, Kuroki T, Adachi T, et al. Development of a novel rat model with pancreatic fistula and the prevention of this complication using tissue-engineered myoblast sheets. *J Gastroenterol*. 2013;48:1081–1089.
15. Tanaka S, Kanetaka K, Fujii M, et al. Cell sheet technology for the regeneration of gastrointestinal tissue using a novel gastric perforation rat model. *Surg Today*. 2017;47:114–121.
16. Matsumoto R, Kanetaka K, Maruya Y, et al. The efficacy of autologous myoblast sheet transplantation to prevent perforation after duodenal endoscopic submucosal dissection in porcine model. *Cell Transplant*. 2020;29:963689720963882.
17. Memon IA, Sawa Y, Fukushima N, et al. Repair of impaired myocardium by means of implantation of engineered autologous myoblast sheets. *J Thorac Cardiovasc Surg*. 2005;130:1333–1341.
18. Saito S, Miyagawa S, Sakaguchi T, et al. Myoblast sheet can prevent the impairment of cardiac diastolic function and late remodeling after left ventricular restoration in ischemic cardiomyopathy. *Transplantation*. 2012;93:1108–1115.
19. Kainuma S, Miyagawa S, Toda K, et al. Long-term outcomes of autologous skeletal myoblast cell-sheet transplantation for end-stage ischemic cardiomyopathy. *Mol Ther*. 2021;29:1425–1438.
20. Miyagawa S, Sawa Y, Taketani S, et al. Myocardial regeneration therapy for heart failure: hepatocyte growth factor enhances the effect of cellular cardiomyoplasty. *Circulation*. 2002;105:2556–2561.
21. Sawa Y, Miyagawa S, Sakaguchi T, et al. Tissue engineered myoblast sheets improved cardiac function sufficiently to discontinue LVAS in a patient with DCM: report of a case. *Surg Today*. 2012;42:181–184.
22. Morita M, Watanabe Y, Akaike T. Protective effect of hepatocyte growth factor on interferon-gamma-induced cytotoxicity in mouse hepatocytes. *Hepatology*. 1995;21:1585–1593.

23. Yao P, Zhan Y, Xu W, et al. Hepatocyte growth factor-induced proliferation of hepatic stem-like cells depends on activation of NF-kappaB. *J Hepatol*. 2004;40:391–398.
24. Ishikawa T, Factor VM, Marquardt JU, et al. Hepatocyte growth factor/c-met signaling is required for stem-cell-mediated liver regeneration in mice. *Hepatology*. 2012;55:1215–1226.
25. Ding BS, Cao Z, Lis R, et al. Divergent angiocrine signals from vascular niche balance liver regeneration and fibrosis. *Nature*. 2014;505:97–102.
26. Mukai Y, Yamada D, Eguchi H, et al. Vitamin D supplementation is a promising therapy for pancreatic ductal adenocarcinoma in conjunction with current chemoradiation therapy. *Ann Surg Oncol*. 2018;25:1868–1879.
27. Matsumura T, Takesue M, Westerman KA, et al. Establishment of an immortalized human-liver endothelial cell line with SV40T and hTERT. *Transplantation*. 2004;77:1357–1365.
28. Sekiya N, Matsumiya G, Miyagawa S, et al. Layered implantation of myoblast sheets attenuates adverse cardiac remodeling of the infarcted heart. *J Thorac Cardiovasc Surg*. 2009;138:985–993.
29. Mitchell C, Willenbring H. A reproducible and well-tolerated method for 2/3 partial hepatectomy in mice. *Nat Protoc*. 2008;3:1167–1170.
30. Makino H, Togo S, Kubota T, et al. A good model of hepatic failure after excessive hepatectomy in mice. *J Surg Res*. 2005;127:171–176.
31. Mikamori M, Yamada D, Eguchi H, et al. MicroRNA-155 controls exosome synthesis and promotes gemcitabine resistance in pancreatic ductal adenocarcinoma. *Sci Rep*. 2017;7:42339.
32. Ji AL, Rubin AJ, Thrane K, et al. Multimodal analysis of composition and spatial architecture in human squamous cell carcinoma. *Cell*. 2020;182:497–514.e22.
33. Friedman SL. Hepatic stellate cells: protean, multifunctional, and enigmatic cells of the liver. *Physiol Rev*. 2008;88:125–172.
34. Schuppan D, Kim YO. Evolving therapies for liver fibrosis. *J Clin Invest*. 2013;123:1887–1901.
35. Gressner AM, Weiskirchen R. Modern pathogenetic concepts of liver fibrosis suggest stellate cells and TGF-beta as major players and therapeutic targets. *J Cell Mol Med*. 2006;10:76–99.
36. Klein D, Demory A, Peyre F, et al. Wnt2 acts as a cell type-specific, autocrine growth factor in rat hepatic sinusoidal endothelial cells cross-stimulating the VEGF pathway. *Hepatology*. 2008;47:1018–1031.
37. Tekkesin N, Taga Y, Sav A, et al. Induction of HGF and VEGF in hepatic regeneration after hepatotoxin-induced cirrhosis in mice. *Hepatogastroenterology*. 2011;58:971–979.
38. Hu J, Srivastava K, Wieland M, et al. Endothelial cell-derived angiopoietin-2 controls liver regeneration as a spatiotemporal rheostat. *Science*. 2014;343:416–419.
39. Miyake K, Miyagawa S, Harada A, et al. Engineered clustered myoblast cell injection augments angiogenesis and muscle regeneration in peripheral artery disease. *Mol Ther*. 2022;30:1239–1251.
40. Funyu J, Mochida S, Inao M, et al. VEGF can act as vascular permeability factor in the hepatic sinusoids through upregulation of porosity of endothelial cells. *Biochem Biophys Res Commun*. 2001;280:481–485.
41. Xu H, Shi BM, Lu XF, et al. Vascular endothelial growth factor attenuates hepatic sinusoidal capillarization in thioacetamide-induced cirrhotic rats. *World J Gastroenterol*. 2008;14:2349–2357.
42. Thabut D, Shah V. Intrahepatic angiogenesis and sinusoidal remodeling in chronic liver disease: new targets for the treatment of portal hypertension? *J Hepatol*. 2010;53:976–980.
43. Iredale JP, Benyon RC, Pickering J, et al. Mechanisms of spontaneous resolution of rat liver fibrosis. Hepatic stellate cell apoptosis and reduced hepatic expression of metalloproteinase inhibitors. *J Clin Invest*. 1998;102:538–549.
44. Kisseleva T, Cong M, Paik Y, et al. Myofibroblasts revert to an inactive phenotype during regression of liver fibrosis. *Proc Natl Acad Sci UA*. 2012;109:9448–9453.
45. Troeger JS, Mederacke I, Gwak GY, et al. Deactivation of hepatic stellate cells during liver fibrosis resolution in mice. *Gastroenterology*. 2012;143:1073–83.e22.
46. Kim WH, Matsumoto K, Bessho K, et al. Growth inhibition and apoptosis in liver myofibroblasts promoted by hepatocyte growth factor leads to resolution from liver cirrhosis. *Am J Pathol*. 2005;166:1017–1028.
47. Okano T, Yamada N, Sakai H, et al. A novel recovery system for cultured cells using plasma-treated polystyrene dishes grafted with poly(N-isopropylacrylamide). *J Biomed Mater Res*. 1993;27:1243–1251.

Long-Term Feasibility of Rescue Reconstruction for Isolated Bile Ducts With Using Cystic Duct in Living Donor Liver Transplantation

Masahiko Kubo, Yoshito Tomimaru, Kunihito Gotoh, Shogo Kobayashi*, Daiki Marukawa, Kazuki Sasaki, Yoshifumi Iwagami, Daisaku Yamada, Hirofumi Akita, Takehiro Noda, Hidenori Takahashi, Tadafumi Asaoka, Masahiro Tanemura, Shigeru Marubashi, Hiroaki Nagano, Keizo Dono, Yuichiro Doki, and Hidetoshi Eguchi

Department of Gastroenterological Surgery, Graduate School of Medicine, Osaka University, Osaka, Japan

ABSTRACT

Background. The isolated bile duct is sometimes observed in the right liver graft of living donor liver transplantation (LDLT). Even though, as a rescue option, it is known to use the recipient's cystic duct (CyD) for duct-to-duct anastomosis, the long-term feasibility of rescue duct-to-CyD (D-CyD) anastomosis remains unclear.

Methods. We prospectively collected data in the right liver-LDLT cohort and compared rescue D-CyD anastomosis (n = 4) with standard duct-to-hepatic duct (D-HD, n = 45) anastomosis (D-CyD group, n = 4).

Results. The observation period was over 5 years (range, 68-171 mo) after LDLT.
The D-CyD group included the following anastomosis procedures: anastomosis between the intrahepatic bile duct of the graft and the CyD of the recipient and anastomosis between the posterior HD and the CyD. Surgical outcomes between the 2 groups are similar, excluding the time for the biliary reconstruction (D-CyD, 116 ± 13 min vs D-HD, 57 ± 3 min). During the period, one recipient in the D-CyD group exhibited postoperative biliary stricture and biliary stone, and 6 recipients underwent those complications in the D-HD group (D-CyD, 25.0% vs D-HD, 13.3%) All recipients in the D-CyD group are presently alive and have not experienced liver dysfunction.

Conclusions. Our findings suggest that rescue D-CyD anastomosis for an isolated bile duct in a right liver LDLT is acceptable as a life-saving option in terms of long-term feasibility.

BECAUSE of their high frequency, biliary complications are regarded as the Achilles' heel of liver transplantation (LT). In a systematic review, Akamatsu et al reported the occurrence of biliary strictures and biliary leakages in 12.8% and 8.2% of LT recipients, respectively [1]. Moreover, they found that these incidence rates were higher after partial liver grafts than after whole liver grafts.

In LT with a partial liver graft, biliary reconstruction used to be performed with a hepaticojejunostomy, because the main indication for living donor LT (LDLT) with a partial liver was pediatric recipients with biliary atresia. However, the indications for LDLT have now been widely expanded thanks to recent advances in surgical techniques and perioperative management. Consequently, in LDLT with a partial liver graft, biliary reconstruction is commonly performed with duct-to-duct (D-D) anastomosis, which has several advantages including no enteric anastomosis, a functional sphincter of Oddi, and an easier endoscopic approach to the anastomotic sites.

In cases with a single bile duct in the partial liver graft, the D-D anastomosis is simple. However, D-D anastomosis is more complicated in cases where the partial liver graft includes multiple ducts—for example, when a right-lobe graft is used. If the partial liver graft includes multiple ducts that are located close together, the anastomosis can be performed between a single orifice created by these ducts of the graft and the hepatic duct (HD) of the recipient. However, this type of anastomosis is

*Address correspondence to Shogo Kobayashi, MD, PhD, Department of Gastroenterological Surgery, Graduate School of Medicine, Osaka University, 2-2-E2, Yamadaoka, Suita, Osaka, 565-0871, Japan. E-mail: skobayashi@gesurg.med.osaka-u.ac.jp

0041-1345/20
https://doi.org/10.1016/j.transproceed.2023.03.086

challenging when the partial liver graft includes multiple bile ducts separated by a wide anatomic distance. It is necessary to consider a rescue biliary reconstruction in such cases.

One rescue method of biliary reconstruction is to use both the cystic duct (CyD) and the HD of the recipient. The anatomic separation of the CyD from the HD potentially enables anastomosis of separated bile ducts in a partial liver graft. Several reports have described the successful use of the CyD for biliary reconstruction in cases of LDLT with a right-lobe liver graft containing separated bile ducts [2–4]. However, no studies have focused on the long-term postoperative outcome of duct-to-CyD (D-CyD) anastomosis performed together with duct-to-HD (D-HD) anastomosis, or compared outcomes between D-CyD anastomosis and the standard D-HD anastomosis.

We have experience with several cases that performed D-CyD anastomosis in LDLT. In our first case, a bile duct branch of the graft had been intentionally left without anastomosis, and was successfully postoperatively anastomosed to the CyD stump using a magnetic compression anastomosis technique [5]. In the present study, based on our experience, we aimed to assess the potential of D-CyD as a rescue option to D-HD by investigating the long-term postoperative outcome of the addition of the D-CyD anastomosis for biliary reconstruction by comparing the outcome of D-CyD anastomosis with that of standard D-HD anastomosis in cases of LDLT with a right-lobe graft.

PATIENTS AND METHODS

Patients

A total of 148 adult patients received LDLT between 1999 and 2018 at the Department of Gastroenterological Surgery, Osaka University Hospital. Of these 148 cases, 76 cases used a right-lobe graft for LDLT. Among the 76 recipients of a right-lobe graft, 49 (64.5%) underwent biliary reconstruction with D-D anastomosis, and 27 (35.5%) underwent hepaticojejunostomy. The present study included 49 recipients who underwent D-D anastomosis with a right-lobe graft. In 4 included recipients (8.2%), D-CyD anastomosis was performed together with D-HD anastomosis (D-CyD group). In the remaining 45 (91.8%) included recipients, only the standard D-HD anastomosis was performed (D-HD group). Ethical approval was given by the Human Ethics Review Committee of the Graduate School of Medicine, Osaka University, and written informed consent was obtained from each of the patients (#21228).

Preoperative Evaluation

Preoperative evaluations for living liver donors and recipients included a work-up with a complete history and physical examination by expert hepatologists, psychiatrists, hepatobiliary/transplant surgeons, and other specialized workup team members, as previously described [6]. The selection of donors and recipients based on these evaluations was approved by the ethics review committee of Osaka University Hospital, as previously described [7]. For each donor, the graft type (left lobe with/without caudate, right lobe, or right posterior section) was determined based on the results of volumetric examination with multidetector computed tomography and drip-infusion cholangiography computed tomography (DIC-CT). Liver volumetric analysis was performed using Virtual Place software version 2.0 (AZE Ltd, Tokyo, Japan) or SYNAPSE VINCENT software (Fujifilm, Tokyo, Japan).

Donor Hepatectomy and LDLT

Donor hepatectomy and LDLT were performed using minimally invasive techniques, as previously described [6,8]. In the donor hepatectomy, to accurately evaluate the bile duct anatomy of the graft, intraoperative cholangiography was performed before cutting the bile duct. In the recipient surgery, the bile duct was carefully handled to avoid sacrificing the surrounding tissues and to preserve the vasculature. Both D-HD and D-CyD anastomoses were performed using interrupted sutures with 6-0 absorbable monofilament. In cases where the CyD of the recipient might be used for biliary reconstruction, care was taken to preserve the CyD itself and the surrounding tissues as much as possible to maintain the blood flow. In LDLT, an external biliary stent was inserted into the biliary anastomotic site.

Postoperative Follow-Up

Postoperative follow-up was performed by regular blood tests and radiographic evaluation, including cholangiography. The amount of immunosuppressive drugs was adjusted by their concentration. Before removing the external biliary stent, cholangiography was performed to exclude any biliary complications, such as biliary leakage or stricture.

Statistical Analysis

All data are reported as the number of patients and percentage, or as mean ± standard deviation. Between-group differences were analyzed for statistical significance by Student t test or Mann-Whitney U test. The cumulative incidence of postoperative biliary stricture was assessed using the Kaplan-Meier method. Statistical analyses were performed using JMP software version 14.0 (SAS Institute Inc.). A P value of less than .05 was considered significant.

RESULTS

Characteristics of Recipients With D-CyD Anastomosis

Table 1 summarizes the clinical characteristics of the 4 recipients who received D-CyD anastomosis together with the standard D-HD anastomosis for biliary reconstruction during LDLT with a right-lobe graft. These recipients included 3 men and 1 woman, with ages ranging from 46 to 64 years old. The disease necessitating LDLT was hepatitis B virus-related cirrhosis in 2 recipients and fulminant hepatic failure in 2 recipients.

In recipients 1 and 2, the D-CyD anastomosis was between the B6 bile duct of the graft and the CyD of the recipient. In recipient 3, the D-CyD anastomosis was between the posterior HD of the graft and the CyD of the recipient. In recipient 4, the

Table 1. Recipient Demographics

No.	Age in Years/Sex	Diagnosis	MELD Score	Intraoperative Blood Loss (mL)	Operation Time (min)	Biliary Reconstruction	Biliary Complication	Outcome
1	53/Male	HBV, cirrhosis	21	59,130	1500	AHD/B7-CHD, B6-CyD	Stricture, stone	Alive without graft loss (171 mo)
2	64/Male	FHF	28	4230	1139	AHD/B7-CHD, B6-CyD	None	Alive without graft loss (69 mo)
3	49/Female	FHF	23	3100	1105	AHD-CHD, PHD-CyD	None	Alive without graft loss (99 mo)
4	46/Male	HBV, cirrhosis	16	2810	1252	PHD/B8-CHD, B5-CyD	None	Alive without graft loss (68 mo)

AHD, anterior hepatic duct; CHD, common hepatic duct; CyD, cystic duct; FHF, fulminant hepatic failure; HBV, hepatitis B virus; MELD, model for end-stage liver disease; PHD, posterior hepatic duct.

D-CyD anastomosis was between the B5 bile duct of the graft and the CyD of the recipient. In recipient 1, the D-CyD anastomosis was added for biliary reconstruction because the standard anastomosis was technically difficult due to the small size of the B6 bile duct, which was overcome using the postoperative recovery magnetic compression anastomosis technique. In the remaining 3 recipients, it was impossible to create a single large orifice from the major bile ducts of the right-lobe graft because they were too separated. The D-CyD anastomosis was performed post-LDLT in recipient 1, and during LDLT in the remaining 3 recipients. More detailed information regarding recipients 1 and 3 has been previously described [5,9].

The follow-up period of the recipients ranged from 68 to 171 months. Recipient 1 exhibited postoperative biliary stricture and biliary duct stone, and both complications were successfully treated using an endoscopic approach. The other 3 recipients exhibited no postoperative biliary complications after the D-CyD anastomosis. All 4 recipients are presently alive and have not experienced liver dysfunction during the postoperative follow-up period. Below we present detailed information about representative recipients (2 and 4).

Recipient 2

Recipient 2 was a 64-year-old man who was scheduled to receive LDLT with a right-lobe graft due to fulminant hepatic failure with hepatic encephalopathy with a model for end-stage liver disease (MELD) score of 28. Because his condition got drastically worse and had no time for the donor to undergo preoperative DIC-CT, an additional intraoperative cholangiography was performed to evaluate the bile duct in the donor at the beginning of the donor hepatectomy (Fig 1A). It revealed that the B6 bile duct was directly confluent to the CyD, separately from the left HD, anterior HD, and B7 bile duct. In bench surgery for the graft, we successfully created a single orifice with the anterior HD and the B7 bile duct. However, it was impossible to create a single orifice with the created anterior HD/B7 bile duct and the separated B6 bile duct because of the distance. Therefore, we performed the anastomosis between the anterior HD/B7 bile duct and the common HD (CHD), the D-CyD anastomosis with the B6 bile duct was performed. The internal diameters of D-CHD and D-CyD were 7 mm and 5 mm, respectively (Fig B and C). External biliary stents were inserted into these 2 anastomoses. The recipient had an uneventful hospital course. At 6 months after LDLT, three-dimensional cholangiography via the inserted external biliary stents revealed patency of the anastomotic sites without leakage or stricture (Fig 1D).

Recipient 4

Recipient 4 was a 46-year-old man diagnosed with end-stage liver disease due to hepatitis B virus. His MELD score was 16. LDLT with a right-lobe graft was planned for his treatment. Preoperative DIC-CT of the donor indicated that the B5 bile duct was confluent separately from the left HD, posterior HD, and B8 bile duct (Fig 2A). Investigation after donor hepatectomy confirmed the independently confluent B5 bile duct observed in the preoperative DIC-CT. In bench surgery for the graft, a single orifice was successfully created with the posterior HD and the B8 bile duct. However, it was impossible to include the separated B5 bile duct into the created posterior HD/B8 bile duct because of the distance. Therefore, we performed the anastomosis between the B5 bile duct of the graft and the CyD of the recipient and the anastomosis between the posterior HD/B8 bile duct of the graft and the CHD of the recipient (Fig 2B and C). The internal diameters of these anastomoses were 4 mm and 1 mm, respectively. External biliary stents were inserted into these 2 anastomoses. The recipient had an uneventful hospital course. At 2 months after LDLT, cholangiography via the inserted external biliary stents confirmed that the contrast medium passed through these anastomotic sites without leakage or stricture (Fig 2D).

Comparison of Surgical Outcome Between the Two Biliary Reconstructions

We checked surgical outcomes between the recipients in the D-CyD and D-HD groups. The 2 groups had similar surgical outcomes, including intraoperative blood loss, or total operation time (Table 2). However, the time for the biliary reconstruction was longer for the 3 cases (recipients 2-4) in which the D-CyD anastomosis was performed during LDLT, compared with the D-HD cases (116 $\pm$ 13 min vs 57 $\pm$ 3 min, $P < .0001$). In terms of intraoperative findings, the biliary anastomosis diameter was smaller in the D-CyD group than in the D-HD group (2.5 $\pm$ 1.5 mm vs 4.0 $\pm$1.7 mm, $P = .2028$).

With regards to postoperative biliary complications, 6 recipients (13.3%) in the D-HD group exhibited a biliary stricture. On the other hand, postoperative biliary stricture was observed in one recipient (25.0%) in the D-CyD group, who underwent the C-CyD anastomosis after LDLT. The incidence of biliary stricture did not significantly differ between the 2 groups, as confirmed by the cumulative incidence assessed using the Kaplan-Meier method (Fig 3). Additionally, one recipient from each group exhibited biliary stone. Notably, the stone in the D-

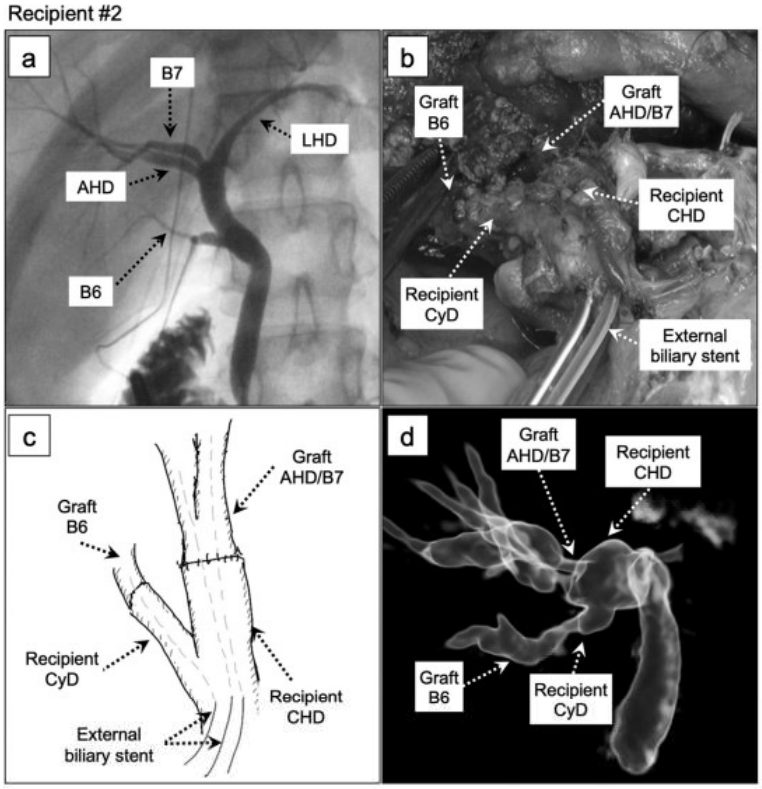

Fig 1. Perioperative imaging of the bile duct in recipient 2. **(A)** Intraoperative cholangiography at the beginning of the donor hepatectomy revealed that the B6 bile duct was directly confluent with the CyD, separately from the LHD, AHD, and B7 bile duct. **(B)** Intraoperative photograph **(C)** and schema of the biliary reconstruction, showing anastomosis between the AHD/B7 bile duct of the graft and the CHD of the recipient, as well as anastomosis between the B6 bile duct of the graft and the CyD of the recipient, with inserted external biliary stents. **(D)** At 6 months after LDLT, three-dimensional cholangiography by corn-beam CT revealed no complications at the anastomotic sites. AHD, anterior hepatic duct; CHD, common hepatic duct; CT, computed tomography; CyD, cystic duct; LDLT, living donor liver transplantation; LHD, left hepatic duct.

CyD group was found in the same patients who exhibited postoperative biliary stricture. No patients in either group exhibited biliary leakage. Thus, the occurrence of biliary complications did not significantly differ between the 2 groups. Recipient 3 in the D-CyD group postoperatively developed acute cellular rejection, which was successfully treated with steroid pulse therapy.

DISCUSSION

In this present study, we assessed the potential of D-CyD as a rescue option to D-HD by investigating the long-term postoperative outcome of biliary reconstruction with D-CyD anastomosis together with D-HD anastomosis for cases of LDLT with a right-lobe graft having multiple separated bile ducts. All 4 of our recipients who had undergone D-CyD anastomosis survived for over 5 years. Furthermore, a checking of the characters of the D-CyD and D-HD groups revealed that the surgical outcome in the D-CyD group was similar to that in the D-HD group. These findings support that the D-CyD anastomosis could be an acceptable life-saving option for biliary reconstruction in LDLT when the standard D-HD anastomosis is because of the anatomic distance separating multiple bile ducts in the graft. This is the first study to demonstrate the long-term postoperative outcome of biliary reconstruction using D-CyD anastomosis together with D-HD anastomosis for LDLT with a right-lobe graft having multiple separated bile ducts.

Several prior reports have described cases of LDLT with a right-lobe graft, in which D-CyD anastomosis was included in the biliary reconstruction. To our knowledge, 9 such cases have been reported [2−4] (Table 3). Among these cases, the longest postoperative follow-up period is 28 months, and 2 of the 9 cases (22.2%) exhibited postoperative biliary obstruction. Moreover, based on the limited previous reports, it remains unclear how the postoperative outcome of D-CyD anastomosis together with D-HD anastomosis compares to that following standard D-HD anastomosis alone, which prompted us to perform the present study to investigate the long-term postoperative outcome.

Carmody et al described biliary reconstruction using the CyD instead of the HD of the recipient in deceased donor liver transplantation [10]. However, it does not mention the purpose of using the CyD, such that it appears that the CyD was simply a substitute for the HD. It does not provide information relevant to outcomes of D-CyD anastomosis for biliary reconstruction in LDLT.

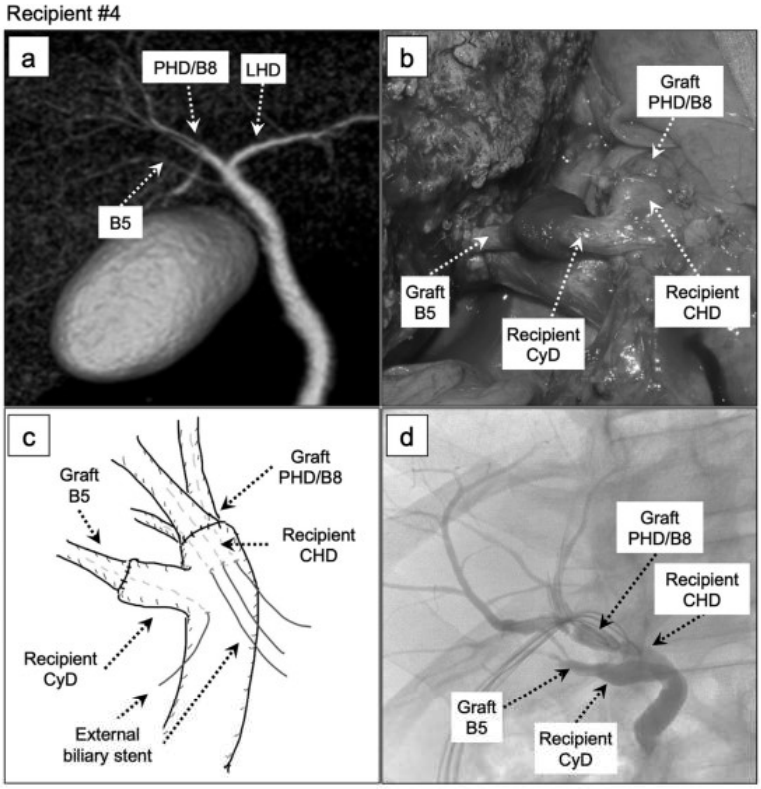

Fig 2. Perioperative imaging of the bile duct in recipient 4. **(A)** Preoperative DIC-CT for the donor indicated that the B5 bile duct was confluent separately from the LHD, PHD, and B8 bile duct. **(B)** Intraoperative photograph **(C)** and schema of the biliary reconstruction, showing anastomosis between the PHD/B8 bile duct of the graft and the CHD of the recipient, as well as anastomosis between the B5 bile duct of the graft and the CyD of the recipient, with inserted external biliary stents. **(D)** At 2 months after LDLT, cholangiography confirmed no complications at the anastomotic sites. CHD, common hepatic duct; CyD, cystic duct; DIC-CT, drip-infusion cholangiography computed tomography; LDLT, living donor liver transplantation; LHD, left hepatic duct; PHD, posterior hepatic duct.

Table 2. Perioperative Features of Recipients With Biliary Reconstruction by D-HD vs D-CyD Anastomosis

Factors		D-HD Anastomosis (n = 45)	D-CyD Anastomosis (n = 4)
Intraoperative blood loss, mL		11,190 ± 9447	17,317 ± 27,881
Total operation time, min		1349 ± 248	1249 ± 179
Biliary reconstruction time, min		57 ± 3	116 ± 13*
Intraoperative biliary duct diameter, mm		4.0 ± 1.7	2.5 ± 1.5*
Postoperative complication			
Biliary complication	Total	6 (13.3%)	1 (25.0%)
	Biliary leakage		0 (0.0%)
	Biliary stricture	6 (13.3%)	1 (25.0%)
	Biliary stones	1 (2.2%)	1 (25.0%)
ACR		10 (22.2%)	1 (25.0%)

Data are presented as the number of patients and percentage, or mean ± standard deviation.
ACR, acute cellular rejection; D-CyD, duct-to-cystic duct; D-HD, duct-to-hepatic duct.
* The data are the average of 3 recipients who received D-CyD anastomosis during liver transplantation.

In our present study, we investigated the detailed clinical course of the 4 cases in which D-CyD anastomosis was performed together with D-HD anastomosis, and we compared these surgical results with those following standard D-HD anastomosis. Among the D-HD group, the incidence of biliary complications was 12.2%. In a systematic review, Akamatsu et al reported that after D-D in LDLT, the incidence rates of biliary stricture and biliary leakage were 19% and 9.5%, respectively [1]. Mizuno et al also reported that among 108 recipients with D-D in LDLT, postoperative biliary stricture and leakage occurred in 13.9% and 5.6%, respectively [11]. Based on these previously reported incidence rates, our D-HD group was

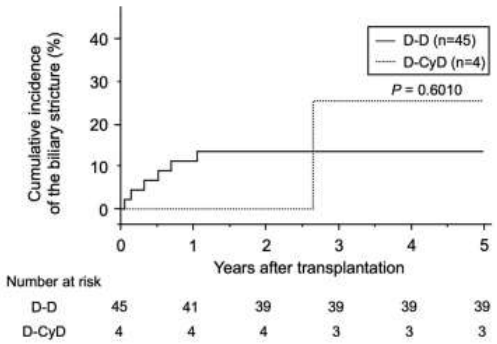

Fig 3. Cumulative incidence of the postoperative biliary stricture after liver transplantation. The incidence rates of stricture in the D-CyD and D-HD groups were assessed using the Kaplan-Meier method. D-CyD, duct-to-cystic duct; D-HD, duct-to-hepatic duct.

judged to be appropriate as a control group for comparison to the D-CyD group. Our present study described 2 novel findings in LDLT with right-lobe graft. First, we present the first observation of a long-term favorable outcome after D-CyD anastomosis. Second, our comparative analysis revealed that biliary reconstruction using D-CyD anastomosis did not negatively affect the surgical outcome compared with the cases with the standard D-HD anastomosis.

While our results suggest a good long-term postoperative outcome of D-CyD anastomosis, several points should be mentioned in relation to performing the D-CyD anastomosis. First, it is important to focus on maintaining the blood flow of the CyD stump of the recipient. It has been reported that preserving blood flow to the bile duct is essential for avoiding postoperative biliary complications in LT [12,13]. Although this concept was originally applied to the bile duct itself, it would also be applicable to the CyD because of their anatomic similarity. For this purpose, in cases where the CyD of the recipient could potentially be used for biliary reconstruction, we were careful to preserve the CyD and its surrounding tissues as much as possible to maintain the blood flow of the CyD. The blood flow at the CyD stump may be checked by cutting the wall of the CyD stump.

The second point is the insertion of the external biliary stent. The necessity of placing a stent inside the lumen of the anastomotic site in LT has been discussed and remains inconclusive [13−15]. Notably, it has been reported that the stent insertion itself is related to postoperative biliary complications [16]. Theoretical advantages of stent insertion include the ability to check bile production, potentially preventing an increase of the inner pressure at the anastomotic site and potentially maintaining the lumen of the anastomotic site via the inserted tube. However, in our opinion, this inconclusiveness is applicable only to the bile duct, not the CyD. Considering that the inside lumen of the CyD is frequently anatomically a spiral due to the valve of Heister [17], tube insertion into the CyD would be reasonable, especially for maintenance of the lumen of the anastomotic site.

Our present study has several limitations. The small number of cases that received the D-CyD anastomosis could have limited the statistical power of between-group comparisons. However, no previous studies have compared the surgical outcomes of D-HD and D-CyD groups after LDLT. Another limitation was the retrospective and single-institution study design. Data collection was based on the medical records available from a single institution, which could have introduced a bias in patient selection. Therefore, when interpreting the present results, one should consider the possible influence of selection bias. However, as mentioned above, the indication for the D-CyD anastomosis was considerably limited. Additionally, the final decision to perform D-CyD anastomosis was based on intraoperative findings. Therefore, it would be impossible to perform a prospective study with a large number of patients.

In conclusion, here we described the long-term outcome of cases in which D-CyD anastomosis was used for biliary reconstruction in LDLT with a right-lobe liver graft containing multiple separated bile ducts. Furthermore, our analysis showed that the surgical outcome of D-CyD anastomosis was not inferior to

Table 3. Reported Cases With D-CyD Anastomosis Including the Present Cases

Published Year	No.	Age in Years /Sex	Diagnosis	Biliary Reconstruction	Postoperative Biliary Complication	Follow-up Period (mo)	Prognosis
2004 (2)	1	50/Male	HBV (HCC)	AHD-RHD, PHD-CyD	None	6	Alive
	2	41/Male	HBV (HCC)	AHD-RHD, PHD-CyD	None	11	Alive
	3	41/Male	HBV	RHD-CyD	None	4	Alive
2004 (3)	4	64/Male	HCV (HCC)	AHD-CyD, PHD-CHD	Obstruction	1	Alive
2005 (4)	5	39/Male	HBV	AHD-CyD, PHD-RHD	None	13	Died
	6	53/Male	HCV (HCC)	AHD-RHD, PHD-CyD	None	28	Alive
	7	58/Male	HCV (HCC)	AHD-CyD, PHD-RHD	None	14	Alive
	8	18/Male	Caroli disease	AHD-RHD, PHD-CyD	None	13	Alive
	9	44/Male	FHF	AHD-CyD, PHD-RHD	None	10	Alive
Current cases	10	53/Male	HBV	AHD/B7-CHD, B6-CyD	Stricture, stone	171	Alive
	11	64/Male	FHF	AHD/B7-CHD, B6-CyD	None	69	Alive
	12	49/Female	FHF	AHD-CHD, PHD-CyD	None	99	Alive
	13	46/Male	HBV	PHD/B8-CHD, B5-CyD	None	68	Alive

AHD, anterior hepatic duct; CyD, cystic duct; CHD, common hepatic duct; D-CyD, duct-to-cystic duct; FHF, fulminant hepatic failure; HBV, hepatitis B virus; HCC, hepatocellular carcinoma; HCV, hepatitis C virus; PHD, posterior hepatic duct; RHD, right hepatic duct.

that of D-HD anastomosis. These results suggest that D-CyD anastomosis is one of the acceptable life-saving options to standard D-HD anastomosis when D-HD anastomosis is complicated by the anatomic distance between multiple bile ducts in a right-lobe graft.

DATA AVAILABILITY

The data that has been used is confidential.

DECLARATION OF COMPETING INTEREST

The authors declare that they have no conflict of interest.

ACKNOWLEDGMENTS

The authors would like to thank San Francisco Edit (https://www.sfedit.net/) for the English language review.

REFERENCES

[1] Akamatsu N, Sugawara Y, Hashimoto D. Biliary reconstruction, its complications and management of biliary complications after adult liver transplantation: a systematic review of the incidence, risk factors and outcome. Transpl Int 2011;24:379–92.

[2] Suh KS, Choi SH, Yi NJ, Kwon CH, Lee KU. Biliary reconstruction using the cystic duct in right lobe living donor liver transplantation. J Am Coll Surg 2004;199:661–4.

[3] Kadry Z, Cintorino D, Foglieni CS, Fung J. The pitfall of the cystic duct biliary anastomosis in right lobe living donor liver transplantation. Liver Transpl 2004;10:1549–50.

[4] Asonuma K, Okajima H, Ueno M, Takeichi T, Zeledon Ramirez ME, Inomata Y. Feasibility of using the cystic duct for biliary reconstruction in right-lobe living donor liver transplantation. Liver Transpl 2005;11:1431–4.

[5] Marubashi S, Nagano H, Yamanouchi E, Kobayashi S, Eguchi H, Takeda Y, et al. Salvage cystic duct anastomosis using a magnetic compression technique for incomplete bile duct reconstruction in living donor liver transplantation. Liver Transpl 2010;16:33–7.

[6] Marubashi S, Kobayashi S, Wada H, Kawamoto K, Eguchi H, Doki Y, et al. Hepatic artery reconstruction in living donor liver transplantation: risk factor analysis of complication and a role of MDCT scan for detecting anastomotic stricture. World J Surg 2013;37:2671–7.

[7] Marubashi S, Nagano H, Eguchi H, Wada H, Asaoka T, Tomimaru Y, et al. Minimum graft size calculated from preoperative recipient status in living donor liver transplantation. Liver Transpl 2016;22:599–606.

[8] Marubashi S, Dono K, Nagano H, Kobayashi S, Takeda Y, Umeshita K, et al. Biliary reconstruction in living donor liver transplantation: technical invention and risk factor analysis for anastomotic stricture. Transplantation 2009;88:1123–30.

[9] Hosoda Y, Tomimaru Y, Marubashi S, Wada H, Eguchi H, Asaoka T, et al. A case of living-donor liver transplantation using the cystic duct for biliary tract reconstruction. Japanese Journal of Transplantation 2015;50:229–33.

[10] Carmody IC, Romano J, Bohorquez H, Bugeaud E, Bruce DS, Cohen AJ, et al. Novel biliary reconstruction techniques during liver transplantation. Ochsner J 2017;17:42–5.

[11] Mizuno S, Inoue H, Tanemura A, Murata Y, Kuriyama N, Azumi Y, et al. Biliary complications in 108 consecutive recipients with duct-to-duct biliary reconstruction in living-donor liver transplantation. Transplant Proc 2014;46:850–5.

[12] Soejima Y, Fukuhara T, Morita K, Yoshizumi T, Ikegami T, Yamashita Y, et al. A simple hilar dissection technique preserving maximum blood supply to the bile duct in living donor liver transplantation. Transplantation 2008;86:1468–9.

[13] Jung DH, Ikegami T, Balci D, Bhangui P. Biliary reconstruction and complications in living donor liver transplantation. Int J Surg 2020;82S:138–44.

[14] Lee SG. A complete treatment of adult living donor liver transplantation: a review of surgical technique and current challenges to expand indication of patients. Am J Transplant 2015;15:17–38.

[15] Ikegami T, Yoshizumi T, Soejima Y, Ohira M, Maehara Y. Appropriate use of stents to prevent biliary complications after living donor liver transplantation. J Am Coll Surg 2018;226:201.

[16] Santosh Kumar KY, Mathew JS, Balakrishnan D, Bharathan VK, Thankamony Amma BSP, Gopalakrishnan U, et al. Intraductal transanastomotic stenting in duct-to-duct biliary reconstruction after living-donor liver transplantation: a randomized trial. J Am Coll Surg 2017;225:747–54.

[17] Pina LN, Samoilovich F, Urrutia S, Rodriguez A, Alle L, Ferreres AR. Surgical considerations of the cystic duct and heister valves. Surg J (N Y) 2015;1:e23–7.

ELSEVIER

Pure Laparoscopic Donor Left Hepatectomy Reduces Postoperative Analgesic Use and Pain Scale

Hiromichi Sato, Kazuki Sasaki, Shogo Kobayashi*, Yoshifumi Iwagami, Daisaku Yamada, Yoshito Tomimaru, Takehiro Noda, Hidenori Takahashi, Yuichiro Doki, and Hidetoshi Eguchi

Department of Gastroenterological Surgery, Graduate School of Medicine, Osaka University, Osaka, Japan

ABSTRACT

Background. Many recent reports have described the efficacy and safety of pure laparoscopic donor hepatectomy (PLDH). Here we investigated the extent to which this technique could reduce patients' experienced pain.

Methods. Among donor left hepatectomy procedures performed between July 2011 and November 2022, we retrospectively analyzed 20 open donor hepatectomy (ODH), 20 laparoscopy-assisted donor hepatectomy (LADH), and 5 PLDH cases. We compared these 3 procedures regarding the total amount of postoperative analgesic use (narcotics and non-narcotics) and the first date when the donor was completely pain-free, as evaluated by the patients using a pain scale.

Results. Total postoperative fentanyl use did not significantly differ among the 3 procedures: median (range), ODH, 0.5 mg (0-2 mg); LADH 1.2 mg (0-7 mg); PLDH, 0.5 mg (0-3.5; $P = .172$). The percentage of patients who completely discontinued analgesics on postoperative day (POD) 5 was significantly higher for PLDH (80%) than for ODH (35%) or LADH (20%) ($P = .041$). The day when 50% of donors were completely pain-free on a pain scale was POD9 for ODH, POD11 for LADH, and POD5 for PLDH, significantly shorter in the PLDH group ($P = .004$).

Conclusion. At our institution, we found that PLDH was a useful technique for postoperative pain management compared with PDH and LADH. Our results suggest that PLDH effectively reduces the duration of postoperative analgesia use. Further studies are warranted as the number of PLDH cases gradually increases.

OPTIONS for liver resection now include laparoscopic surgery and robot-assisted surgery, and although the first priority is to ensure safety and effectiveness, "patient-friendly" surgery has become increasingly desired [1−6]. Many recent studies described the efficacy and safety of pure laparoscopic donor hepatectomy (PLDH) in liver donor surgery [7,8]. Minimally invasive techniques, including laparoscopy-assisted donor hepatectomy (LADH), have been reported to reduce postoperative complications in liver donor surgery, decrease postoperative hospital stay, and decrease postoperative analgesic use [9].

Although PLDH has been the focus of attention in recent years, most statistics regarding postoperative pain are based on a combined analysis of PLDH and LADH, and there is no clear determination of whether PLDH truly has a positive impact on patients' pain. Several reports discuss the differences in pain between open donor hepatectomy (ODH) and PLDH [10−13] (Table 1). It is important to investigate this subject further because PLDH is a recently introduced procedure and only limited data regarding pain is available. Furthermore, the conclusions in the literature are mixed; all published comparisons are based on pain scales, with no discussion about the actual

*Address correspondence to Shogo Kobayashi, MD, PhD, Department of Gastroenterological Surgery, Graduate School of Medicine, Osaka University, 2-2-E2, Yamadaoka, Suita, Osaka 565-0871, Japan E-mail: skobayashi@gesurg.med.osaka-u.ac.jp

0041-1345/20
https://doi.org/10.1016/j.transproceed.2023.03.019

Table 1. Previous Reports on the Relationship Between PLDH and Pain.

Authors	Subject of Comparison	Surgical Procedures	Conclusions
Broering et al [10]	ODH vs PLDH	Left lateral sectionectomy	Pain scores were significantly lower in the PLDH group
Park et al [11,12]	ODH vs PLDH	Right hepatectomy	Reduced use of patient-controlled analgesia in PLDH
Jeong et al [13]	ODH vs PLDH	Right hepatectomy	The numerical pain rating scale did not significantly differ between the 2 groups

ODH, open donor hepatectomy; PLDH, pure laparoscopic donor hepatectomy.

amount and frequency of analgesic use, and there are no comparisons between PLDH and LADH.

In the present study, we investigated the extent to which PLDH could reduce patients' experienced pain.

PATIENTS AND METHODS

Patient Eligibility

Among the donor left hepatectomy procedures performed between July 2011 and November 2022, we retrospectively analyzed 20 ODH, 20 LADH, and 5 PLDH cases. We compared these 3 procedures regarding the total amount of postoperative analgesic use (narcotics and non-narcotics) and the first date on which the donor was completely pain-free, as evaluated by the patients using a pain scale.

At our institution, the indication for PLDH is limited to only left lobe hepatectomy (including lateral segmentectomy). Therefore, we also selected ODH and LADH cases performed for only left lobe hepatectomy. After surgery, patients were taken directly to the general ward unless there were intraoperative problems. Fluid intake was started on the first postoperative day, and food intake was started around the third postoperative day, with consideration of the patient's medical condition. Intravenous fentanyl was administered immediately after surgery, and its use was extended depending on the patient's pain level. Postoperative analgesics are not routinely administered as a protocol but are prescribed as needed at the discretion of the physician in charge. The patients themselves rated their experienced pain as +, ±, or −, and the nurse in charge for the day would record this rating in the patient's chart daily. The first day a

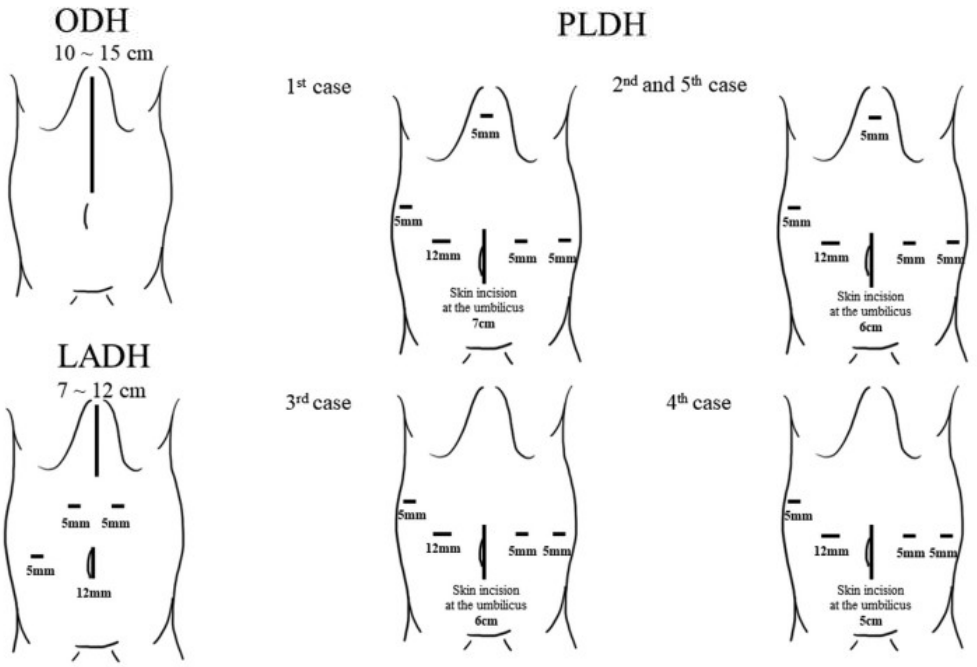

Fig 1. Port placements for open donor hepatectomy, laparoscopy-assisted donor hepatectomy, and 4 pure laparoscopic donor hepatectomy cases. LADH, laparoscopy-assisted donor hepatectomy; ODH, open donor hepatectomy; PLDH, pure laparoscopic donor hepatectomy.

Table 2. Baseline Patient Characteristics and Postoperative Results.

	ODH (n = 20)	LADH (n = 20)	PLDH (n = 5)	P Value
Age, y	35 (24-62)	39.5 (20-54)	30 (26-35)	.129
Female:male (% female)	9: 11 (45%)	10: 10 (50%)	3: 2 (60%)	.831
Procedure classification, lateral segmentectomy: left lobectomy (% lateral segmentectomy)	11: 9 (55%)	14: 6 (70%)	5: 0 (100%)	.154
Blood loss, mL	250 (30-2930)	200 (20-1168)	20 (0-130)	.010*
Operation time, min	405 (319-483)	422 (326-671)	345 (333-411)	.061
Postoperative day of oral food intake	3 (3-5)	3 (2-3)	3 (2-3)	.084
Time to first flatus, d	3 (1-4)	2.5 (1-4)	3 (2-3)	.905
Time to first stool, d	4.5 (2-6)	4.5 (2-7)	5 (4-6)	.203
Clavien-Dindo grade II or higher	0 (0%)	0 (0%)	0 (0%)	1.000

Values are expressed as median (range) or n (%).
LADH, laparoscopy-assisted donor hepatectomy; ODH, open donor hepatectomy; PLDH, pure laparoscopic donor hepatectomy.
* $P < .05$ by Kruskal-Wallis test.

patient rated their pain as − was defined as the day when the pain completely disappeared.

The primary endpoint was the date patients rated their pain as completely gone. The secondary endpoints were the amount of analgesics used (narcotics and non-narcotics), the number of times non-narcotic analgesics were used as needed on the fifth postoperative day or later, and the percentage of patients completely off analgesics on the fifth postoperative day.

Port Placements for 4 PLDH Cases

Figure 1 shows the port arrangements for ODH and LADH and in 4 cases of PLDH. In general, the PLDH cases required a reduced number of ports and a shorter length of the incision.

Statistical Analysis

Data are presented as mean and standard deviation or median and range. The Kruskal-Wallis and log-rank tests were used to investigate the relationship among ODH, LADH, and PLDH. A 2-tailed value of $P < .05$ was considered statistically significant. Statistical analyses were conducted using Statcel, version 4 (OMS; Higashikurume, Tokyo, Japan).

RESULTS

Patient Characteristics and Postoperative Results

Table 2 shows the patients' background information. The 3 groups did not significantly differ with respect to age (P = .129), sex (P = .831), or proportion of procedures that were lateral segmentectomy (P = .154).

With regard to postoperative outcomes, blood loss was significantly lower in the PLDH group: median (range), ODH, 250 mL (30-2930 mL); LADH, 200 mL (20-1168 mL); PLDH, 20 mL (0-130 mL) (P = .010). Operative time did not significantly differ among the 3 groups (P = .061). The 3 groups also did not significantly differ in the number of days of postoperative oral food intake (P = .084), days to first flatus (P = .905), or days to first stool (P = .203). Complications of Clavien-Dindo grade 2 or higher did not occur in any of the 3 groups.

Postoperative Analgesic Use (if Any) and Total Amount Used (Narcotic and Non-Narcotic)

Table 3 shows the use of analgesics, their dosage, and when analgesic use stopped. The 3 groups did not significantly differ in the total postoperative fentanyl dose (P = .172), anti-inflammatory drug dose (P = .971), or the number of uses of non-narcotic analgesics as needed after postoperative day (POD) 5 (P = .205). Notably, total postoperative acetaminophen use was significantly higher in the ODH group: median (range), ODH, 1500 mg (0-9000 mg); LADH, 0 mg (0-14,500 mg); PLDH, 0 mg (0-2000 mg) (P = .005). Additionally, the percentage of patients who completely discontinued analgesic use at POD5 was significantly higher in the PLDH group (80%) than in the ODH group (20%) and LADH group (35%) (P = .041).

Table 3. Relationship Between Histologic Therapeutic Effect and Tumor Reduction Rate

	ODH (n = 20)	LADH (n = 20)	PLDH (n = 5)	P Value
Total postoperative fentanyl use, mg	0.5 (0-2)	1.2 (0-7)	0.5 (0-3.5)	.172
Total postoperative nonsteroidal anti-inflammatory drugs use, mg	600 (0-2500)	600 (100-2530)	500 (300-1080)	.971
Total postoperative acetaminophen use, mg	1500 (0-9000)	0 (0-14,500)	0 (0-2000)	.005*
Times non-narcotic analgesics were used as needed after POD 5	3.5 (0-33)	5.5 (0-33)	0 (0-9)	.205
Percentage of patients completely off analgesics on POD5	7 (35%)	4 (20%)	4 (80%)	.041*

Values are expressed as the median (range) or n (%).
LADH, laparoscopy-assisted donor hepatectomy; ODH, open donor hepatectomy; PLDH, pure laparoscopic donor hepatectomy; POD, postoperative day.
* $P < .05$ by Kruskal-Wallis test.

Days Until 50% of Donors Were Completely Pain-Free on a Pain Scale

The POD when 50% of donors were completely pain-free, as self-reported using a pain scale, was POD9 in the ODH group, POD11 in the LADH group, and POD5 in the PLDH group. This happened significantly faster in the laparoscopic group (Fig 2; $P = .004$).

DISCUSSION

The results of the present study demonstrated that, at our institution, PLDH was a useful technique for postoperative pain management while maintaining safety compared with ODH and LADH. This reduction of pain may facilitate postoperative weaning and prevent delirium.

Previous reports have shown that LADH [14−17] and PLDH [7,10−13] were associated with reduced pain compared with ODH. In addition to liver resection, laparoscopic techniques are reportedly useful for pain reduction in appendectomy [18], gastrectomy [19], and nephrectomy [20]. Robotic liver donor surgeries have been widely performed recently, with demonstrated usefulness and safety [21,22].

At our institution, we found that LADH was less useful than ODH in pain, as it required more analgesics, and patients tended to feel pain long after the operation. Patient ratings using the postoperative pain scale were poorer after LADH than ODH, possibly because the postoperative acetaminophen use was higher after ODH (Table 3). The open wound in LADH is larger than in ODH, and inserting a port site makes patients more sensitive to pain (Fig 1). Reports from other centers vary, with some reporting that LADH and ODH did not differ in the amount, duration, or frequency of analgesic use [23] and others reporting that LADH is associated with better pain scales [14−16], number of analgesic uses [15], and duration of analgesic use [17]. Jeong et al [13] even found that PLDH and ODH did not significantly differ in the numeric pain rating scale (Table 1). These variations in results may be because of the combined effects of differences between institutions regarding intraoperative anesthesia management, wound length, and the number of port holes, which may prevent us from reaching the same conclusions.

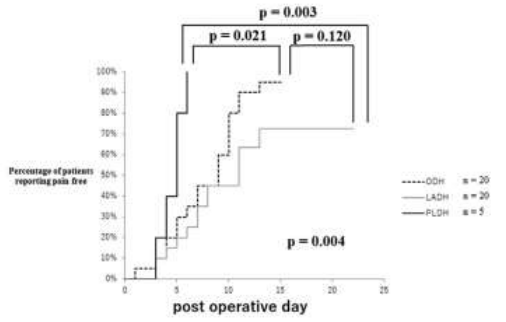

Fig 2. Percentage of patients reporting that they are pain free. *P* values were determined by the log-rank test for comparison among 3 groups. LADH, laparoscopy-assisted donor hepatectomy; ODH, open donor hepatectomy; PLDH, pure laparoscopic donor hepatectomy.

Although we found that PLDH is useful for reduced analgesia use, unlike ODH/LADH, the indication for PLDH is limited to only left hepatectomy at our institution. Other institutions have reported using PLDH for right hepatectomy [11−13,24], and the indication for PLDH should be carefully expanded with increasing experience.

Limitations of the present study include that it was a single-center retrospective study and included only a small number of PLDH cases.

CONCLUSIONS

In conclusion, although PLDH is still in its infancy and requires further study, the present results suggest that it effectively reduces postoperative analgesia use. Notably, the number of analyzed PLDH cases was small, and the subject should be re-examined as the number of cases gradually increases.

DISCLOSURES

The authors declare that they have no known competing financial interests or personal relationships that could have appeared to influence the work reported in this paper.

REFERENCES

[1] Cai JP, Chen W, Chen LH, Wan XY, Lai JM, Yin XY. Comparison between robotic-assisted and laparoscopic left hemi-hepatectomy. Asian J Surg 2022;45:265–8.

[2] Chong CC, Fuks D, Lee KF, Zhao JJ, Choi GH, Sucandy I, et al. Propensity score-matched analysis comparing robotic and laparoscopic right and extended right hepatectomy. JAMA Surg 2022; 157:436–44.

[3] Kamel MK, Tuma F, Keane CA, Blebea J. National trends and perioperative outcomes of robotic-assisted hepatectomy in the USA: a propensity-score matched analysis from the National Cancer Database. World J Surg 2022;46:189–96.

[4] Labadie KP, Droullard DJ, Lois AW, Daniel SK, McNevin KE, Gonzalez JV, et al. IWATE criteria are associated with perioperative outcomes in robotic hepatectomy: a retrospective review of 225 resections. Surg Endosc 2022;36:889–95.

[5] Sucandy I, Shapera E, Syblis CC, Crespo K, Przetocki VA, Ross SB, et al. Propensity score matched comparison of robotic and open major hepatectomy for malignant liver tumors. Surg Endosc 2022;36:6724–32.

[6] Zwart MJW, Gorgec B, Arabiyat A, Nota CLM, van der Poel MJ, Fichtinger RS, et al. Pan-European survey on the implementation of robotic and laparoscopic minimally invasive liver surgery. HPB (Oxford) 2022;24:322–31.

[7] Bekheit M, Khafagy PA, Bucur P, Katri K, Elgendi A, Abdel-Salam WN, et al. Donor safety in live donor laparoscopic liver procurement: systematic review and meta-analysis. Surg Endosc 2015;29:3047–64.

[8] Marubashi S, Nagano H. Laparoscopic living-donor hepatectomy: review of its current status. Ann Gastroenterol Surg 2021;5:484–93.

[9] Li H, Zhang JB, Chen XL, Fan L, Wang L, Li SH, et al. Different techniques for harvesting grafts for living donor liver

transplantation: a systematic review and meta-analysis. World J Gastroenterol 2017;23:3730–43.

[10] Broering DC, Elsheikh Y, Shagrani M, Abaalkhail F, Troisi RI. Pure laparoscopic living donor left lateral sectionectomy in pediatric transplantation: a propensity score analysis on 220 consecutive patients. Liver Transpl 2018;24:1019–30.

[11] Park J, Kwon CHD, Choi GS, Lee SK, Kim JM, Oh J, et al. One-year recipient morbidity of liver transplantation using pure laparoscopic versus open living donor right hepatectomy: propensity score analysis. Liver Transpl 2019;25:1642–50.

[12] Park J, Kwon DCH, Choi GS, Kim SJ, Lee SK, Kim JM, et al. Safety and risk factors of pure laparoscopic living donor right hepatectomy: comparison to open technique in propensity score-matched analysis. Transplantation 2019;103:e308–16.

[13] Jeong JS, Wi W, Chung YJ, Kim JM, Choi GS, Kwon CHD, et al. Comparison of perioperative outcomes between pure laparoscopic surgery and open right hepatectomy in living donor hepatectomy: propensity score matching analysis. Sci Rep 2020;10:5314.

[14] Choi HJ, You YK, Na GH, Hong TH, Shetty GS, Kim DG. Single-port laparoscopy-assisted donor right hepatectomy in living donor liver transplantation: sensible approach or unnecessary hindrance? Transplant Proc 2012;44:347–52.

[15] Marubashi S, Wada H, Kawamoto K, Kobayashi S, Eguchi H, Doki Y, et al. Laparoscopy-assisted hybrid left-side donor hepatectomy. World J Surg 2013;37:2202–10.

[16] Makki K, Chorasiya VK, Sood G, Srivastava PK, Dargan P, Vij V. Laparoscopy-assisted hepatectomy versus conventional (open) hepatectomy for living donors: when you know better, you do better. Liver Transpl 2014;20:1229–36.

[17] Zhang X, Yang J, Yan L, Li B, Wen T, Xu M, et al. Comparison of laparoscopy-assisted and open donor right hepatectomy: a prospective case-matched study from China. J Gastrointest Surg 2014;18:744–50.

[18] Rao AD, Tan CBD, Singaporewalla Md RM. Laparoscopic appendectomy translates into less analgesics and faster return to work in Asia. JSLS 2022;26 e2022.00006.

[19] Garbarino GM, Laracca GG, Lucarini A, Piccolino G, Mercantini P, Costa A, et al. Laparoscopic versus open surgery for gastric cancer in western countries: a systematic review and meta-analysis of short- and long-term outcomes. J Clin Med 2022;11:3590.

[20] Nazemi T, Galich A, Sterrett S, Klingler D, Smith L, Balaji KC. Radical nephrectomy performed by open, laparoscopy with or without hand-assistance or robotic methods by the same surgeon produces comparable perioperative results. Int Braz J Urol 2006;32:15–22.

[21] Broering DC, Elsheikh Y, Alnemary Y, Zidan A, Elsarawy A, Saleh Y, et al. Robotic versus open right lobe donor hepatectomy for adult living donor liver transplantation: a propensity score-matched analysis. Liver Transpl 2020;26:1455–64.

[22] Troisi RI, Elsheikh Y, Alnemary Y, Zidan A, Sturdevant M, Alabbad S, et al. Safety and feasibility report of robotic-assisted left lateral sectionectomy for pediatric living donor liver transplantation: a comparative analysis of learning curves and mastery achieved with the laparoscopic approach. Transplantation 2021;105:1044–51.

[23] Kitajima T, Kaido T, Iida T, Seo S, Taura K, Fujimoto Y, et al. Short-term outcomes of laparoscopy-assisted hybrid living donor hepatectomy: a comparison with the conventional open procedure. Surg Endosc 2017;31:5101–10.

[24] Gamez B, Benitez J, Puelma F, Jarufe N. Pure laparoscopic living donor right hepatectomy (with video). J Surg Case Rep 2021;2021:rjab394.

Clinical Journal of Gastroenterology (2023) 16:709–714
https://doi.org/10.1007/s12328-023-01827-5

CASE REPORT

Rituximab administration one week before ABO-incompatible liver transplantation due to drug-induced acute liver failure with hepatic coma: a case report

Kazuki Sasaki[1] · Shogo Kobayashi[1] · Yoshifumi Iwagami[1] · Daisaku Yamada[1] · Yoshito Tomimaru[1] · Takehiro Noda[1] · Hidenori Takahashi[1] · Yuichiro Doki[1] · Hidetoshi Eguchi[1]

Received: 20 April 2023 / Accepted: 26 June 2023 / Published online: 20 July 2023

Abstract
In cases of acute liver failure (ALF) with hepatic coma, early liver transplantation, including ABO-incompatible (ABOi) living donor liver transplantation (LDLT), should be considered. The ABO antibody barrier can be reduced using plasma exchange (PE) and the anti-CD20 antibody rituximab. Plasma exchange is also performed for drug-induced ALF and is effective for desensitization. Rituximab treatment usually requires 14 days. There is presently no established desensitization protocol for ABOi-LDLT for ALF. Here, we report a case of drug-induced ALF with hepatic coma, which was treated with ABOi-LDLT using PE and rituximab 8 days prior to surgery. A 33-year-old female, with a history of headaches for which she was taking analgesics daily, developed drug-induced ALF with hepatic coma. Her ABOi sister desired to become a liver donor. We initiated desensitization using rituximab (500 mg) and mycophenolate mofetil (MMF, 2000 mg/day), followed by five sessions of PE. Eight days after rituximab administration, ABOi-LDLT with splenectomy was performed. Postoperatively, the patient received local infusion via portal vein for 14 days and immunosuppression with tacrolimus, methylprednisolone, and MMF. No episode of cellular or antibody-mediated rejection (AMR) was observed. The patient was discharged uneventfully 56 days after ABOi-LDLT with no problems up to 15 months after the transplant.

Keywords ABO-incompatible living donor liver transplantation · Rituximab · Antibody-mediated rejection · Plasma exchange

Abbreviations

ALF	Acute liver failure
ABOi	ABO-incompatible
LDLT	Living donor liver transplantation
APAP	Acetaminophen
MMF	Mycophenolate mofetil
AMR	Antibody-mediated rejection
DBD	Donor after brain death
PE	Plasma exchange
CHDF	Continuous hemodiafiltration

✉ Shogo Kobayashi
skobayashi@gesurg.med.osaka-u.ac.jp

Kazuki Sasaki
ksasaki@gesurg.med.osaka-u.ac.jp

Yoshifumi Iwagami
yiwagami@gesurg.med.osaka-u.ac.jp

Daisaku Yamada
dyamada@gesurg.med.osaka-u.ac.jp

Yoshito Tomimaru
ytomimaru@gesurg.med.osaka-u.ac.jp

Takehiro Noda
tnoda@gesurg.med.osaka-u.ac.jp

Hidenori Takahashi
htakahashi8@gesurg.med.osaka-u.ac.jp

Yuichiro Doki
ydoki@gesurg.med.osaka-u.ac.jp

Hidetoshi Eguchi
heguchi@gesurg.med.osaka-u.ac.jp

[1] Department of Gastroenterological Surgery, Graduate School of Medicine, Osaka University, 2-2-E2, Yamadaoka, Suita, Osaka 565-0871, Japan

CMV Cytomegalovirus
POD Postoperative day
IVIG Intravenous immunoglobulin

Introduction

Acute liver failure (ALF) with hepatic coma requires urgent multidisciplinary treatment, including liver transplantation. In Europe and the US, ALF is most often caused by acetaminophen (APAP) intoxication, but in Japan, APAP is rare and ALF is most commonly caused by viral diseases [1]. APAP is an antipyretic analgesic that can be easily obtained as an over-the-counter drug. According to the Japan Poison Information Center, the lethal dose of APAP is 13–25 g for adults [2]. The glutathione precursor *N*-acetylcysteine is a specific agent for treating APAP intoxication [3]. However, if the timing is missed, APAP intoxication may progress to ALF and require liver transplantation. The prognosis is good when liver transplantation is performed for ALF, but Japan has an especially small number of brain-dead liver transplant donors. In 2022, the International Registry in Organ Donation and Transplantation (IRODat) ranked Japan as 52nd worldwide for deceased donor liver transplants, with 0.48 cases per million people [4]. Because of this, living donor liver transplantation (LDLT) is frequently considered [5] and, since an ABO-compatible living donor is not always available, ABO-incompatible (ABOi)-LDLT is often required.

ABOi-LDLT used to have a poor prognosis due to antibody-mediated rejection (AMR) [6]. However, the introduction of rituximab has eliminated the difference between ABOi and ABO-compatible transplants [7]. Notably, it is generally recommended to initiate desensitization with rituximab 2–3 weeks prior to transplantation [8], but the urgency of ALF may not allow for this timing. Over the last decade, limited reports have described successful desensitization protocols for ABOi-LDLT due to ALF [9–12], and no standardized protocol has yet been established. Another problem is that when considering LT for drug-induced ALF, it is sometimes difficult to obtain a medical history due to the patient's impaired consciousness. Moreover, there are no guidelines for determining the indication for LT in patients with undeniable suicide attempts, leaving the institution to make a difficult decision [13].

In the present report, we describe a case of drug-induced ALF. After careful discussion, the indication of LT was determined and the patient was rescued by ABOi-LDLT with desensitization, including PE and rituximab administration, 8 days prior to LT. We also performed a literature review of ABOi-LDLT for ALF.

Case report

A 33-year-old woman, with no medical issues other than a history of chronic headache for which she took analgesics daily, was discovered unconscious in her room. No suicide note was found. She was transported to the nearest emergency room. Drug intoxication was suspected. The patient was treated with gastric lavage, activated charcoal, and laxative administration, and was sedated and intubated with midazolam and fentanyl. The following day, the laboratory test results were as follows: AST 12,919 IU/L, ALT 9369 IU/L, T-Bil 2.97 mg/dL, D-Bil 1.65 mg/dL, D-/T-Bil ratio 0.55, and PT < 10%. The patient was later found to be negative for autoantibodies and viral infections. CT scanning revealed no infection, no liver atrophy or ascites, and no cerebral edema. Later that day, the patient's family brought an empty bag (equivalent to 13.2 g of APAP), indicating that the patient had developed ALF due to APAP overdose. However, since her blood APAP concentration was 8.7 μg/dL at 16 h after admission, no N-acetylcysteine was administered. Because the possibility of ALF caused by drug-induced liver injury (DILI) was considered at that time, hydrocortisone pulses and plasma exchange (PE) were performed to suppress hepatic inflammation after discussion with hepatology specialists. At the same time, the requirement for a liver transplant was discussed with our facility.

The predicted mortality rate was 30–50% according to the scoring system used to predict the mortality of patients with fulminant hepatitis and LOHF [14]. Therefore, a liver transplantation was considered necessary to save the patient's life. However, because she was unconscious, it was unclear whether the patient had taken drug for suicide or as an overdose for analgesia. In the discussion regarding transplantation indication, the opinion was stated that even if it was a suicide attempt, every effort should be made, including liver transplantation. On the other hand, due to the scarcity of donor after brain death (DBD) and its reliance on DBD goodwill, it was considered that it might be unethical to use a DBD for a patient who may attempt suicide. Notably, since the family is the surrogate decision-maker for a patient with impaired consciousness, if the family wishes to donate the liver, then the patient should be considered for transplantation. Our hospital's liver transplantation review committee approved LDLT but not brain-dead liver transplant, pending the patient's recovery from impaired consciousness and confirmation of their wish to be transplanted. At the local hospital, the patient received intensive treatment—including hydrocortisone pulses, plasma exchange (PE), and high-flow continuous hemodiafiltration (CHDF), as well as the administration of flumazenil and naloxone to antagonize sedatives. Finally, the patient regained

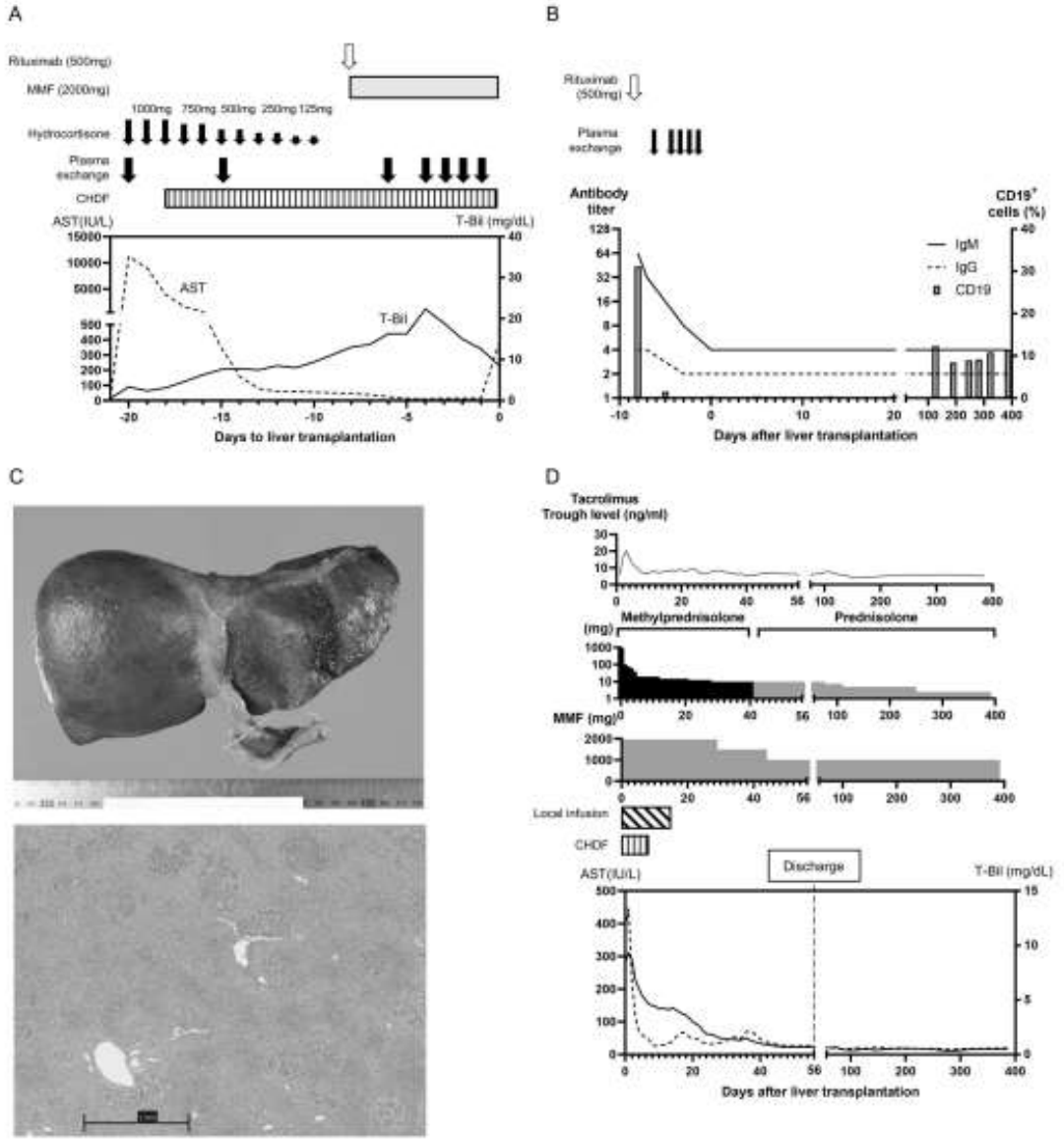

Fig. 1 **A** Preoperative courses of treatment before living donor liver transplantation. **B** Changes in anti-A antibody titers (IgM, IgG) and CD19$^+$ cells (%).**C** Gross and histological findings of resection specimens. **D** Postoperative courses of treatment after living donor liver transplantation

consciousness 10 days after losing consciousness. After the situation and the need for a liver transplant was explained, the patient expressed a desire for a liver transplant and was sent to our hospital.

The patient was blood type B, and the available donor was blood type A. Therefore, to prepare for ABOi-LDLT, desensitization was performed using 500 mg of rituximab and 2000 mg/day of mycophenolate mofetil (Fig. 1A). Tar stools and suspected gastrointestinal bleeding occurred on the day of rituximab administration. Upper gastrointestinal endoscopy revealed no bleeding source. Daily platelet transfusions controlled bleeding tendency. At 3 days after

rituximab treatment, $CD19^+$ cells (%) decreased from 31 to 0.3% (Fig. 1B). After an additional five performances of PE, the anti-A IgM titer decreased from 1:64 to 1:4. At 8 days after rituximab treatment, the patient received LDLT with a left lobe and caudal lobe, along with splenectomy. During operation, 1000 mg of methylprednisolone was administered intravenously. A catheter was placed in the portal vein for local infusion. The operation time was 700 min, blood loss was 1630 mL, graft volume/standard liver volume ratio was 39.7%, and graft-to-recipient weight ratio was 0.85. The resected liver weight was 580 g. The gross appearance of the liver showed marked atrophy (Fig. 1C). Histologically, the specimen showed extensive hemorrhagic necrosis of the parenchyma, inflammatory cell infiltration (mainly of lymphocytes and hemosiderin-phagocytic histiocytes), and residual hepatocyte masses in the form of islands. These findings were consistent with acute hepatitis.

The patient received triple immunosuppression (with tacrolimus, methyl prednisolone, and mycophenolate mofetil), as well as local infusion of corticosteroids and prostaglandin E1 via portal, with systemic administration of gabexate mesilate for 14 days postoperatively (Fig. 1D). The patient left CHDF on postoperative day (POD) 5 and was transferred to the general ward 20 days after surgery. The anti-A IgM/IgG titer was monitored daily for a month, and no increase was detected (Fig. 1B). There was no need for PE postoperatively. No signs of acute cellular rejection or AMR were detected. From around 4 months postoperatively, an increase of $CD19^+$ cells (%) was observed, which did not cause any problems (Fig. 1B). Cytomegalovirus (CMV) antigenemia was observed at POD 20, after 8 days of prophylactic ganciclovir. Although the patient had no symptoms, 900 mg Valixa was started on POD 54 due to a rise in CMV-positive cells. Other than that, the course of recovery was uneventful.

According to a psychiatric interview conducted near the time of hospital discharge, the patient denied suicidal ideation, but drug overdose was suspected. She was advised to comply with correct medication dosage and use and was discharged at POD 56. The patient now regularly visits a psychiatric clinic and is supported by her family. She has since been doing well, with no problems for 15 months after the transplant.

Discussion

The presently reported case illustrates two key points. The first point is that a patient with drug-induced ALF was successfully saved by ABOi-LDLT, with rituximab and MMF starting 8 days prior to LDLT, together with plasma exchange, splenectomy, and local infusion, without experiencing postoperative AMR or acute cellular rejection. The protocol we followed in this case was based on what we had previously used for elective ABOi-LDLT, and reduced the time from rituximab administration to transplantation to 8 days [15]. During the desensitization period, no specific adverse events occurred. CMV antigenemia developed after transplantation, but could be treated with ganciclovir without developing CMV infection. The second point is that this was a case of drug-induced ALF with hepatic coma, in which ABOi-LDLT was required to save the patient's life, but the decision regarding the indication for LT was controversial because the possibility of a suicide attempt could not be excluded.

Table 1 summarizes the ABOi-LDLT desensitization protocols with rituximab for ALF, which have been reported over the last 10 years, from 2014 to 2023. Protocols were divided into three categories: I) rituximab and IVIG; II) rituximab, PE, and bortezomib; and III) rituximab, PE, and splenectomy. The timing of rituximab administration ranged from about two weeks before LT (III-1 and III-2) to a couple of days prior to LT (I-2, III-1, and III-2), or intraoperatively (I), or the day after LT (II) [8–12]. Yasuda et al. reported that no AMR occurred when rituximab was administered two weeks before LT, followed by high-flow CHDF (III-3 and III-4). However, AMR developed with a protocol in which rituximab was administered 3 days prior to surgery and combined with PE (III-1 and III-2) [10]. Although the timing of PE was not described in detail, a study of the kinetics of rituximab showed that PE within 3 days of rituximab administration eliminates 50% of rituximab [16]. In our case (III-5), PE was performed 2 days after rituximab administration due to the progression of jaundice; however, $CD19^+$ cells were found to have almost disappeared by 3 days after rituximab administration. The timing of PE should be carefully considered in any desensitization protocol that combines PE and rituximab.

There is controversy regarding splenectomy and local infusion. Table 1 describes two cases of local infusion (III-1 and III-5) and five cases of splenectomy (III). Prior to the availability of rituximab, local infusion and splenectomy played an important role in the control of AMR [17]. However, in protocols using rituximab for ABOi-LDLT, splenectomy has no immunologic benefit [18], and catheter-related complications have been reported in local infusion [10].

PE was not performed in the combined IVIG and rituximab protocols (I) described by Shen et al. [9] and Lee B et al. [12]. Shen et al. prevented AMR with rituximab and low-dose IVIG for 10 days postoperatively. Lee B et al. prevented AMR with high-dose IVIG for 3 days postoperatively, even in a case with a high preoperative titer of anti-donor isoagglutinin (1:1024) and positive T-/B-cell crossmatch. In Japan, IVIG is currently approved for preoperative desensitization in anti-donor antibody-positive renal transplantation,

Table 1 Reported studies of ABOi-LDLT desensitization therapy using rituximab in the past 10 years

Desensitization protocol	#	Primary Disease (n)	PE	Purpose for PE	Timing of rituximab	IVIG	Additional regimen	Accommodation without AMR
I: Rituximab + IVIG	I-1 [9]	HBV (32) DILI (2) Cryptogenic (1)	No		POD 0	POD 0–10	None	Partially (33/35)
	I-2 [12]	HBV (1)	No		POD − 3	POD 0–3	None	Yes
II: PE + Rituximab + Bortezomib	II-1 [11]	HBV (7) AIH (1)	Yes	Antibody reduction	POD 1	No	None	Partially (7/8)
III: PE + Rituximab + Splenectomy	III-1 [10]	Cryptogenic (1)	Yes	Antibody reduction	POD − 3	No	Local infusion	No
	III-2 [10]	Cryptogenic (1)	Yes	Antibody reduction	POD − 3	No	None	No
	III-3 [10]	AIH (1)	Yes	Antibody reduction	POD − 14	No	None	Yes
	III-4 [10]	AIH (1)	Yes	Antibody reduction	POD − 15	No	None	Yes
	III-5*	DILI (1)	Yes	Antibody and drug reduction	POD − 8	No	Local Infusion	Yes

LDLT living donor liver transplantation, *ABOi* ABO-incompatible, *PE* plasma exchange, *IVIG* intravenous immunoglobulin, *DILI* drug-induced liver injury, *PNF* primary non-function, *AIH* autoimmune hepatitis, *AMR* antibody-mediated rejection

*Current case

but it is not covered by insurance for ABOi-LDLT. However, IVIG may be a promising treatment option for this purpose.

Lee WC et al. recently published a quick preparation protocol using bortezomib for ABOi-LDLT due to ALF (II). Bortezomib is a proteasome inhibitor used to target plasma cell depletion in multiple myeloma and primary macroglobulinemia. Some reports [19, 20] have already shown the efficacy of bortezomib as a treatment for AMR. The desensitization protocol is based on the administration of 3.5 mg of bortezomib at 4.75 ± 1.58 days preoperatively to deplete plasma cells, followed by PE to remove antibodies, and postoperative removal of B cells with rituximab administered at POD 1. However, IgM and IgG isoagglutinin titers were observed to rebound in four and five patients, respectively, and AMR developed in 1 out of 8 patients. There remains a need for optimization regarding the dose, timing, and frequency of bortezomib administration.

When planning liver transplantation for drug-induced ALF with hepatic coma, the question is often raised of whether the drug use was intentional (i.e., suicidal) or accidental. In the reports listed in Table 1, the primary disease was most commonly HBV (81.6%) and rarely from DILI. Unlike HBV, ALF caused by DILI may raise ethical issues. The patient's impaired consciousness makes it difficult for them to comprehend the situation. Regarding organ transplantation, the small number of organs acquired through the altruism of a DBD should not be lost due to another suicide attempt or suicide. Interestingly, liver transplant outcomes are the same for patients with and without a history of suicide or drug addiction [21, 22]. Following transplantation in cases of APAP-induced ALF, the subsequent rate of suicide has been reported to be approximately 6% [21]. On the other hand, it has been reported that the long-term prognosis is worse for cases of LT for APAP-induced ALF compared to LT for chronic liver disease, with 35% continuing to have social and psychiatric problems postoperatively [23]. In our present case, the patient was fortunate to regain consciousness, her willingness to undergo transplantation was confirmed, and the transplantation saved her life. When a patient is unconscious, the decision must be left to a surrogate decision-maker, but it has been suggested that it is more appropriate to make a decision according to the patient's best interests, when medically indicated, rather than considering what the patient wants [24]. In the absence of apparent contraindications (e.g., infection, growing cerebral edema, or other organ damage), it appears reasonable to explore liver transplantation. However, careful judgement is required regarding the indication for liver transplantation.

Here, we report our experience with a case of ABOi-LDLT for drug-induced ALF with hepatic coma, which is relatively rare in Japan, and required discussion about the indication of LT. A good postoperative course, without development of AMR or other serious complications, was

achieved by reducing the duration of rituximab desensitization (which usually takes two weeks) to eight days, with combined treatment with PE, based on the protocol used in elective ABOi-LDLT. While various desensitization protocols for ABOi-LDLT have been reported, the optimal desensitization duration and protocol have not yet been established. There remains a need for further investigation through clinical trials.

Author contributions KS wrote the manuscript. SK, YI, DY, YT, TN, HT, YD, and HE participated in assessment and discussion. All the authors read and approved the final manuscript.

Declarations

Conflict of interest The authors declare that they have no conflict of interest.

Human/animal rights All procedures followed were in accordance with the ethical standards of the responsible committee on human experimentation (institutional and national) and with the Helsinki Declaration of 1975, as revised in 2008(5).

Informed consent Informed consent was obtained from all patients included in this study.

References

1. Nakao M, Nakayama N, Uchida Y, et al. Nationwide survey for acute liver failure and late-onset hepatic failure in Japan. J Gastroenterol. 2018;53:752–69.
2. https://www.j-poison-ic.jp/system/pmasters/view2/%3Finfoid%3DO00900. Accessed 17 Apr 2023.
3. Heard KJ. Acetylcysteine for acetaminophen poisoning. N Engl J Med. 2008;359:285–92.
4. https://www.irodat.org/. Accessed 17 Apr 2023.
5. Yamashiki N, Sugawara Y, Tamura S, et al. Outcomes after living donor liver transplantation for acute liver failure in Japan: results of a nationwide survey. Liver Transpl. 2012;18:1069–77.
6. Demetris AJ, Jaffe R, Tzakis A, et al. Antibody-mediated rejection of human orthotopic liver allografts. A study of liver transplantation across ABO blood group barriers. Am J Pathol. 1988;132:489–502.
7. Umeshita K, Eguchi S, Egawa H, et al. Liver transplantation in Japan: registry by the Japanese liver transplantation society. Hepatol Res. 2019;49:964–80.
8. Egawa H, Teramukai S, Haga H, et al. Impact of rituximab desensitization on blood-type-incompatible adult living donor liver transplantation: a Japanese multicenter study. Am J Transpl. 2014;14:102–14.
9. Shen T, Lin BY, Jia JJ, et al. A modified protocol with rituximab and intravenous immunoglobulin in emergent ABO-incompatible liver transplantation for acute liver failure. Hepatobiliary Pancreat Dis Int. 2014;13:395–401.
10. Yasuda M, Ikegami T, Imai D, et al. The changes in treatment strategies in ABOi living donor liver transplantation for acute liver failure. J Med Invest. 2015;62:184–7.
11. Lee WC, Cheng CH, Lee CF, et al. Quick preparation of ABO-incompatible living donor liver transplantation for acute liver failure. Clin Transplant. 2021;e14555.
12. Lee B, Cho JY, Han H-S, et al. Long-term outcomes of emergency ABO-incompatible living donor liver transplantation using a modified desensitization protocol for highly sensitized patients with acute liver failure: a case report. Ann Hepatobiliary Pancreat Surg. 2021;25:571–4.
13. Rhodes R, Aggarwal S, Schiano TD. Overdose with suicidal intent: ethical considerations for liver transplant programs. Liver Transpl. 2011;17:1111–6.
14. Naiki T, Nakayama N, Mochida S, et al. Novel scoring system as a useful model to predict the outcome of patients with acute liver failure: Application to indication criteria for liver transplantation. Hepatol Res. 2012;42:68–75.
15. Kobayashi S, Nagano H, Marubashi S, et al. Successful adult ABO incompatible living donor liver transplantation: experience with double infusion through the hepatic artery and portal vein. Hepatogastroenterology. 2011;58:503–7.
16. Puisset F, White-Koning M, Kamar N, et al. Population pharmacokinetics of rituximab with or without plasmapheresis in kidney patients with antibody-mediated disease. Br J Clin Pharmacol. 2013;76:734–40.
17. Tanabe M, Shimazu M, Wakabayashi G, et al. Intraportal infusion therapy as a novel approach to adult ABO-incompatible liver transplantation. Transplantation. 2002;73:1959–61.
18. Raut V, Mori A, Kaido T, et al. Splenectomy does not offer immunological benefits in ABO-incompatible liver transplantation with a preoperative rituximab. Transplantation. 2012;93:99–105.
19. Lee C-F, Eldeen FZ, Chan K-M, et al. Bortezomib is effective to treat acute humoral rejection after liver transplantation. Transpl Proc. 2012;44:529–31.
20. Tajima T, Hata K, Okajima H, et al. Bortezomib against refractory antibody-mediated rejection after ABO-incompatible living-donor liver transplantation: dramatic effect in acute-phase? Transplant Direct. 2019;5: e491.
21. Karvellas CJ, Safinia N, Auzinger G, et al. Medical and psychiatric outcomes for patients transplanted for acetaminophen-induced acute liver failure: a case-control study. Liver Int. 2010;30:826–33.
22. Simmons OL, Meinzer C, Rule J, et al. Liver transplantation for acetaminophen-induced acute liver failure: role of psychiatric comorbidity in listing decisions and outcomes. Dig Dis Sci. 2020;65:1861–8.
23. Khan LR, Oniscu GC, Powell JJ. Long-term outcome following liver transplantation for paracetamol overdose. Transpl Int. 2010;23:524–9.
24. Brewster LP, Palmatier J, Manley CJ, et al. Limitations on surrogate decision-making for emergent liver transplantation. J Surg Res. 2012;172:48–52.

Sasaki et al. Surgical Case Reports (2023) 9:143
https://doi.org/10.1186/s40792-023-01723-7

CASE REPORT

Open Access

Successful endovascular embolization of the common hepatic artery for pseudoaneurysm associated with pancreatic fistula after liver transplantation: a case report

Kazuki Sasaki[1], Tadafumi Asaoka[1,2], Shogo Kobayashi[1*], Yoshifumi Iwagami[1], Daisaku Yamada[1], Yoshito Tomimaru[1], Takehiro Noda[1], Hiroshi Wada[1,3], Kunihito Gotoh[1,4], Hidenori Takahashi[1], Noboru Maeda[5], Yasushi Kimura[6], Yusuke Ono[6], Yuichiro Doki[1] and Hidetoshi Eguchi[1]

Abstract

Background After orthotopic liver transplantation (OLT), complications such as hepatic artery stenosis, thrombosis, and bleeding are possible. Hepatic artery pseudoaneurysms (HAP) are prone to rupture, rupture hemorrhage, and increased mortality risk. Endovascular treatment of HAP may result in recurrence, even after successful embolization with thrombin. Formation of a HAP in the common hepatic artery (CHA) is challenging because the CHA is the only artery in the liver graft after OLT. Therefore, CHA embolization in HAP is not an initial option. We report a case of HAP at the CHA after OLT that was treated with endovascular therapy, resulting in the occlusion of the CHA with coil embolization, achieving a radical cure.

Case presentation A 59-year-old man with decompensated hepatitis C virus cirrhosis underwent deceased donor whole-liver transplantation after graft failure of a living donor liver transplantation. After the second transplantation, the patient developed infectious narrow-necked HAP at the CHA associated with postoperative pancreatic fistula. Repeated transcatheter arterial embolization with thrombin and n-butyl-2-cyanoacrylate was unsuccessful, as confirmed by postprocedure angiography, which revealed recanalization and regrowth of the HAP. Eight months after the first transcatheter arterial embolization, the patient presented with a chief complaint of abdominal pain due to an enlarged HAP. Angiography of the superior mesenteric artery (SMA) revealed a collateral bypass around the bile duct from the SMA to the liver graft. Coil embolization of the HAP in the CHA completely occluded the HAP without complications. More than 2 years after coil embolization, the liver graft function test results remained within normal limits without HAP recurrence.

Conclusions HAP at the CHA after liver transplantation can be fatal if ruptured. Because the liver is a highly angiogenic organ, even if initial treatment is not successful, radical treatment to occlude the CHA with HAP is possible if sufficient collateral vessels are developed.

Keywords Hepatic artery pseudoaneurysm, Orthotopic liver transplantation, Endovascular treatment, n-2-Butyl-cyanoacrylate

*Correspondence:
Shogo Kobayashi
skobayashi@gesurg.med.osaka-u.ac.jp
Full list of author information is available at the end of the article

Introduction

Orthotopic liver transplantation (OLT) is practiced worldwide and is regarded as a standard procedure for end-stage liver disease, with 10,418 transplants performed through December 2020 in Japan [1]. Despite improvements in surgical techniques and immunological maintenance, severe biliary and vascular complications can occur after OLT, leading to graft failure and patient death.

Hepatic artery-related complications such as hepatic artery thrombosis (HAT), stenosis (HAS), and pseudoaneurysm (HAP) are rare but can occur after OLT. Their incidences are 3.5%, 2–13%, and 1.1–2.5% for HAT, HAS, and HAP, respectively [2–4]. Among these, HAP is the most serious complication [2, 5], with the risk of sudden life-threatening rupture that leads to graft loss and high mortality (53–69%) [4]. HAP after OLT often presents with nonspecific symptoms such as fever, abdominal discomfort, and gastrointestinal bleeding. Early diagnosis of HAP through close monitoring is crucial to prevent life-threatening hemorrhages with shock and high mortality. The location of the HAP depends on its etiology. Intrahepatic HAP is related to iatrogenic injuries, such as percutaneous transhepatic intervention or liver biopsy. Extrahepatic HAP is associated with anastomotic problems, local infection, bilio-enteric anastomosis [4], bile leakage, or postoperative pancreatic fistula.

Therapeutic approaches for HAP include surgical management and interventional radiology. Surgical treatments include HAP resection, ligation, and subsequent retransplantation or bypass with a saphenous vein graft [6], autologous radial artery, or inferior mesenteric artery [7]. For endovascular treatment, coil embolism, covered stent, endovascular balloon occlusion [8], and embolic agents, such as thrombin and *n*-butyl-2-cyanoacrylate (NBCA) are used [9, 10]. Surgery has traditionally been the treatment for HAP after OLT; however, minimally invasive interventional radiological approaches have recently become common [3, 11]. However, in some cases, the patient's condition and the HAP location make simultaneous graft stenting and arterial embolization difficult.

A particular challenge is the treatment of a HAP formed at the common hepatic artery (CHA) because the CHA is usually the only arterial blood supply pathway to the liver graft. Therefore, CHA embolization in cases of HAP is not an initial option. We report a case of HAP in the CHA after liver transplantation. Although recurrence of HAP was observed after initial treatment with NBCA and thrombin infusion, coil embolization of the CHA with HAP was finally performed. A radical cure was achieved due to the formation of collateral flow to the liver graft via the superior mesenteric artery (SMA) that developed during that period.

Case presentation

A 59-year-old male with decompensated hepatitis C virus cirrhosis (Child–Pugh score of 10 [C], and a Model for End-stage Liver Disease score of 31) underwent living donor liver transplantation (LDLT) using a left liver plus caudate lobe graft from his spouse. The patient developed partial liver infarction because of a portal vein thrombus extending from the main to the left portal branches, leading to liver graft failure. After that, the patient underwent deceased donor liver transplantation (DDLT) using a whole-liver graft on postoperative day 43 (Additional file 1: Fig. S1). A portal vein was reconstructed between the recipient's superior mesenteric vein and the graft portal vein with the donor's left common iliac vein graft interposition using end-to-end anastomosis. The biliary duct was constructed using duct-to-duct anastomosis.

After DDLT, aspartate aminotransferase levels decreased immediately (Fig. 1), but the patient developed a postoperative pancreatic fistula (grade B, according to the International Study Group of Pancreatic Fistula). *Candida* species were cultured in the fluid drainage, and the fistula was relieved by conservative treatment. Seven months after the surgery, the patient was transferred to a nursing hospital.

One month after the transfer (postoperative day 261), the patient experienced acute abdominal discomfort around the epigastrium. Abdominal computed tomography revealed a 4-cm cystic lesion in the pancreatic head (Fig. 2A). Abdominal ultrasonography revealed a to-and-fro wave pattern in the cyst (Fig. 2B). Angiography of the celiac artery confirmed HAP in the CHA (Fig. 2C-a). Because the HAP had a narrow neck shape, thrombin (800 U) was injected under balloon protection of the proper hepatic artery (PHA) (Fig. 2C-b). After this procedure, the HAP disappeared, and the hepatic artery was patent (Fig. 2C-c). Daily doppler abdominal ultrasonography was performed. On the third day, doppler abdominal ultrasonography showed that the blood flow resumed in the mass. Embolization was performed with thrombin under IVR (Interventional Radiology). However, during the third relapse, the HAP was recanalized repeatedly and occluded by embolization with NBCA (1:2 NBCA: Lipiodol). No collateral formation was observed at this point.

The HAP resolved for a while. However, abdominal pain and fever were later observed, thus confirming the fifth HAP recurrence 8 months after the first thrombin infusion (postoperative day 517). Angiography showed that the neck of the HAP had widened to 1 cm, and the PHA diameter had narrowed (Fig. 3A). Another NBCA

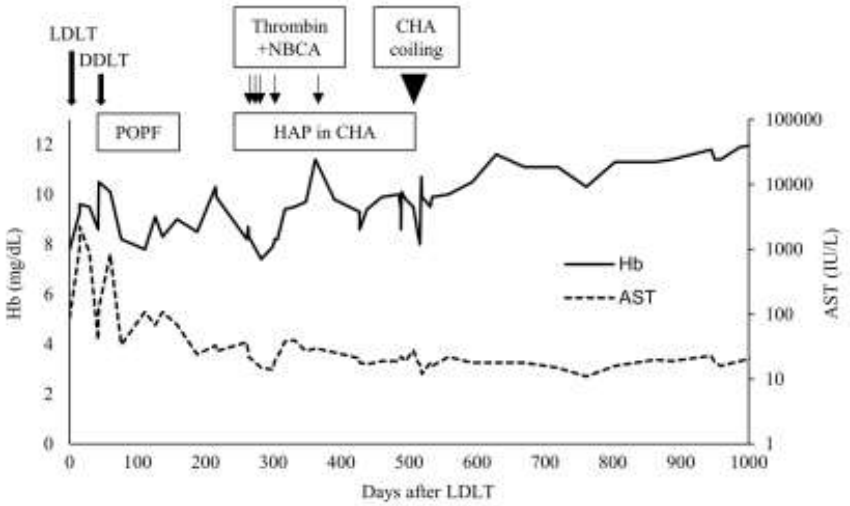

Fig. 1 The postoperative course of the patient. One month after LDLT, the patient underwent DDLT due to liver graft failure resulting from a portal vein thrombus extending from the main to the left portal branch. Approximately 8 months after LDLT, a HAP developed in the CHA and was controlled by thrombin and NBCA injections; however, the HAP was recanalized repeatedly. Finally, coil embolization was performed on the HAP and CHA, and the patient survived recurrence-free for more than 500 days. *AST* aspartate aminotransferase, *CHA* common hepatic artery, *DDLT* deceased donor liver transplantation, *HAP* hepatic artery pseudoaneurysm, *LDLT* living donor liver transplantation, *NBCA* *n*-2-butyl-cyanoacrylate, *POPF* postoperative pancreatic fistula

injection into the HAP or stent graft was unsuitable because of the widened neck and the small diameter of the PHA. Fortunately, the liver graft was enhanced by a collateral bypass around the bile duct from the SMA (Fig. 3B) and under from left gastric vein with balloon occlusion of CHA (Additional file 2: Fig. S2). Given the collateral vasculature; we believe CHA embolization is safe. Coil embolization (Target and Penumbra) of the HAP and CHA under balloon protection was performed (Fig. 3C). After embolization, angiography confirmed complete HAP occlusion and blood flow to the liver graft through the SMA (Fig. 3D). Additionally, abdominal ultrasonography showed that the intrahepatic arterial waveforms were visible after coil embolization (Fig. 3E). After that, the patient's clinical course was uneventful. Liver function test results remained within normal limits. The patient was discharged on day 20 after coil embolization and has remained stable without abscess or HAP recurrence for over 2 years.

Discussion

Along with HAT, HAS, portal vein thrombosis, and portal vein stenosis, HAP is another vascular complication that can occur after OLT [12]. Although HAPs are rare, they can lead to severe outcomes, including graft loss and even death. Therefore, early detection and prompt treatment of HAP before rupture are crucial.

Table 1 summarizes reports of the treatment of extrahepatic pseudoaneurysms after liver transplantation over the past 10 years (from 2013 to 2022). Because there have been several types of cases, including ruptured and unruptured HAP, it is difficult to uniformly compare the treatments to determine which is best. Surgical treatment includes revascularization, hepatic artery (HA) ligation, and repeat liver transplantation. Boleslawski showed the benefit of HA ligation for ruptured HAP with high mortality [13]. Among 17 patients with ruptured HAP, 6 of 10 of those patients with HA ligation achieved long-term survival. Interestingly, some patients who achieved long-term survival without repeat transplantation underwent HA ligation without ischemic bile duct injury. Regarding endovascular therapy, the usefulness of endovascular therapies such as coil embolization and stent grafting has been reported [3, 4, 9, 14]. Kadohisa et al. reported three cases of ruptured HAP treated with embolization [14]. The HA was completely occluded. One patient was successfully treated with autologous vein graft, and another was successfully treated with liver transplantation; however, one patient died of liver abscess and sepsis while waiting for the formation of collateral channels.

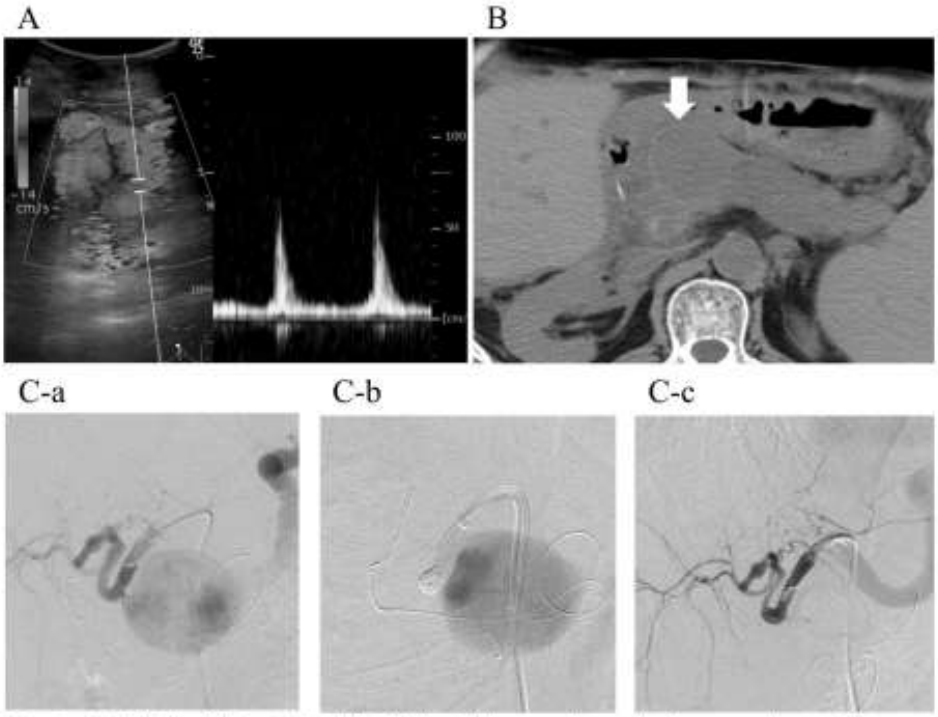

Fig. 2 Diagnosis of the HAP in the CHA 8 months after LDLT. **A** Abdominal ultrasonography revealing a 4-cm mass with a to-and-fro wave pattern at the neck of the lesion on Doppler. **B** Plain abdominal computed tomography imaging showing a 4-cm cystic lesion in the area of the pancreatic head. **C-a** Celiac angiography revealing a narrow-neck type HAP in the CHA and a tortuous PHA. **C-b** Under balloon protection of the PHA, thrombin was injected into the HAP. **C-c** Post-procedure angiography showing complete occlusion of the HAP and a good flow to the graft liver. *CHA* common hepatic artery, *HAP* hepatic artery pseudoaneurysm, *LDLT* living donor liver transplantation, *PHA* proper hepatic artery

In our case, HAP in the CHA after liver transplantation was successfully treated with CHA embolization because of the collateral vasculature to the liver graft that developed around the bile duct. HAP generally develops after OLT, where a local infection has injured the artery wall at the anastomotic site because of technical difficulties during anastomosis completion or due to iatrogenic effects from procedures such as angioplasty for arterial stenosis. In this case, a HAP developed in the CHA and not at the anastomotic site. The retrospective imaging evaluation revealed a portal vein thrombus during DDLT, which required a jump graft through the SMV to the back of the pancreas in the presence of severe adhesions. The GDA was considered to have been sacrificed during dissection around the CHA for hemostasis. In fact, the GDA was visible on angiography before DDLT, but it was not visible on postoperative day 14 (Additional file 1: Fig. S1). And this, combined with the postoperative pancreatic fistula, may have led to the development of HAP at the GDA stump.

NBCA is generally a permanent embolic reagent that polymerizes in the blood. It is injected in a mixture with

(See figure on next page.)

Fig. 3 Coil embolization of the HAP in the CHA. Coil embolization of the recanalized HAP 8 months after the first endovascular treatment. **A** Celiac angiogram of the HAP in the CHA. The HAP neck had widened, and the diameter of the PHA had narrowed compared to the first endovascular treatment. **B** SMA angiography image of the collateral vascular network around the bile duct (arrow). **C** Coil embolization performed on the HAP and CHA. **D** Post-procedural angiography of the SMA showing preserved flow to the graft via a vascular network around the bile duct. **E** Abdominal ultrasonography showing the intrahepatic arterial waveforms after coil embolization of the CHA. *CHA* common hepatic artery, *HAP* hepatic artery pseudoaneurysm, *PHA* proper hepatic artery, *SMA* superior mesenteric artery

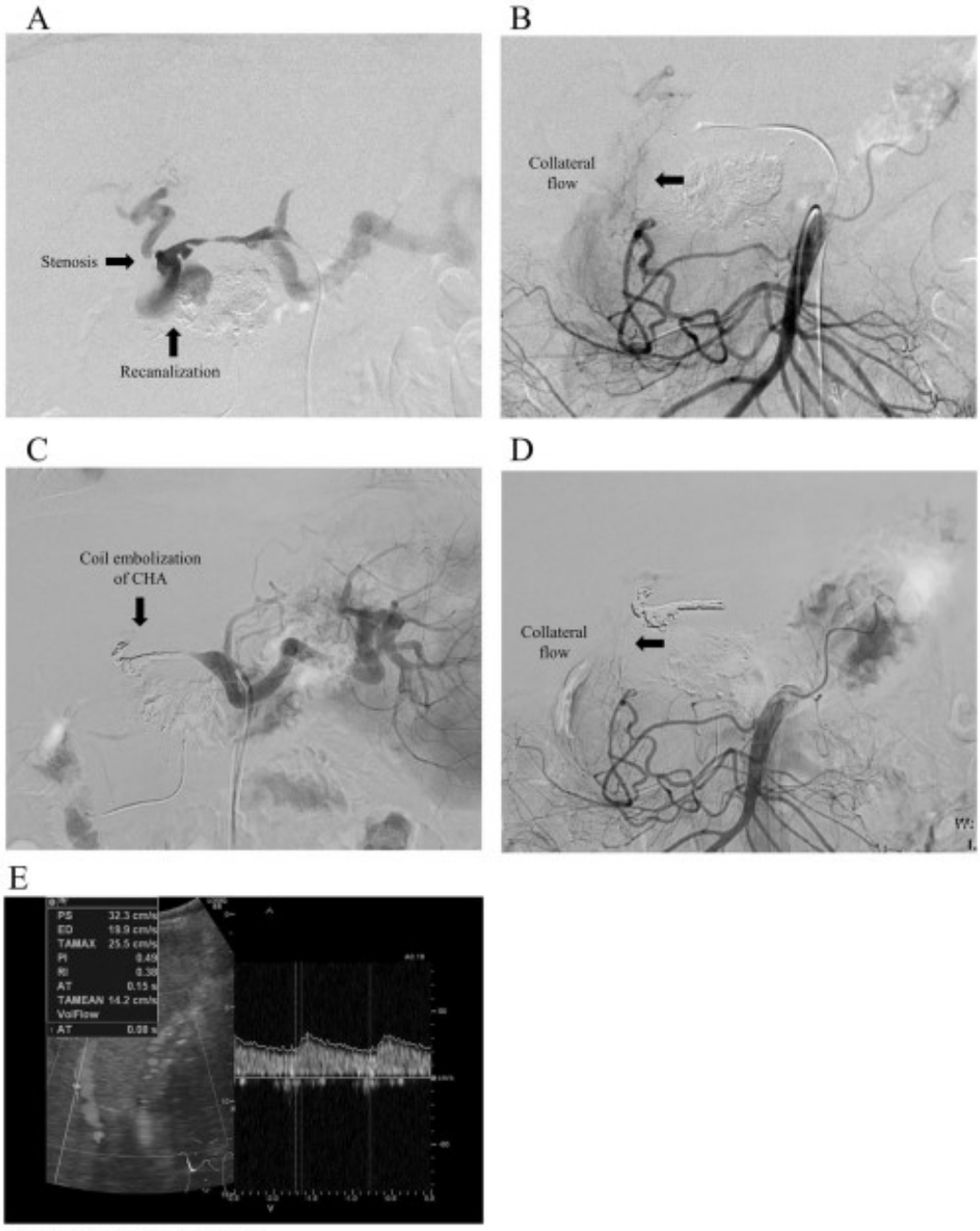

Fig. 3 (See legend on previous page.)

Table 1 Case series regarding extrahepatic HAP after liver transplantation 2013–2022

Year	Author	N	Onset (day) median, range	Clinical presentation (n)	Surgical treatment (n)	Endovascular therapy (n)	None (n)	Outcome alive/total
2013	Saad	20	48, 1–1098	Hypotension (12) GI-bleeding (7) Sepsis (2) Dropped hematocrit without symptoms (1)	Surgery (2)			1/2
						Embolization (4) (selective embolization (1))		1/4
						Stent-graft (8)(+ ReOLT (1))		6/8
					ReOLT (5)			5/5
							None (1)	0/1
2013	Panaro	9	39.6, 22–92	Bleeding (4), fever (3) asymptomatic (3)	Revascularization with saphenous bypass (9) (+ ReOLT (1))			8/9
2013	Boleslawski	17	29, 2–92	Hemo peritoneum (10) GI-bleeding (5) Hemobilia (1) Hematoma (1)	Anastomosis revision (5) (+ ReOLT (1))			1/5
					HA ligation (10)(+ ReOLT (3))			6/10
						Embolization (1)		0/1
							None (1)	0/1
2014	Volpin	16	13, 4–100	Shock (10) GI-bleeding (4) Bleed through drains (5) Abdominal pain (8)	Excision + revascularization (7)			4/7
					Ligation (5)(+ ReOLT (1))			2/5
						Embolization (1)		1/1
						Covered stent (1)		1/1
							None (2)	0/2
2017	Thorat	2[a]	7, 2.5 Mo	Bleeding (2)		Stent graft (2)		2/2
2022	Kadohisa	3	41, 68, 19 Mo	GI-bleeding (3)		Embolization (3) (+ revascularization (1) + ReOLT(1))		2/3
2023	This case	1	7 Mo	Abdominal pain, fever		Embolization (1)		1/1

[a] Extrahepatic HAP cases were extracted from original reports. *Mo* Month, *ReOLT* re-orthotopic liver transplantation, *HA* hepatic artery

Lipiodol for the embolization of pseudoaneurysms [15], aneurysms [16], arteriovenous malformations [17], and varices. The advantage of NBCA over coil embolization is that it can be applied to tortuous vessels, unlike coil embolization. However, recanalization can occur after injection [18]. In our case, we initially did not perform coil embolization because of the risk of occluding the native PHA, leading to graft ischemia. We also did not choose a stent graft because a suitable size was unavailable owing to the tortuous artery. Thus, we chose thrombin and NBCA as initial treatments. Despite the disappearance of HAP immediately after injection, NBCA could have been washed out by the high arterial pressure of the CHA during the ensuing months. Because NBCA was not a definitive treatment in the present case, we finally switched to coil embolization of the HAP in the CHA.

Neovascularization of the liver is often observed after OLT, especially when HAT is involved [19–22]. There have been few reports of HAP treatment that involves waiting for the formation of collateral channels. According to Panaro et al., the mean interval between the diagnosis of hepatic artery thrombosis and neovascularization of the liver was 4.1 months (range, 3–5.5 months) [20]. Four factors have been cited in the development of neovascularization after DDLT: late hepatic artery thrombosis (>30 days), early hepatic artery stenosis (<30 days), thrombosis at the anastomotic site, and Roux-en-Y anastomosis [20]. The trigger for neovascularization is unknown; however, the assumed mechanism is that prolonged liver hypoxia due to HAT or stenosis induces the expression of vascular endothelial growth factor and hypoxia-inducible factor 1-α, leading to angiogenesis from the surrounding tissue to the liver [22]. Neovascularization has been reported in various vessels, including the omentum and mesenteric, subcostal, lumbar, renal, and iliac arteries [20, 22]. The connective tissue around the common bile duct and the hilar plate is usually preserved during donor hepatectomy to ensure sufficient blood flow to the bile duct after transplantation. In this patient, 8 months after the first thrombin embolization (517 days after LDLT), we confirmed collateral formation around the bile duct; however, we did not know the timing of the collateral vessel development. We do know that

during the third relapse (286 days after the LDLT), it was not confirmed from SMA angiography (data not shown). We speculate that arterial stenosis and repeated thrombin or NBCA injections may have led to chronic ischemia of the liver, inducing neovascularization.

Conclusions

This case illustrates the need to pay special attention to patients with risk factors for HAP after OLT, such as local infections. In such cases, regular ultrasound or computed tomography imaging should be performed to enable the early recognition of HAP and management of this life-threatening condition. Neovascularizing the liver after OLT could benefit graft survival by allowing the embolizing of a HAP in the CHA if needed. Fortunately, in this case, because of the collateral bypass formed around the bile duct more than 500 days after LDLT, HAP in the CHA was cured without complications by endovascular treatment with NBCA, thrombin, and coil embolization.

Abbreviations

HAP	Hepatic artery pseudoaneurysm
CHA	Common hepatic artery
OLT	Orthotopic liver transplantation
SMA	Superior mesenteric artery
NBCA	*N*-Butyl-2-cyanoacrylate
LDLT	Living donor liver transplantation
DDLT	Deceased donor liver transplantation
PHA	Proper hepatic artery
AST	Aspartate aminotransferase
POPF	Postoperative pancreatic fistula
IVR	Interventional radiology

Supplementary Information

The online version contains supplementary material available at https://doi.org/10.1186/s40792-023-01723-7.

Additional file 1: Fig. S1. The hypothesized location of the HAP in the CHA. A) Drawing before DDLT (a), after DDLT (b) and 7 months after DDLT(c). Before DDLT, portal vein thrombosis was observed. During DDLT, PV reconstructed using the donor's left common iliac vein graft interposition from the SMV, passed from the back of the pancreas to the head and anastomosed with the donor portal vein. During this process, GDA was sacrificed. Postoperative pancreatic fistula developed. Seven months after DDLT, a pseudoaneurysm formed at the GDA stump. B Angiogram before DDLT showing GDA, CHA, and PHA (a). Maximum Intensity Projection (MIP) image of POD14 (b) and POD49 (c). 3D constructed contrast-enhanced CT image 7 months after DDLT (d). The GDA seen preoperatively is obscured after DDLT. A hepatic pseudoaneurysm was detected on the GDA stump. CHA: common hepatic artery; PHA: proper hepatic artery; GDA: gastroduodenal artery.

Additional file 2: Fig. S2. Angiography prior to coil embolization of the HAP in the CHA. A. Angiography from LGA with balloon occlusion of CHA showed intrahepatic artery via collateral tract. BAngiography from SMA showed intrahepatic artery via IPDA and peribiliary collateral tract. Arrows indicate intrahepatic arteries via collateral channels. LGA: left gastric artery, IPDA: inferior pancreaticoduodenal artery.

Acknowledgements
Not applicable.

Author contributions
All authors read and approved the final manuscript.

Funding
This study received no funding or grant support.

Availability of data and materials
Data sharing is not applicable to this article as no datasets were generated or analyzed during the current study.

Declarations

Ethics approval and consent to participate
All the procedures were performed in accordance with the ethical standards of the appropriate version of the Declaration of Helsinki.

Consent for publication
Informed consent was obtained from the patient for the publication of this report.

Competing interests
The authors declare that they have no competing interests.

Author details
[1]Department of Gastroenterological Surgery, Graduate School of Medicine, Osaka University, 2-2 E2 Yamadaoka, Suita, Osaka 565-0871, Japan. [2]Department of Gastroenterological Surgery, Osaka Police Hospital, Osaka, Japan. [3]Department of Gastroenterological Surgery, Osaka International Cancer Institute, Osaka, Japan. [4]Department of Surgery, National Hospital Organization Osaka National Hospital, Osaka, Japan. [5]Department of Diagnostic and Interventional Radiology, Osaka International Cancer Institute, Osaka, Japan. [6]Department of Diagnostic and Interventional Radiology, Osaka University Graduate School of Medicine, Suita, Japan.

Received: 10 May 2023 Accepted: 31 July 2023
Published online: 10 August 2023

References

1. Japanese Liver Transplantation Society. Liver Transplantation in Japan—Registry by the Japanese Liver Transplantation Society. Available from: http://jlts.umin.ac.jp/.
2. Marshall MM, Muiesan P, Srinivasan P, Kane PA, Rela M, Heaton ND, et al. Hepatic artery pseudoaneurysms following liver transplantation: incidence, presenting features and management. Clin Radiol. 2001;56:579–87.
3. Saad WE, Dasgupta N, Lippert AJ, Turba UC, Davies MG, Kumer S, et al. Extrahepatic pseudoaneurysms and ruptures of the hepatic artery in liver transplant recipients: endovascular management and a new iatrogenic etiology. Cardiovasc Intervent Radiol. 2013;36:118–27.
4. Volpin E, Pessaux P, Sauvanet A, Sibert A, Kianmanesh R, Durand F, et al. Preservation of the arterial vascularisation after hepatic artery pseudoaneurysm following orthotopic liver transplantation: long-term results. Ann Transplant. 2014;19:346–52.
5. Fistouris J, Herlenius G, Bäckman L, Olausson M, Rizell M, Mjörnstedt L, et al. Pseudoaneurysm of the hepatic artery following liver transplantation. Transplant Proc. 2006;38:2679–82.
6. Panaro F, Miggino M, Bouyabrine H, Carabalona JP, Berthet JP, Canaud L, et al. Reversed saphenous bypass for hepatic artery pseudoaneurysm after liver transplantation. Ann Vasc Surg. 2013;27:1088–97.
7. Asonuma K, Ohshiro H, Izaki T, Okajima H, Ueno M, Kodera A, et al. Rescue for rare complications of the hepatic artery in living donor liver transplantation using grafts of autologous inferior mesenteric artery. Transpl Int. 2004;17:639–42.
8. Stephenson K, Kalkwarf K, Giorgakis E. Application of resuscitative endovascular balloon occlusion in post-transplant mycotic hepatic artery pseudoaneurysm rupture in the setting of Aspergillus Constellatus bacteremia. Ann Hepatobiliary Pancreat Surg. 2021;25:126–31.

9. Thorat A, Lee CF, Wu TH, Pan KT, Chu SY, Chou HS, et al. Endovascular treatment for pseudoaneurysms arising from the hepatic artery after liver transplantation. Asian J Surg. 2017;40:227–31.
10. Páez-Carpio A, Serrano E, Zarco F, Fondevila C, Burrel M. Arterio-biliary fistula caused by a hepatic artery pseudoaneurysm in a recently performed liver transplant: successful resolution and long-term liver implant preservation using a covered coronary stent. CVIR Endovasc. 2020;3:93.
11. Piardi T, Lhuaire M, Bruno O, Memeo R, Pessaux P, Kianmanesh R, et al. Vascular complications following liver transplantation: a literature review of advances in 2015. World J Hepatol. 2016;8:36–57.
12. Frongillo F, Lirosi MC, Nure E, Inchingolo R, Bianco G, Silvestrini N, et al. Diagnosis and management of hepatic artery complications after liver transplantation. Transplant Proc. 2015;47:2150–5.
13. Boleslawski E, Bouras AF, Truant S, Liddo G, Herrero A, Badic B, et al. Hepatic artery ligation for arterial rupture following liver transplantation: a reasonable option. Am J Transplant. 2013;13:1055–62.
14. Kadohisa M, Inomata Y, Sakisaka M, Sugawara Y, Hibi T. Massive duodenal ulcer bleeding due to the ruptured hepatic artery pseudoaneurysm after living donor liver transplantation. Surg Case Rep. 2022;8:199.
15. Ou HY, Concejero AM, Yu CY, Huang TL, Chen TY, Tsang LL, et al. Hepatic arterial embolization for massive bleeding from an intrahepatic artery pseudoaneurysm using N-butyl-2-cyanoacrylate after living donor liver transplantation. Transpl Int. 2011;24:e19–22.
16. Guziński M, Kurcz J, Kukulska M, Neska M, Garcarek J. Embolization of a true giant splenic artery aneurysm using N8CA glue—case report and literature review. Pol J Radiol. 2015;80:155–8.
17. Tatsuta T, Endo T, Watanabe K, Hasui K, Sawada N, Igarashi G, et al. A successful case of transcatheter arterial embolization with n-butyl-2-cyanoacrylate for pancreatic arteriovenous malformation. Intern Med. 2014;53:2683–7.
18. Matsumoto K, Ushijima Y, Tajima T, Nishie A, Hirakawa M, Ishigami K, et al. Recanalization of splenic artery aneurysm after transcatheter arterial embolization using N-butyl cyanoacrylate. Cardiovasc Intervent Radiol. 2010;33:187–90.
19. Dydynski PB, Bluth EI, Altmeyer W, Devun DA, Milburn JM. Collateral transformation of the hepatic artery after liver transplantation. AJR Am J Roentgenol. 2008;191:546–9.
20. Panaro F, Gallix B, Bouyabrine H, Ramos J, Addeo P, Testa G, et al. Liver transplantation and spontaneous neovascularization after arterial thrombosis: "the neovascularized liver" Transpl Int. 2011;24:949–57.
21. Fouzas I, Sklavos A, Bismpa K, Paxiadakis I, Antoniadis N, Giakoustidis D, et al. Hepatic artery thrombosis after orthotopic liver transplantation: 3 patients with collateral formation and conservative treatment. Transplant Proc. 2012;44:2741–4.
22. Casadaban L, Parvinian A, Tzvetanov IG, Jeon H, Oberholzer J, Benedetti E, et al. Unconventional extrahepatic neovascularization after transplant hepatic artery thrombosis: a case report. Transplant Proc. 2013;45:2841–4.

Publisher's Note

https://doi.org/10.1016/j.hpb.2023.01.020 HPB

ORIGINAL ARTICLE

Interventional treatment for portal vein complications utilizing a hybrid operating room after liver transplantation

Hiroyuki Hakoda[1], Nobuhisa Akamatsu[1], Eisuke Shibata[2], Hidemasa Takao[2], Akihiko Ichida[1], Yoshikuni Kawaguchi[1], Junichi Kaneko[1], Osamu Abe[2] & Kiyoshi Hasegawa[1]

[1]Artificial Organ and Transplantation Division, Department of Surgery, Graduate School of Medicine, The University of Tokyo, Tokyo, Japan, and [2]Department of Radiology, Graduate School of Medicine, The University of Tokyo, Tokyo, Japan

Abstract

Background: Vascular complications after liver transplantation (LT) can be lethal and require immediate treatment to prevent graft failure. Nowadays, with interventional radiology (IR), approaches such as the percutaneous transhepatic (PTH) and transileocolic venous (TIC), have become major treatment options. We reviewed the safety and efficacy of a hybrid operating room (OR) for portal vein complications after LT.

Methods: Patients who underwent IR for post-LT vascular complications in the hybrid OR from May 2014 to May 2022 were enrolled. Patients who underwent post-LT IR in conventional angiography rooms were excluded.

Results: Nine patients developed portal vein complications; eight after living donor LT and one after deceased donor LT. Six patients had portal vein stenosis, two had portal vein thrombosis, and one had both. In the hybrid OR, PTH and TIC were used in five and three cases, respectively. The Rendezvous technique was used in one case. Angioplasty was performed in all patients. A stent was placed in four patients. The portal venous pressure gradient across the stenotic site significantly decreased after IR (P &= 0.031). The IR success rate in the hybrid OR was 100%.

Conclusion: The hybrid OR enables us to accomplish IR for post-LT vascular complications safely and effectively.

Received 26 December 2022; accepted 30 January 2023

Correspondence

Artificial Organ and Transplantation Division, Department of Surgery, Graduate School of Medicine, The University of Tokyo, 7-3-1 Hongo, Bunkyo-ku, Tokyo, 113-8655, Japan. E-mail: hasegawa-2su@h.u-tokyo.ac.jp

Introduction

Developments in surgical techniques and immunosuppressive therapies have contributed to excellent outcomes for recipients of liver transplantation (LT)[1]; however, surgical complications still require immediate treatment with an appropriate strategy. Vascular complications may directly lead to graft dysfunction and failure and require prompt and appropriate management. The portal vein (PV) complications such as stenosis (PVS) and thrombosis (PVT) are reportedly infrequent, ranging from 2% to 15% [2,3]; however, the management of such complications remains demanding and challenging.

There are several treatment strategies for the complications. Revision surgery has been an early option after LT; however, it has become less common after the development of interventional radiology (IR). IR is currently the gold standard for the treatment of post-LT PV complications. A hybrid OR has recently become a major tool for abdominal vessels.

In this study, we investigated the efficacy and safety of IR in the hybrid OR for the treatment of post-LT PV complications.

Meeting presentation: None.

Methods

Patient data

We retrospectively reviewed the medical records of all adults (age≥18) who underwent LT at the University of Tokyo Hospital from May 2014 (Hybrid OR introduction) to May 2022.

We selected patients who developed post-LT PV complications, that were treated using IR in the hybrid OR. Patients who underwent IR for post-LT vascular complications in the angiography rooms were excluded.

This retrospective study was approved by the Institutional Ethics Committee of the University of Tokyo [No: 2158-(6)].

Clinical diagnosis of PV stenosis/occlusion

The diagnosis of PV stenosis/occlusion was fundamentally based on the morphological findings of CE-CT,[4] and confirmed via direct venography performed by a radiologist.

Interventional treatment in a hybrid OR

Interventional treatment was performed in a hybrid OR, consisting of a conventional OR and an angiography system, which offers high-resolution DSA. The hybrid OR was preferred in cases requiring a long operative time (>2 h) and stent placement. In the hybrid OR, patients requiring percutaneous transhepatic (PTH) and transileocolic venous (TIC) approaches were prepared with general anesthesia.

All IR procedures were performed in collaboration with the transplant surgeons and experienced radiologists. Vascular sheaths were first inserted into the targeted PV-SMV system using the PTH or TIC approach. In the TIC approach, the surgeons exposed the ileocecal vein and placed the sheath through a small laparotomy. In cases of severe anastomotic stricture or severe thrombosis for which balloon dilation alone was not satisfactory, an intravascular metallic stent was implanted. After the procedure, the anticoagulant agents were administered as long as the patient had no contraindication to anticoagulant therapy.

Statistical analysis

We used the Wilcoxon signed-rank sum test using JMP Pro 16.2 (SAS Institute, Cary, NC, USA). The threshold for significance was set at $P < 0.05$.

Results

A total of 833 patients underwent either LDLT (n = 770) or DDLT (n = 60) between January 1996 and May 2022 at our institution. Fourteen patients developed post-LT PVS or PVT

Table 1 Patients' characteristics

Case	Age	Sex	Liver disease	LT procedure	Liver graft	Initial symptoms	PV complications	Interval from LT (day)	Approach	Treatment procedures	Operation time (min)	Discharge from Treatment (day)	IVR complications
1	67	M	HBV-LC	LDLT	LLG	Renal dysfunction	PVS	107	TIC	TA, stent placement	75	5[b]	none
2	50	M	HCV-LC, HCC	LDLT	LLG	Inflammation at blood test	PVT (Grade IV[a])	1261	TIC	TA, thrombectomy	226	22	hematoma, fever
3	34	F	Wilson's disease	LDLT	RLG	Accidently	PVS	109	PTH	PTA, shunt embolization	178	4	none
4	59	M	HCV-LC	DDLT	RTriSG	Consciousness disorder	PVS and PVT (Grade II[a])	120	TIC→ PTH	PTA, stent placement	324	7	none
5	28	F	LC due to biliary atresia	LDLT	LLG	Fever	PVS	13	PTH	PTA	103	32[b]	none
6	58	M	HBV/ HDV-LC, HCC	LDLT	RLSG	Elevated serum levels of hepatic enzymes	PVS	277	PTH	PTA, stent placement	107	6	none
7	52	F	CTLN2	APOLT	LLG	Elevated serum levels of hepatic enzymes	PVT (Grade II[a])	3	TIC	thrombolysis, TA, stent placement	156	29[b]	hematoma, infection
8	55	M	NASH-LC	LDLT	RLG	Elevated serum levels of hepatic enzymes	PVS	18	PTH	PTA	65	20[b]	none
9	64	M	HCV-LC, HCC, Banti syndrome	LDLT	RLG	Anemia, melena	PVS	158	PTH	PTA	98	1	none

M: male, F: female, LC: liver cirrhosis, HCV-LC: hepatitis C virus-related liver cirrhosis, HBV-LC: hepatitis B virus-related liver cirrhosis, HBV/HDV-LC: hepatitis B virus and hepatitis D visurs-coinfection-related liver cirrhosis, HCC: hepatocellular carcinoma, CTLN2: adult-onset type II citrullinemia, NASH: non-alcoholic steatohepatitis, LDLT: living donor liver transplantation, DDLT: deceased donor liver transplantation, APOLT: auxiliary partial orthotopic liver transplantation, PV: portal vein, PVT: portal vein thrombosis, PVS: portal vein stenosis, LLG: left liver graft, RLG: right liver graft, RTriSG: right trisegment graft (right liver split graft), RLSG: right lateral sector graft.
[a] Grade under Yerdel classification of PVT, PTH: percutaneous transhepatic approach, TIC: transileocolic venous approach, PTA: percutaneous transluminal angioplasty, TA: transluminal angioplasty, IR: interventional radiology.
[b] Patients who had been hospitalized since LT when they underwent IR.

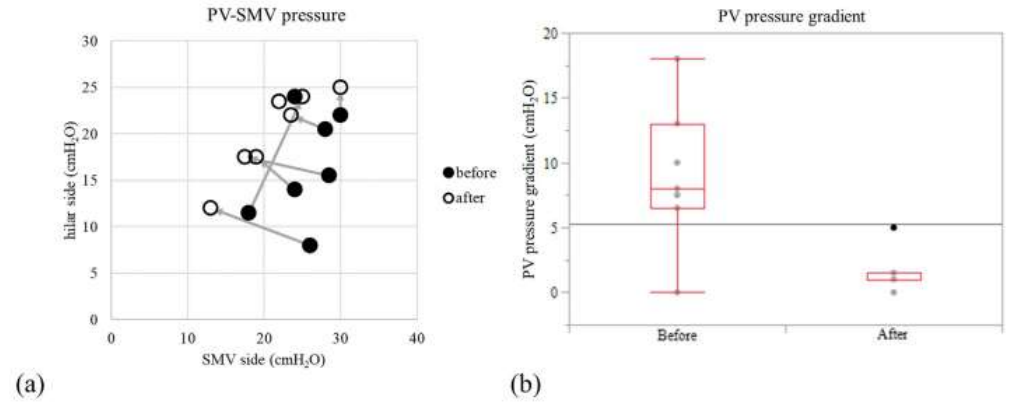

Figure 1 (a): The scatter plot of portal vein pressure before and after treatment (b): The box-and-whisker plot of the pressure gradient before and after the treatment in the hybrid operation room The pressure gradients were significantly decreased after the treatment (P = 0.031, Wilcoxon signed-rank sum test).

requiring IR between May 2014 and May 2022, accounting for 4.8% (14/294) of all LT cases during the period. The development of either or both PV complications was observed in 5% (30/593) of patients during January 1996 to April 2014, that is, before the introduction of the hybrid OR. The incidences of PV complications were comparable throughout the study period. In the post-IR group, nine of the 14 cases with PV complications were treated in the hybrid OR using the present technique. During the same period, five of the 14 patients with PV complications underwent IR in the conventional angiography room. Relatively mild stenosis (<50%) of the PV anastomosis was identified in all cases. Detailed characteristics of those treated with the hybrid OR are presented in Table 1. In eight patients LDLT had been performed, and in one DDLT.

Six patients had PVS and three had PVT. One patient had both PVS and PVT. Thrombosis was classified according to the Yerdel classification.[5]

PTH and TIC approaches were used in five and three cases, respectively. In one case, the TIC approach was first selected, and the IR was completed using the rendezvous technique with the PTH approach.

Angioplasty was performed in all cases. The PV pressure gradient across the stenotic site significantly decreased after IR (P = 0.03, Fig. 1). A metallic stent was placed in 4 cases (50%). Complications after IR occurred in only two cases, which were mild (Table 1). The technical success rate and the patency after IR were both 100%.

In the group before the introduction of the hybrid OR, 10 and 20 patients underwent IR and operation for PV complications, respectively. The rate of the direct approach to PV (open surgery) was high in this group owing to the earlier cohort.

Discussion

The causes of PVS or PVT after LDLT are thought to be associated with the relatively short length of the donor PV, PV diameter mismatch between the donors and recipients, and pre-existing PVT in recipients.[2]

Post-LT PV complications have several treatment options such as revision surgery and IR, including thrombolysis, thrombectomy, and angioplasty.[6] However, surgical procedures are associated with high morbidity and mortality rates because of severe postoperative adhesions, scar tissues around vessels, or limited length of the vein structures.[7] Although there are possible treatment options if PVS occurs early after LT, surgical treatment is not the first choice.[8]

IR in the OR with fluoroscopic guidance can be performed under general anesthesia, which provides the following benefits: general anesthesia relieves pain, ventilatory respiration control facilitates a safe and precise procedure, and recipients can tolerate the long procedure. Additionally, the approach can be immediately converted to TIC when the PTH approach fails or requires a rendezvous technique.

The hybrid OR provides higher resolution on DSA.[9] Since the hybrid OR combines the beneficial features of conventional OR and angiography room, it can be especially useful for treating post-LT vascular complications which require the most meticulous IR management among all abdominal surgeries.

In conclusion, IR in hybrid OR is a safe and effective treatment for PV-SMV complications after LT.

Funding information

This work was not supported by any grants.

Acknowledgment

We would like to thank Editage (www.editage.com) for English language editing.

Conflict of interest

None declare.

References

1. Andrews JC. (2004) Vascular complications following liver transplantation. *Semin Intervent Radiol* 21:221–233.
2. Wei BJ, Zhai RY, Wang JF, Dai DK, Yu P. (2009) Percutaneous portal venoplasty and stenting for anastomotic stenosis after liver transplantation. *World J Gastroenterol* 15:1880–1885.
3. Miraglia R, Maruzzelli L, Caruso S, Milazzo M, Marrone G, Mamone G *et al.* (2009) Interventional radiology procedures in adult patients who underwent liver transplantation. *World J Gastroenterol* 15:684–693.
4. Kyoden Y, Tamura S, Sugawara Y, Matsui Y, Togashi J, Kaneko J *et al.* (2008) Portal vein complications after adult-to-adult living donor liver transplantation. *Transpl Int* 21:1136–1144.
5. Yerdel MA, Gunson B, Mirza D, Karayalçin K, Olliff S, Buckels J *et al.* (2000) Portal vein thrombosis in adults undergoing liver transplantation: risk factors, screening, management, and outcome. *Transplantation* 69: 1873–1881.
6. Ko GY, Sung KB, Gwon DI. (2021) The application of interventional radiology in living-donor liver transplantation. *Korean J Radiol* 22: 1110–1123.
7. Cheng YF, Ou HY, Tsang LL, Yu CY, Huang TL, Chen TY *et al.* (2010) Vascular stents in the management of portal venous complications in living donor liver transplantation. *Am J Transplant* 10:1276–1283.
8. Cavalcante A, Zurstrassen CE, Carnevale FC, Pugliese RPS, Fonseca EA, Moreira AM *et al.* (2018) Long-term outcomes of transmesenteric portal vein recanalization for the treatment of chronic portal vein thrombosis after pediatric liver transplantation. *Am J Transplant* 18:2220–2228.
9. Sawai Y, Kokudo T, Sakamoto Y, Takao H, Kazami Y, Nishioka Y *et al.* (2019) Stent placement for benign portal vein stenosis following pancreaticoduodenectomy in a hybrid operating room. *Biosci Trends* 12:641–644.

Original research article

IJAO The International Journal of Artificial Organs

Thick silk fibroin vascular graft: A promising tissue-engineered scaffold material for abdominal vein grafts in middle-sized mammals

The International Journal of Artificial Organs
2024, Vol. 47(3) 190–197

DOI: 10.1177/03913988241234547
journals.sagepub.com/home/jao
Sage

Kaito Fukuda[1], Junichi Kaneko[1], Sho Kiritani[1], Yui Sawa[1], Masaaki Morito[1], Mariko Tanaka[2], Tetsuo Ushiku[2], Chieh-Jen Cheng[3], Takashi Tanaka[3], Ryo Tanaka[3], Tetsuo Asakura[4], Yoshikuni Kawaguchi[1], Nobuhisa Akamatsu[1] and Kiyoshi Hasegawa[1]

Abstract

Abdominal vein replacement with synthetic tissue-engineered vascular grafts constructed from silk-based scaffold material has not been reported in middle-sized mammals. Fourteen canines that underwent caudal vena cava replacement with a silk fibroin (SF) vascular graft (15 mm long and 8 mm diameter) prepared with natural silk biocompatible thread were allocated to two groups, thin and thick SF groups, based on the graft wall thickness. The short-term patency rate and histologic reactions were compared. The patency rate at 2 weeks after replacement in the thin and thick SF groups was 50% and 88%, respectively ($p = 0.04$). CD31-positive endothelial cells covered the luminal surface of both groups at 4 weeks. The elastic modulus of the thick SF graft was significantly better than that of the thin SF graft (0.0210 and 0.0007 N/m^2, $p < 0.01$). Roundness of thick SF groups ($o = 0.8$ mm) was better than thin SF ($o = 2.0$ mm). There was significant difference between the groups ($p = 0.01$). SF vascular grafts are a promising tissue-engineered scaffold material for abdominal venous system replacement in middle-sized mammals, with thick-walled grafts being superior to thin-walled grafts.

Keywords

Hepatobiliary pancreatic surgery, venous replacement, silk fibroin, synthetic vascular graft

Date received: 30 October 2023; accepted: 7 February 2024

[1]Hepato-Biliary-Pancreatic Surgery Division, Department of Surgery, Graduate School of Medicine, The University of Tokyo, Bunkyo-ku, Tokyo, Japan
[2]Department of Pathology, Graduate School of Medicine, The University of Tokyo, Bunkyo-ku, Tokyo, Japan
[3]Department of Veterinary Surgery, Tokyo University of Agriculture and Technology, Fuchu, Tokyo, Japan
[4]Department of Biotechnology, Tokyo University of Agriculture and Technology, Koganei, Fuchu, Tokyo, Japan

Corresponding authors:
Junichi Kaneko, Hepato-Biliary-Pancreatic Surgery Division, Department of Surgery, Graduate School of Medicine, The University of Tokyo, 7-3-1 Hongo, Bunkyo-ku, Tokyo 113-8655, Japan.
Email: jkaneko-gi@umin.ac.jp

Kiyoshi Hasegawa, Hepato-Biliary-Pancreatic Surgery Division, Department of Surgery, Graduate School of Medicine, The University of Tokyo, 7-3-1 Hongo, Bunkyo-ku, Tokyo 113-8655, Japan.
Email: kihase-tky@umin.ac.jp

Introduction

Complete excision is currently the only curative treatment option for hepatobiliary pancreatic cancer. Although this cancer often invades major abdominal venous systems, such as the hepatic veins, inferior vena cava, portal vein, and superior mesenteric vein,[1–3] there was no better synthetic vascular grafts than expanded polytetrafluoroethylene as a material for those venous replacement.

For artery replacement, fully synthesized vascular grafts constructed from expanded polytetrafluoroethylene are frequently used. Although expanded polytetrafluoroethylene vascular grafts have been applied for vein replacement in hepato-biliary-pancreatic surgery,[4] their use is limited due to low-flow thrombogenicity without endothelialization and higher graft infection rates in contaminated tissue beds under digestive fluids.[5] Additionally, fully synthetic vascular grafts remain in the human body permanently and the long-term effects are unclear. To date, no alternative tissue-engineered venous grafts or scaffolds have been reported.

Silk fibroin (SF) is a promising tissue-engineered scaffold material derived from silk fiber with good biocompatibility, high affinity for cells, and susceptibility to proteolytic degradation in vivo without antigenicity.[6] Artery replacement in a rat model using double-raschel knitted SF vascular grafts coated with an SF sponge has been reported.[6,7] A recent study reported that SF application for rat vein replacement produced a better short-term outcome than expanded polytetrafluoroethylene, with acceptable patency and vascular remodeling.[8] The potential for extrapolation of these findings of better patency from our previous study in rats to a larger animal such as humans, however, is unknown. Veins comprise a low-pressure system, which, in humans, generally ranges from 8 to 10 mmHg with the central venous pressure ranging from 0 to 6 mmHg.[9] The intra-abdominal pressure of middle- and large-sized mammals is higher than that of small mammals. For example, the intra-abdominal pressure of a rat is 2.2 mmHg,[10] whereas it is 7.4 mmHg in canines and ranges from 5 to 15 mmHg in humans.[11,12] A higher intra-abdominal pressure than venous pressure can cause veins to collapse. A highly elastic synthetic vascular graft, therefore, could potentially collapse and obstruct sooner.

To explore the application of SF grafts in clinical practice, it is important to evaluate wider and longer synthetic SF vascular grafts in middle-sized mammals. The present study examined the patency rate and histologic reaction of thick and thin SF vascular grafts, thick and thin SF films with different wall strengths, as replacements for the caudal vena cava in a middle-sized mammal (canine).

Materials and methods

SF vascular grafts coated with an SF sponge

The vascular SF grafts were prepared as follows. SF double-raschel knit tubes with SF threads from *Bombyx mori* were prepared by two-needle stitch knitting on a computer-controlled double-raschel knit machine (Fukui Warp Knitting Co Ltd, Fukui City, Japan).[13] In detail, fertilized eggs of *Bombyx mori* were supplied by Gunma Sericultural Technology Center, and the larvae were reared in Asakura laboratory by feeding them an artificial diet (Silk Mata 2M, Nippon Nosan Kogyo Corp., Tokyo, Japan). *B. mori* cocoons were obtained. Marseille soap and sodium carbonate were purchased from Miyoshi soap Corp., Japan and Tokyo chemical industry Co., Ltd., Tokyo, Japan. A silk fiber was of 42 Deniers. For use in canines, the inner diameter was 8 mm. The SF fibers contained a small amount of silk sericin to maintain thread strength and avoid SF thread breakage in the knitting process. Therefore, the knit SF tube had to be degummed in a mixture of sodium carbonate (0.08% w/v) and Marseille soap (0.12% w/v) solution at 95°C for 2 h to remove the remaining silk sericin. Removal of silk sericin was confirmed by scanning electron microscope (Real surface view microscope VE-7800, Keyence, Tokyo, Japan).[14]

Thin coating (thin SF group). An expanded polytetrafluoroethylene rod was inserted into the knit SF tube. The rod covered with the SF tube was immersed into a pipe filled with a mixed aqueous solution of SF and glycerin (as a porogen) at a 1:1 (w/w) ratio for coating. Preparation of the SF aqueous solution was described previously.[15] The pipe was placed in a desiccator under a reduced pressure of 100 hPa until no air bubbles were observed on the coated surface of the SF tube.

Thick coating (thick SF group). A SF tube was set in a coaxial pipe and a mixed aqueous solution of SF and glycerin was poured into the gap between the pipe and SF tube. In details, the difference between the fabrication method of thin and thick coating was as follows: for thin coatings, the SF tube was removed from the pipe before freezing at −20°C, and then only the SF tube was freeze-dried later. On the other hand, for thick coatings, the SF tube was freeze-dried with the pipe at the same time, while still immersed in the solution.

The SF tubes of both groups were frozen at −20°C overnight before immersing in distilled water. Both SF grafts were freeze-dried and kept in a refrigerator until implantation into an animal.

Scanning SF grafts and measurement of physical properties

The knitted pattern of the SF fibers from the outside surface and a cross-section of 8-mm diameter SF grafts were observed by scanning electron microscopy (JSM-6360LA, Japan Electron Optics Laboratory Ltd., Tokyo, Japan).

Sample size was 10 mm long, 8 mm in diameter and total six SF grafts were used (three thick SF and three thin SF, respectively). The breaking strengths of the SF graft were measured using a tabletop material tester (EZ-graph,

SIMAZU Coup., Kyoto, Japan)[16]. Each sample SF vascular graft was placed in the testing machine and slowly extending it until they broke (Supplemental Figure 1A). The load cell was 100 N, and the stretching rate was 2 mm/min.

The compressive elastic modulus of the knitted grafts (10 mm long, 8 mm in diameter) was also determined using the same tabletop material tester. The load cell was 5 N, and the compression rate was 2 mm/min. The elastic modulus (N/mm^2), when compressed to 25% of the diameter, was calculated with the following formula: Elastic Modulus (Young's modulus), $E = \sigma$ (compressive stress)/ε (Δdiameter / diameter, strain) using analysis software (TRAPEZIUM, SIMAZU Coup., Kyoto, Japan; Supplemental Figure 1B, C).

Animal model

The study protocols (I-P16-034) and (R03-32) were approved by the University of Tokyo and the Tokyo University of Agriculture and Technology Animal Ethics Committee in accordance with the Japanese and ARRIVE (Animal Research: Reporting of In Vivo Experiments) guidelines. We used female beagles (Kitayama Labes Co.,Ltd., Nagano, Japan) weighing 8–17 kg. All canines were kept in cages for 2–4 weeks with a 12-h light/dark cycle. The canines were fasted overnight before undergoing the surgical procedure.

Surgical procedure

All surgical procedures were performed by hepato-biliary-pancreatic surgeons (KF, SK, and JK). The canines underwent general anesthesia using midazolam (0.2 mg/kg: Sandoz K.K, Tokyo, Japan) and buprenorphine (0.02 mg/kg; Nissin Co, Kanagawa, Japan) as premedication followed by intravenous injection of propofol (3 mg/kg body weight, titrated to effect; JMS Co., Ltd, Hiroshima, Japan) for induction and isoflurane (1.3%–1.6%; Pfizer, New York, NY, USA) for maintenance anesthesia by a veterinarian (C.C.). Cefazolin (20 mg/kg; Nichi-Iko Pharmaceutical Co, Ltd, Toyama, Japan) was given intravenously at the time of induction. No postoperative antibiotics were administered.

The caudal vena cava was exposed from the bifurcation of the renal veins to the bifurcation of the iliac veins, and all branches of the caudal vena cava were ligated and divided with 3-0 silk (Alfresa Pharma CO., Osaka, Japan) knotted sutures using an electric scalpel. After intravenous injection of unfractionated heparin (100 IU/kg; AY Pharmaceuticals Co., Ltd, Tokyo, Japan), the proximal and distal portions of the caudal vena cava were clamped with vascular clips. Approximately 15 mm of the caudal vena cava was removed and replaced with the SF vascular graft (15 mm long, 8 mm in diameter) by continuous sutures using 6-0 Prolene (Johnson & Johnson med Co., Raritan, NJ, USA), starting with two stay sutures 180° apart at both the cranial and caudal sides, then suturing the back wall, followed by the front wall. The cranial and caudal sides of the vascular graft were de-clamped (Figure 2). Anticoagulants, Dalteparin (100 U/kg three-times-daily, Nichi-Iko Pharmaceutical Co, Ltd, Toyama, Japan) was given subcutaneously for 7 days.. Clopidogrel (Sawai Pharmaceutical Co, Ltd, Osaka, Japan) was given orally at day 0 with a loading dose of 4 mg/kg followed by 2 mg/kg once daily on days 1, 2, 3, 5, and 7.

Patency assessment

The patency of the SF graft vascular grafts was monitored extracorporeally by Doppler ultrasonography (EnVisor M25040A; Phillips, Tokyo, Japan) on postoperative days 1, 3, 5, and 7, and then every week for 4 weeks, and then every month. Graft occlusion was defined as the absence of a color Doppler signal. In the absence of a color Doppler signal, the canine was anesthetized as mentioned above, and the graft was grossly and pathologically evaluated.

Histologic analysis

At 4 weeks after surgery or at the time of confirming an occlusion, the canines underwent general anesthesia as described above. The grafts were carefully removed with the surrounding tissue. Cross-sections of the middle of the SF grafts were fixed in 20% formalin, embedded in paraffin, and sectioned (4-μm thick, Tissue-Tek Auto Section, Sakura Finetek Japan Co., Ltd.) for hematoxylin and eosin staining. Elastica van Gieson staining was applied to detect elastic and collagen fibers. Immunohistochemical staining was performed as previously reported.[17] The sections were incubated with primary antibodies, including alkaline phosphatase-conjugated anti-alpha smooth muscle actin (anti-αSMA; clone 1A4, MilliporeSigma, St. Louis, MO, USA), anti-rat CD 31 antibody (clone TLD-3A12, BD Biosciences, San Jose, CA, USA), and anti-podoplanin antibody (ab11936, Abcam, Cambridge, MA, USA) followed by incubation with biotinylated anti-mouse immunoglobulin (Ig) G secondary antibody (DAKO, Glostrup, Denmark).

Roundness was measured on each cross-section of thin and thick SF grafts in hematoxylin and eosin staining, was calculated with the following formula: roundness (mm, diameter measurement method) = difference between circumscribed and inscribed circle in diameter / 2. The analysis was performed using Image J software (version 1.44; National Institute of Mental Health Bethesda, MD, USA).[18]

To know thickness of normal native caudal vena cava of canine, hematoxylin and eosin, and EVG staining were performed.

Rats were also anesthetized and grossly and pathologically evaluated at 1 month and 12 months after surgery. To

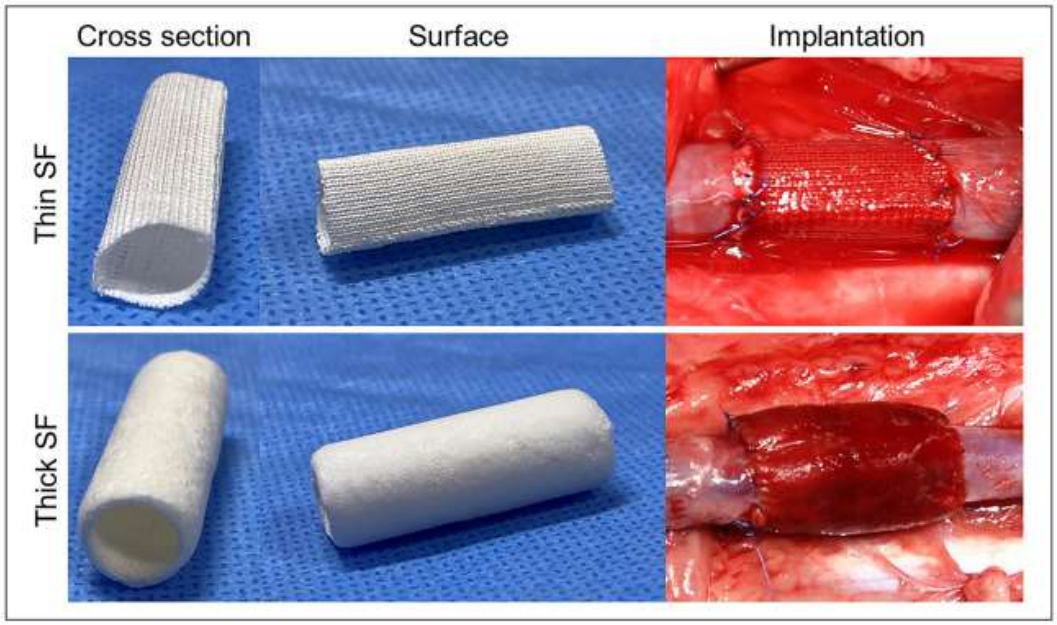

Figure 1. Thin SF had a reticulate appearance on gross examination, whereas the thick SF had a sponge-like appearance with a soft texture. In both SF groups, the graft turned red after implantation in canine (8.0 mm in diameter, 15 mm length) because the blood cells infiltrated the interfiber space, but did not leak out of the graft.

determine the degree of degradation, semi-quantitative analysis was used to evaluate the ratio of SF fibers and infiltrated tissue area of a representative cross-section of the SF graft wall. SF fibers, observed as aggregations of transparent dots on a representative cut surface, were encircled by yellow lines on a histologic image by three surgeons (KF, JK, and YS). The area of infiltrated autologous cells—the other area of the whole SF graft wall—was encircled with a blue line. The ratio of the remaining SF fiber area (yellow) to autologous cells (blue) was determined to calculate the area of 1 cut surface of the SF graft that was replaced by autologous cells at 1 and 12 months. The analysis was performed using Image J software (version 1.44; National Institute of Mental Health Bethesda, MD, USA).[18]

Statistical analysis

Continuous variables are expressed as the median and range. The backgrounds of each group were compared using the Mann–Whitney *U* test or Student *t* test. The log-rank test was used to compare the patency rate. A *p*-value less than 0.05 was considered statistically significant. Statistical analysis was conducted using software (JMP Pro version 16.0.0; SAS Institute, Cary, NC, USA).

Results

Appearance, scanning electron microscopy of SF grafts, and measurement of its physical properties

Thin SF grafts had a reticulate appearance on gross examination, whereas the thick SF grafts had a sponge-like appearance with a soft texture (Figure 1). After implantation, the color of grafts in both SF groups changed to red because blood cells infiltrated the interfiber space, but did not leak out of the graft. Scanning electron microscopy images, including the surfaces and cross-sections of SF grafts coated with SF sponges, are shown in Figure 2. The images revealed a reticulate and sponge-like appearance of both the thin and thick SF surfaces. In the cross-section, the thickness of the thin SF was 500 µm, whereas the thick SF graft thickness was 1500 µm. The cross-section view revealed that two-thirds of the external side of the thick SF grafts was coated with SF sponge.

Breaking strength was not significantly different between the thin and thick SF groups (35.5 and 42.2, $p=0.29$), whereas the elastic modulus differed significantly (0.0210 and 0.0007 N/m^2, $p<0.01$, Figure 2a, b). Stress–strain curve was shown in Supplemental Figure 2.

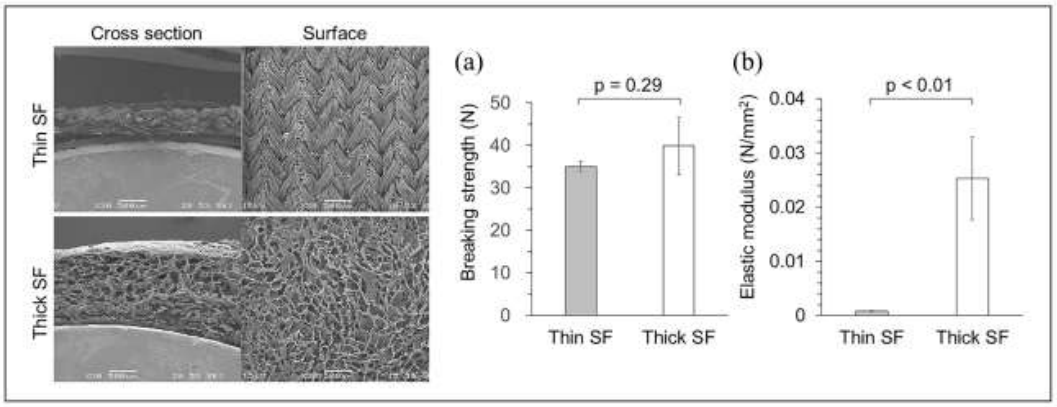

Figure 2. Scanning electron microscopy images including the surfaces and cross-sections of SF grafts coated with SF sponges are shown. Breaking strength did not differ significantly between the thin and thick SF groups (35.5 and 42.2, $p = 0.29$), whereas the elastic modulus was significantly different between groups (0.0210 and 0.0007 N/m^2, $p < 0.01$).

Animal model

We implanted 12 canines, 4 with the thin SF graft (thin SF group) and 8 with the thick SF graft (thick SF group). The median weight of the thin SF group was 8.0 kg (range 7.6–8.8) and that of the thick SF group was 8.2 (range 7.5–9.4), indicating no significant difference between groups ($p = 0.864$). The median diameter (8.0 mm vs 8.0 mm; $p = 1.000$) and length (15 mm [range 15–19 mm] vs 15 mm [range 15–15], $p = 0.296$) of the replaced caudal vena cava were not significantly different between the groups.

The inferior vena cava of two rats (13–14 weeks of age, weighing 400 g) were replaced by thin and small SF grafts (3 mm diameter, 10 mm length).

Graft patency

A representative Doppler ultrasonography result showing the flow inside the SF graft, indicating better venous flow, is shown in Figure 3a, b. Although the thin SF graft seemed to show slight stenosis of the intra-luminal diameter compared with the other parts of the canine caudal vena cava (Figure 3a), the thick SF graft seemed to have the same intra-luminal diameter (Figure 3b).

On postoperative day 1 (24 h later), the intra-luminal diameters differed significantly between the thin and thick SF vascular grafts (2.23 and 4.27 mm, respectively, $p < 0.01$, Figure 3) The patency rate is shown in Figure 4. Although there was no significant difference between the groups (log-rank, $p = 0.18$), there was a significant difference at day 14 (Student's t test, $p = 0.04$). At 28 days later, 50% (4/8) of the thick SF grafts were patent.

In the two rats, the grafts were patent at both 1 and 12 months, with no complications.

Histologic analysis

Hematoxylin and eosin staining of the thin and thick SF vascular grafts is shown in Figure 5. The graft lumens of both groups remained patent, but the walls of the thin SF grafts were deformed (Figure 5a) compared with those of the thick SF grafts (Figure 5b). In both the thin and thick SF vascular grafts, cellular proliferation was observed around the SF fibers, and the luminal surfaces were covered by flat cells (Figure 5). Elastica van Gieson staining of the SF vascular grafts revealed collagen fibers around the SF fibers, but no elastic fibers, (Figure 5, EVG). CD31 was expressed on the luminal surface of both SF vascular graft types (Figure 5, CD31). Anti-alpha smooth muscle actin antibody staining of the SF vascular grafts was positive (Figure 5, αSMA).

Roundness of thick SF groups ($o = 0.8$ mm) was better than thin SF ($o = 2.0$ mm). There was significant difference between the groups ($p = 0.01$).

Hematoxylin and eosin and EVG staining of normal native caudal vena cava of canine showed that wall thickness was around 1200 μm (Supplemental Figure 3a, b). It was approximately two times thicker than native caudal vena cava of rat, around 600 μm in previous our report [8].

Discussion

This is the first report of SF vascular grafts for abdominal venous replacement in a canine model. We found that SF vascular grafts require a certain modulus of elasticity to have less deformity and better patency in middle-sized mammals. Furthermore, 89.5% of the SF vascular wall at 12 months was substituted by autologous cells, indicating better SF vascular graft degradation ability in rat.

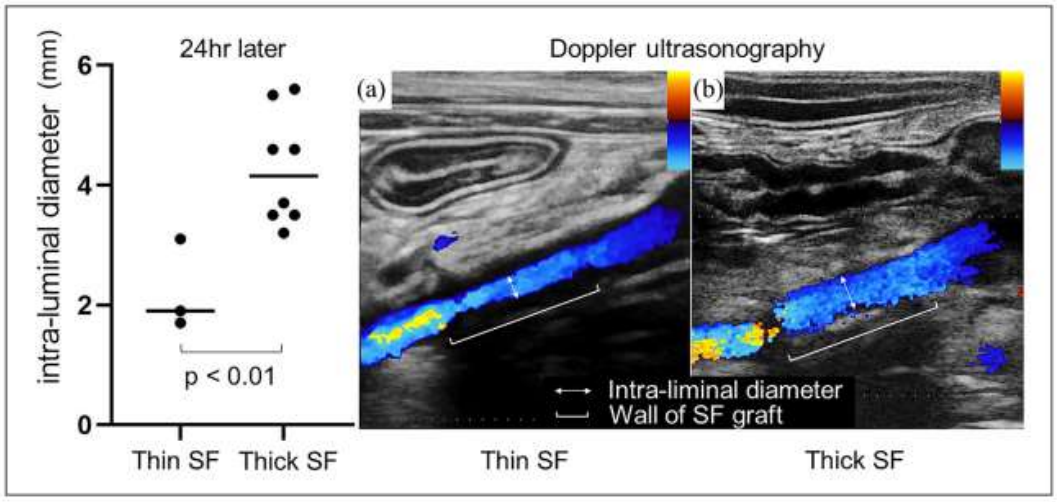

Figure 3. A representative Doppler ultrasonography result showing colored flow inside of the SF graft, indicating better venous flow as shown in (a) and (b). Although the thin SF grafts exhibited slight stenosis of the intra-luminal diameter compared with the other parts of the canine caudal vena cava (a), the thick SF was not stenotic (b). The intra-luminal diameter of the thin and thick SF vascular grafts was significantly different on postoperative day 1 (2.23 mm vs 4.27 mm, respectively, $p < 0.01$). Note, yellow color (a and b) indicated high velocity with disturbed flow, suggesting stenosis of anastomosis.

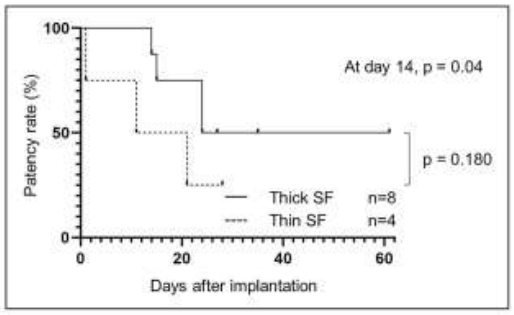

Figure 4. Although there was no overall significant difference in the patency of the grafts between groups (log-rank, $p = 0.18$), a significant difference was detected at day 14 (Student's t test, $p = 0.04$). At 28 days, 50% of the grafts in the thick SF group were patent (4/8).

Unlike the arterial system, vein walls do not have much elasticity due to a lack of, or fewer, elastic fibers in mammals. Contrary to our expectation, the thick SF grafts with a certain modulus of elasticity had better patency. In present study, we concluded that tortuous wall with narrow lumen due to inferior of roundness of thin SF grafts made inside narrower and led to earlier occlusion. As patency rate was shown in Figure 4, initial experiment using thin SF graft resulted in early obstruction, with 75% occlusion within 21 days (at day 14, $p = 0.04$). This led us to decide to increase the elasticity by adding thickness to the SF grafts, creating a new thick SF graft. We found that synthetic SF vascular grafts for the abdominal venous system should have a better modulus of elasticity, at least 40 N/mm^2 in canine caudal vena cava replacement model. The flexibility of the venous wall is another crucial point for maintaining a certain luminal diameter, but the thin SF grafts tended to collapse soon after insertion into the canine abdominal vein. As mentioned in the introduction, the larger the mammal's body size, the higher the intra-abdominal pressure.[11] We found that a certain wall strength was required to maintain the luminal diameter, even for synthetic vein grafts. Further studies are needed to determine the precise correlation among venous pressure, intrabdominal pressure, wall strength of the SF vascular graft, and the change in flexibility after replacement.

Matsumura et al.[19] reported graft stenosis that occurred at 1 month after venous replacement using 8-mm diameter biodegradable scaffolds consisting of polyglycolide knitted fibers with a 3.6-mm intra-liminal diameter. They suggested that stenotic changes may lead to tissue regeneration disorders, blood flow disturbance, and more thrombogenesis. In the present study, we found that stenosis developed at 24 h after replacement. The intra-liminal diameter of the thick SF vascular graft (4.3 mm) was larger than that of the thin SF graft (2.2 mm). The venous system has low pressure, however, and vascular grafts require higher elasticity to avoid stenosis and maintain better patency. Intramural thrombus was another problem and 50% of the thick SF grafts became obstructed within 4 weeks. A previous report

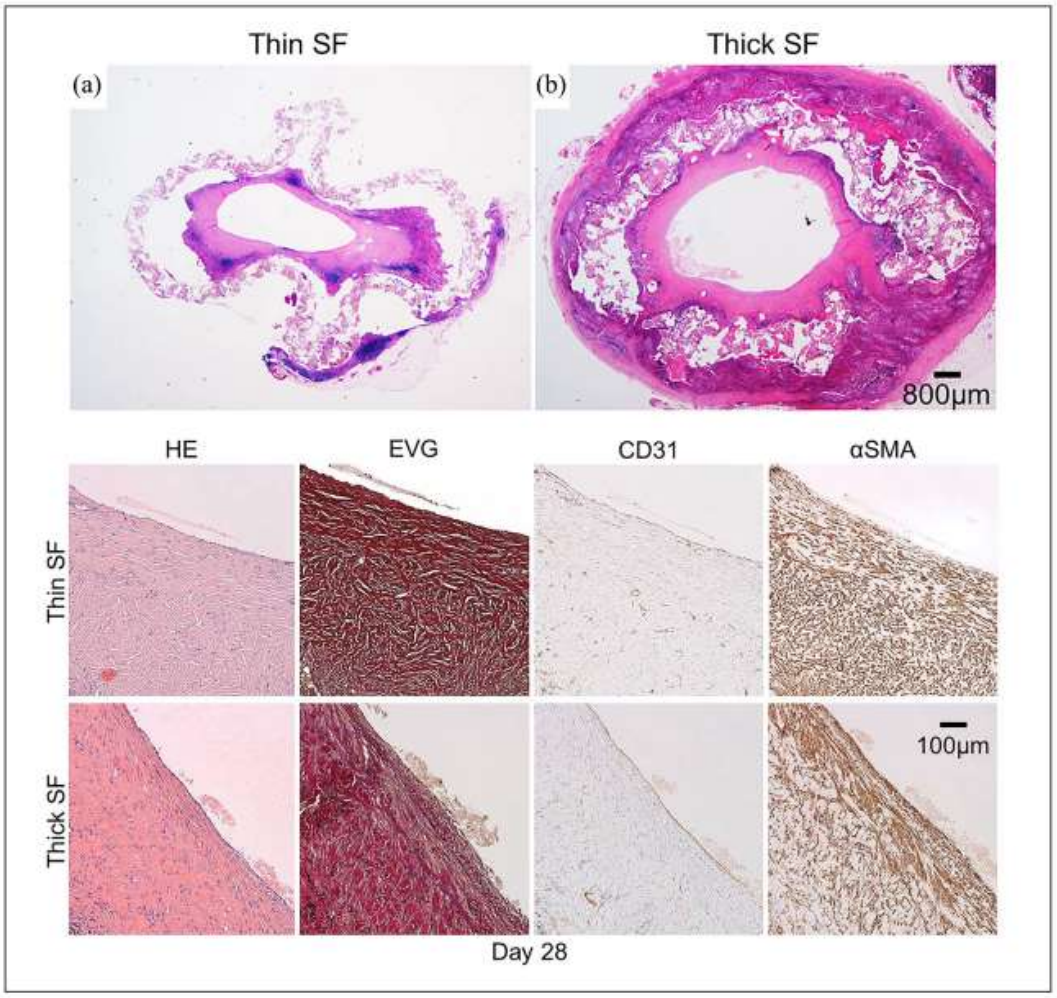

Figure 5. Hematoxylin and eosin staining of thin and thick SF vascular grafts is shown. The lumens of both the thin and thick grafts remained patent, but the wall of the thin SF graft was deformed (a) compared with the thick SF graft (b). In both the thin and thick SF vascular grafts, cellular proliferation was observed around the SF fibers, and the luminal surfaces were covered by flat cells. Elastica van Gieson staining of the SF vascular graft revealed collagen fibers (red) around the SF fibers, but no elastic fibers (EVG). CD31 was expressed on the luminal surface of both SF vascular graft types (CD31). Anti-alpha smooth muscle actin (αSMA) antibody staining of the SF vascular grafts was positive and adjacent to CD31-positive cells.

confirmed that endothelialization occurs within 4 weeks after venous replacement in rat,[8] and the present study is the first to confirm endothelialization in a canine model with a SF vascular graft. Early after placement of the SF vascular graft, however, the graft developed low-flow thrombogenicity without endothelialization. SF vascular grafts may need to be coated with a heparin-like substance coating to avoid early intramural thrombus development, and this requires further study.

Although we did not establish tolerance against bacterial infection in this study, autologous cells were seeded into the SF fibers of present the SF vascular grafts in canine. Outcome might allow SF vascular grafts to tolerate bacterial infection, but further studies are needed.

In conclusion, thick SF vascular grafts were better than thin SF vascular grafts as a promising tissue-engineered scaffold material for abdominal vein replacement in middle-sized mammals.

Author contributions

Conceptualization: S.K., J.K., R.T., and T.A. Methodology: J.K., R.T., M.T., T.U., and T.A. Data curation: K.F., S.K., Y.S., M.M., C.C., T.T., and J.K. Formal Analysis: S.K., J.K., M.T., and T.U. Writing—original draft: K.F. and J.K. Writing—review & editing: Y.K., N.A., and K.H. Funding acquisition and Project administration: J.K. and K.H. Supervision: Y.K., N.A., and K.H. All authors read and approved the final version of the manuscript for submission.

Declaration of conflicting interests

The author(s) declared no potential conflicts of interest with respect to the research, authorship, and/or publication of this article.

Funding

The author(s) disclosed receipt of the following financial support for the research, authorship, and/or publication of this article: This study was funded by NIPRO Corp., Tokyo, Japan., and the work was supported by grant no. 19K09191 (Kaneko) from the Ministry of Education, Culture, Sports, Science, and Technology of Japan, as an academic-industrial collaboration.

ORCID iDs

Junichi Kaneko https://orcid.org/0000-0002-1284-5639
Kiyoshi Hasegawa https://orcid.org/0000-0001-8734-740X

Supplemental material

Supplemental material for this article is available online.

References

1. Lynch SM, Vrieling A, Lubin JH, et al. Cigarette smoking and pancreatic cancer: a pooled analysis from the pancreatic cancer cohort consortium. *Am J Epidemiol* 2009; 170: 403–413.
2. Demir IE, Jäger C, Schlitter AM, et al. R0 versus R1 resection matters after pancreaticoduodenectomy, and less after distal or total pancreatectomy for pancreatic cancer. *Ann Surg* 2018; 268: 1058–1068.
3. Klaiber U, Leonhardt CS, Strobel O, et al. Neoadjuvant and adjuvant chemotherapy in pancreatic cancer. *Langenbecks Arch Surg* 2018; 403: 917–932.
4. Chu CK, Farnell MB, Nguyen JH, et al. Prosthetic graft reconstruction after portal vein resection in pancreaticoduodenectomy: a multicenter analysis. *J Am Coll Surg* 2010; 211: 316–324.
5. Shell DHt, Croce MA, Cagiannos C, et al. Comparison of small-intestinal submucosa and expanded polytetrafluoroethylene as a vascular conduit in the presence of gram-positive contamination. *Ann Surg* 2005; 241: 995–1001; discussion 1001–1004.
6. Asakura T, Tanaka T and Tanaka R. Advanced silk fibroin biomaterials and application to small-diameter silk vascular grafts. *ACS Biomater Sci Eng* 2019; 5: 5561–5577.
7. Enomoto S, Sumi M, Kajimoto K, et al. Long-term patency of small-diameter vascular graft made from fibroin, a silk-based biodegradable material. *J Vasc Surg* 2010; 51: 155–164.
8. Kiritani S, Kaneko J, Ito D, et al. Silk fibroin vascular graft: a promising tissue-engineered scaffold material for abdominal venous system replacement. *Sci Rep* 2020; 10: 21041.
9. Tansey EA, Montgomery LEA, Quinn JG, et al. Understanding basic vein physiology and venous blood pressure through simple physical assessments. *Adv Physiol Educ* 2019; 43: 423–429.
10. Lee T and Yoon SM. The role of intra-abdominal pressure measurement in Awake rat cystometry. *Int Neurourol J* 2013; 17: 44–47.
11. Smith SE and Sande AA. Measurement of intra-abdominal pressure in dogs and cats. *J Vet Emerg Crit Care* 2012; 22: 530–544.
12. Milanesi R and Caregnato RC. Intra-abdominal pressure: an integrative review. *Einstein* 2016; 14: 423–430.
13. Aytemiz D, Sakiyama W, Suzuki Y, et al. Small-diameter silk vascular grafts (3 mm diameter) with a double-raschel knitted silk tube coated with silk fibroin sponge. *Adv Healthc Mater* 2013; 2: 361–368.
14. Yagi T, Sato M, Nakazawa Y, et al. Preparation of double-raschel knitted silk vascular grafts and evaluation of short-term function in a rat abdominal aorta. *J Artif Organs* 2011; 14: 89–99.
15. Asakura T, Kuzuhara A, Tabeta R and Saito H. Conformational characterization of Bombyx mori silk fibroin in the solid state by high-frequency carbon-13 cross polarization-magic angle spinning NMR, x-ray diffraction, and infrared spectroscopy. *Macromolecules* 1985; 18: 1841–1845.
16. Saotome T, Hayashi H, Tanaka R, et al. Introduction of VEGF or RGD sequences improves revascularization properties of Bombyx mori silk fibroin produced by transgenic silkworm. *J Mater Chem B* 2015; 3: 7109–7116.
17. Sata M, Saiura A, Kunisato A, et al. Hematopoietic stem cells differentiate into vascular cells that participate in the pathogenesis of atherosclerosis. *Nat Med* 2002; 8: 403–409.
18. Schneider CA, Rasband WS and Eliceiri KW. NIH Image to ImageJ: 25 years of image analysis. *Nat Methods* 2012; 9: 671–675.
19. Matsumura G, Nitta N, Matsuda S, et al. Long-term results of cell-free biodegradable scaffolds for in situ tissue-engineering vasculature: in a canine inferior vena cava model. *PLoS ONE* 2012; 7: e35760.

DOI: 10.1002/jhbp.1357

ORIGINAL ARTICLE

Two-step artificial intelligence algorithm for liver segmentation automates anatomic virtual hepatectomy

Yusuke Kazami[1] | **Junichi Kaneko**[1] | **Deepak Keshwani**[2] | **Yoshiro Kitamura**[2] | **Ryugen Takahashi**[1] | **Yuichiro Mihara**[1] | **Akihiko Ichida**[1] | **Yoshikuni Kawaguchi**[1] | **Nobuhisa Akamatsu**[1] | **Kiyoshi Hasegawa**[1]

[1]Hepato-Biliary-Pancreatic Surgery Division, Department of Surgery, Graduate School of Medicine, The University of Tokyo, Tokyo, Japan

[2]Imaging Technology Center, Fujifilm Corporation, Tokyo, Japan

Correspondence
Kiyoshi Hasegawa, Hepato-Biliary-Pancreatic Surgery Division, Department of Surgery, Graduate School of Medicine, The University of Tokyo, 7-3-1 Hongo, Bunkyo-ku, Tokyo 113-8655, Japan.
Email: hasegawa-2su@h.u-tokyo.ac.jp

Funding information
Fujifilm Corporation; Ministry of Education, Culture, Sports, Science, and Technology of Japan, Grant/Award Number: 19K09191

Abstract

Background: Anatomic virtual hepatectomy with precise liver segmentation for hemilivers, sectors, or Couinaud's segments using conventional three-dimensional simulation is not automated and artificial intelligence (AI)-based algorithms have not yet been applied.

Methods: Computed tomography data of 174 living-donor candidates for liver transplantation (training data) were used for developing a new two-step AI algorithm to automate liver segmentation that was validated in another 51 donors (validation data). The Pure-AI (no human intervention) and ground truth (GT, full human intervention) data groups were compared.

Results: In the Pure-AI group, the median Dice coefficients of the right and left hemilivers were highly similar, 0.95 and 0.92, respectively; sectors, posterior to lateral: 0.86–0.92, and Couinaud's segments 1–8: 0.71–0.89. Labeling of the first-order branch as hemiliver, right or left portal vein perfectly matched; 92.8% of the second-order (sectors); 91.6% of third-order (segments) matched between the Pure-AI and GT data.

Conclusions: The two-step AI algorithm for liver segmentation automates anatomic virtual hepatectomy. The AI-based algorithm correctly divided all hemilivers, and more than 90% of the sectors and segments.

KEYWORDS

anatomic virtual hepatectomy, artificial intelligence, automatic liver segmentation, automatic liver vessel extraction, deep learning

1 | INTRODUCTION

Liver cancer is the third leading cause of cancer death, with an estimated 0.8 million deaths in 2020.[1] Hepatectomy is crucial treatment for liver cancer[2] and colorectal liver metastases.[3] To ensure a safe hepatectomy and avoid postoperative liver failure, preoperative virtual hepatectomy with three-dimensional (3D) simulation has become the standard procedure for surgical planning and intraoperative navigation to precisely estimate the liver resection volume.[4,5]

Based on the Brisbane 2000 terminology,[6] the liver is anatomically divided and segmented into two hemilivers, four sectors(section), and eight segments corresponding

to the perfusion area of the portal vein (PV) according to the Couinaud classification. While anatomic hepatectomy is critical to maximize the functional future liver remnant volume and minimize cancer recurrence,[4,7,8] precise liver segmentation by conventional 3D simulation remains challenging.[9,10] Currently, anatomic virtual hepatectomy has not been automated, and conventional software requires verification and correction by expert surgeons and radiologists.

Artificial intelligence (AI) has attracted high attention for developing new algorithms for medical image pattern recognition, but an AI-based algorithm for liver segmentation has not been reported. Furthermore, no evaluation method exists for verifying the accuracy of AI algorithms for this purpose.

In the present study, we report a new two-step AI algorithm aiming at automating liver segmentation and evaluate its accuracy and quality from the viewpoint of liver surgeons.

2 | METHODS

Between 2012 and 2019, consecutive 284 donor candidates for living-donor liver transplantation with no history of any disease underwent computed tomography (CT) at the University of Tokyo Hospital during the donor evaluation steps. Among them, 59 donor candidates were excluded due to a thicker CT slice, 5-mm thick CT data. CT images from the remaining 225 donor candidates were included in the study. The retrospective cohort study was approved by the local ethics committee of the University of Tokyo Hospital (2018201NI). An opt-out statement was publicly disclosed (http://plaza.umin.ac.jp/htokyotransplant/results/index.html). None of the donor candidates were opposed to being included in the present study.

2.1 | CT scanning

Multidetector row CT was performed with a tube voltage of 120 kVp (Aquillion; Canon Medical Systems Corporation). The CT images (1-mm thick) were obtained at 0.85-mm intervals by scanning for 20, 25, and 75 s, respectively, after injecting an iodine-based contrast media (Omnipaque 350; Daiichi Pharmaceutical; 2 mL/kg bodyweight, maximum dose of 100 mL) within 30 s. The late portal phase, scanning at 75 s, was used for the study.

2.2 | Training and validation data

The training and validation data comprised CT from 174 and 51 donor candidates obtained from 2012 to 2017, and 2018 to 2019 (Figure 1). The donor characteristics were collected.

In the training data, the outer edge of the whole liver, PV, and hepatic vein (HV) branches were extracted from the CT data of each of the 174 donors to develop the first and the second step of the AI algorithm. The first step of the AI algorithm to extract the PV and HV from the CT data has been previously reported[11] (Synapse Vincent, version 6, Fujifilm Corp.). To develop the second step of the AI, 2 experts, hepato-biliary surgeons with 10 and 9 years of experience (YK and RT, respectively), made corrections and labeled each of the PV and HV branches to define the two hemilivers, four sectors, and eight segments for liver segmentation, as described later. Two other experts, two senior experts, hepato-biliary surgeons with 20 years of experience (JK, KH), confirmed the labeled and segmented PV branches or discussed the anatomy with them in a clinical meeting for consistency of the evaluation. These experts provided the PV branch labeling and segmentation of the training data were used for the deep learning. Then,

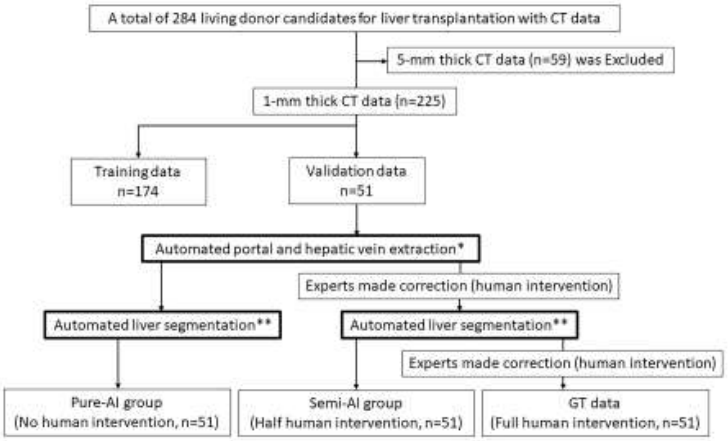

FIGURE 1 Flow-chart of the Pure- and Semi-AI groups and GT data. *The first step of artificial intelligence (AI); **the second step of AI; CT, computed tomography; GT, ground truth.

two-step artificial intelligence algorithm was evaluated in the validation data.

2.3 | Pure- and Semi-AI, and ground truth data groups

In the validation step, three groups were created. The Pure-AI group (no human intervention, $n=51$) comprised the data for which no corrections were made, as shown in Figure 1. The Semi-AI group (half human intervention, $n=51$) comprised the data for which the experts made corrections after the first AI step. The experts also made corrections after each of the AI steps, classifying the errors as missing (i.e., failing to extract) or misclassifying (i.e., successful extraction but labeled incorrectly) the PV and HV branches after the first AI step, and mis-dividing the liver segmentation after the second AI step. These data were defined as the ground truth (GT) data (full human intervention, $n=51$). The time required to make the corrections for each case was recorded.

2.4 | Portal vein branch labeling

All PV branches were labeled and categorized as first to third-order PV branches: hemiliver (first-order branches; right, left), sector (same as "section", second-order branches; posterior, anterior, medial, lateral), and segment (third-order branches; Couinaud's segments 1–8), based on the Tokyo terminology for the updated Brisbane 2000 system.[6,12]

The first-order branches were defined as those branching off the main trunk of the PV. Second-order branches were defined as those directly arising from the right and umbilical portion of the left PV. Anatomic variations, for example, a trifurcation, a separate and sole right posterior vessel branching off the main trunk of the PV, were categorized as a second-order branches of the PV. A third-order branch was defined as any Couinaud's segment branch, for example, a branch coming from a third-order branch as a different Couinaud's segment branch that was categorized as a third-order branch. For example, when a segment 5 branch arose from a segment 8 branch, both branches were categorized as third-order branches.

2.5 | Couinaud's concept of liver segmentation

The right hemiliver comprises two sectors, posterior and anterior sectors. The posterior sector is made up of superior segment 7 and inferior segment 6, and the anterior sector is made up of superior segment 8 and inferior segment 5. The left hemiliver also comprises two sectors, medial and lateral, which are separated by the falciform and round ligaments. The left medial sector is not divided and comprises single segment 4.[13] The left lateral sector is divided into two segments (superior segment 2 and inferior segment 3). Segment 1 is defined by a small PV branch that could not be defined as a second-order branch into any sector, branching directly from the main trunk or a first-order branch of the PV. Segmentation also depends on the hepatic vein (HV). The Rex-Cantlie line with the middle HV divides the right and left hemilivers. The right HV is segmented into posterior and anterior sectors, and the left HV is divided into segments 2 and 3 as an intersegmental plane.[14]

2.6 | Deep learning-based algorithm for automated segmentation

To extract the PV and HV, the first step of the AI algorithm used a method that has previously been reported.[11] In the second step, input data from the CT imaging and 3D reconstruction model of the liver, and the PV trees are evaluated in two substeps. First, the PVs are divided into four sector branches, including segment 1. Second, the PVs are subdivided into eight segment branches. Then, Voronoi tessellation is applied to the labeled PV tree to compute the perfusion area of each PV branch as shown in Figure 2a.

A 3D fully convolutional neural network (FCN) is used for the PV labeling task. A 3D FCN has two parts, an encoder and decoder, as illustrated in Figure 2b. The encoder part consists of consecutive convolution, pooling, and nonlinear activation layers. Due to several pooling layers in the encoder, the feature maps generated from the encoder had small spatial dimensions. The decoder, which consists of several up-sampling layers and convolution layers, maps the encoder feature maps to spatial dimensions the same as that of the input image.

For the task of classifying the PV into sector branches, the FCN is trained to label the PV into five branch clusters, that is, posterior, anterior, medial, and lateral sectors, and segment 1. The inputs for the neural network are the CT images, PV mask, HV mask, and liver mask, defining the area outside the masked areas as a negative (0 valued) image. The neural network was trained to output labeled PV branches such that each voxel in the labeled image belongs to one of the five branch clusters. The weights of each of the layers in the neural network are trained such that the output PV-labeling tree is as close to the GT PV-labeling tree. The training was done using a backpropagation algorithm,[15] which is a standard algorithm used in

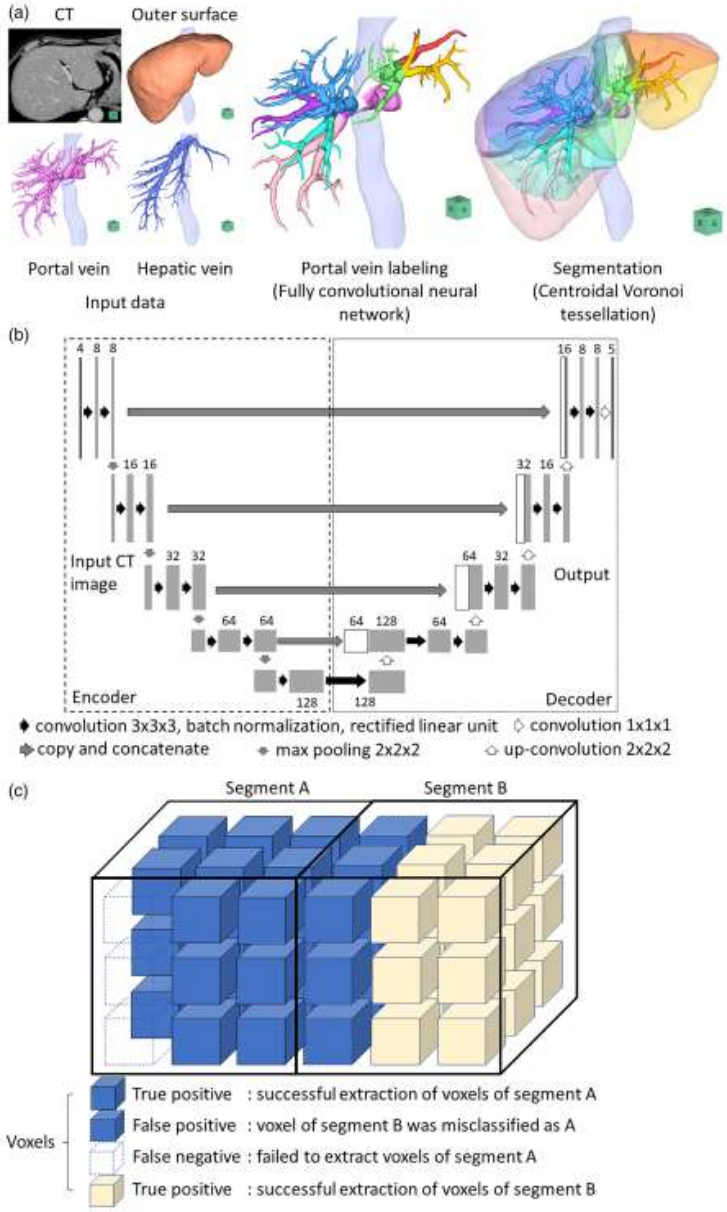

FIGURE 2 Overview of the liver segmentation training in the AI, deep learning-based algorithm. (a) In the second step of the AI-based algorithm, two substeps were used to automate the PV labeling into segment PV branches. The input data is the CT image and 3D reconstruction model of the liver, and PV and HV trees. First, all PV branches are divided into the four sector branches and segment 1. Second, they are subdivided into the eight segment branches. Then, Voronoi tessellation is applied to the labeled branches to compute the perfusion area. (b) A 3D fully convolutional neural network (FCN) was used for the PV labeling task. The 3D FCN has two parts, an encoder and decoder. (c) All areas of the hemiliver, sectors, and Couinaud's segments are represented as an aggregation of voxels with following attribution, hemiliver (right or left), sector (posterior, anterior, medial, and lateral), and segment (1–8). Accuracy was calculated on the difference of attribution of each voxel between Pure- /Semi-AI groups and the ground truth data as shown in the figure.

deep learning that utilizes a multi-class dice loss function (Figure S1) as shown in the following equation. Multi-class refers to the five branch clusters, that is, posterior, anterior, medial, lateral sectors, and segment 1.

$$\text{Loss} = 1 - \frac{1}{C}\sum_{c=1}^{C}\frac{2*\sum_i p_i(c)g_i(c)}{\sum_i p_i(c)+g_i(c)}, i\forall PV_i = 1$$

Here, $p_i(c)$ is the predicted probability for voxel i being class c (e.g., c = anterior sector, as one of the 5 branch clusters), $g_i(c)$ is the GT, so-called ground truth probability map which takes a value of 0 to 1, for voxel i being class c. When voxel i is located in class c and $g_i(c)$ is close to 1, $p_i(c)$ takes value of close to 1; if no, $p_i(c)$ takes value of close to 0. C is the total number of classes; five for this task. Loss was computed only for PV voxels (PV_i=1), the regions

outside the PV mask ($PV_i = 1$) are ignored and were not included in the training.

To further subdivide the portal branches associated with each sector, three separate 3D FCNs for the posterior, anterior, and lateral sectors were used. Each 3D FCN used the same input data for the division into sectors, and outputs 2 class label images of the PVs. For example, one 3D FCN was trained to separate the lateral PV into segments 2 and 3. The architecture of the neural network was similar to that shown in Figure 2b, except that the final scoring layer ($1 \times 1 \times 1$ convolution) outputs two images instead of five. The loss function used for training the 3D FCN for segment labeling was similar to the above equation with $C = 2$ because the total number of output classes was 2. Additionally, for each of the 3D FCNs, the loss was computed only over voxels i that belong to the posterior, anterior, and lateral regions, respectively. The following equation shows the loss computation for the 3D FCN trained to separate the lateral PV into segments 2 and 3, respectively. In the equation, PL is the GT label of PV at voxel i.

$$\text{Loss} = 1 - \frac{1}{C}\sum_{c=1}^{C} \frac{2 * \sum_i p_i(c) g_i(c)}{\sum_i p_i(c) + g_i(c)}, i \forall PL_i = 2 \mid PL_i = 3$$

Once a PV branch enters one of the areas and travels a certain distance, the label of the PV should not change and was added to the post-processing as a rule-based constraint.

2.7 | Accuracy of automated segmentation

All areas of the hemiliver, sectors, and Couinaud's segments were represented as an aggregation of voxels classified with each of the three attributes (hemiliver [left or right], sector [posterior, anterior, medial and lateral], and segment[1–8]) on the 3D simulation data as shown in Figure 2c. Attribution of these voxels for the Pure- and Semi-AI groups, and GT data were compared to determine the true positive, false positive, and false negative rates, and the similarities among the Pure- and Semi-AI groups, and the GT data. The Dice coefficient,[16] which ranges between 0 and 1, with 1 signifying the greatest similarity[17] was applied. The formula is given as,

$$\frac{2\ \text{true positives}}{2\ \text{true positives} + \text{false positive} + \text{false negative}}$$

Segmentation was evaluated by comparing the accuracy of the automated PV branch labeling and volumes of automated segmentation among the Pure- and Semi-AI groups, and the GT data.

2.8 | Preliminary clinical data

In the clinical setting, the Pure-AI algorithm has been used for preoperative 3D simulation since April 2023. Clinical data, including blood loss, operation time, estimated liver volume, and actual graft liver weight of 10 consecutive donors, was collected during March 2023 ($n = 5$, right 3/left 2, No-AI group, Synapse Vincent, version 5.5), and April 2023 ($n = 5$, right 3/left 2, Pure-AI group, version 6.8).

2.9 | Statistical analysis

The donor characteristics data are expressed as the median and range. The categorical data of the training and validation data were compared using Fisher's exact test or the chi-squared test as appropriate. Continuous data were compared using the Mann–Whitney U test or the Kruskal–Wallis test. Pearson's correlation coefficient was used to test correlations between the Pure- or Semi-AI groups and the GT data. Group variability was assessed using Bland–Altman plots with 95% limits of agreement using mean values and standard deviations.[18] All statistical tests were performed using JMP software (version 15; SAS Institute). A p value of $<.05$ was considered statistically significant.

3 | RESULTS

The median age of training data was 34 years (range: 20–65) with 92 men and 82 women, whereas validation data was 46 years (range:21–64), 26 men and 25 women. The median age was significantly different ($p < .001$); however, the gender between the data did not differ significantly ($p = .874$). The median body mass index and body surface area of the training data were 22.2 (range: 14.5–33.2) and 1.65 (1.24–2.09); the validation data were 21.9 (16.6–30.6) and 1.65 (range: 1.34–2.14), respectively. These were not significantly different between the groups ($p = .524$ and $p = .666$, respectively, Table S1).

3.1 | Comparing voxel attribution

In the Pure-AI group, the median numbers of voxels in the right and left hemiliver were 2115319 (range: 1144805–4881676) and 912842 (range: 315938–1639720),

TABLE 1 Accuracy of each segmentation.

	Pure-AI			Semi-AI			p-value
	Sensitivity	Specificity	Dice coefficient	Sensitivity	Specificity	Dice coefficient	Sensitivity/specificity/Dice coefficient
Hemiliver							
Right	0.95 (0.86–0.99)	0.99 (0.99–0.99)	0.95 (0.90–0.99)	1.00 (0.92–1.00)	0.99 (0.99–1.00)	0.99 (0.94–1.00)	
Left	0.92 (0.84–0.98)	0.99 (0.99–0.99)	0.92 (0.85–0.98)	1.00 (0.95–1.00)	0.99 (0.99–1.00)	0.99 (0.90–1.00)	
Sector							
Posterior	0.92 (0.60–0.99)	0.99 (0.99–0.99)	0.92 (0.49–0.96)	1.00 (0.85–1.00)	1.00 (0.99–1.00)	0.99 (0.62–1.00)	All, <.001
Anterior	0.91 (0.67–0.97)	0.99 (0.99–0.99)	0.91 (0.74–0.97)	1.00 (0.69–1.00)	0.99 (0.99–1.00)	0.99 (0.82–1.00)	
Medial	0.87 (0.29–0.99)	0.99 (0.99–0.99)	0.86 (0.45–0.95)	0.99 (0.78–1.00)	0.99 (0.99–1.00)	0.99 (0.82–1.00)	
Lateral	0.91 (0.77–0.96)	0.99 (0.99–0.99)	0.91 (0.81–0.95)	1.00 (0.86–1.00)	0.99 (0.99–1.00)	0.99 (0.91–1.00)	
Segment							
1	0.78 (0.18–0.94)	0.99 (0.99–0.99)	0.71 (0.30–0.86)	0.95 (0.75–1.00)	1.00 (0.99–1.00)	0.97 (0.70–1.00)	
2	0.86 (0.05–0.94)	0.99 (0.99–0.99)	0.82 (0.08–0.91)	1.00 (0.61–1.00)	0.99 (0.99–1.00)	0.99 (0.34–1.00)	
3	0.87 (0.21–0.97)	0.99 (0.99–0.99)	0.85 (0.34–0.94)	1.00 (0.18–1.00)	1.00 (0.99–1.00)	0.99 (0.29–1.00)	
4	0.87 (0.29–0.99)	0.99 (0.99–0.99)	0.86 (0.45–0.95)	0.99 (0.78–1.00)	0.99 (0.99–1.00)	0.99 (0.82–1.00)	
5	0.88 (0.21–0.97)	0.99 (0.99–0.99)	0.82 (0.34–0.95)	1.00 (0.19–1.00)	0.99 (0.99–1.00)	0.95 (0.32–1.00)	
6	0.91 (0–0.99)	0.99 (0.99–1.00)	0.84 (0–0.93)	1.00 (0.34–1.00)	0.99 (0.99–1.00)	0.93 (0.34–1.00)	
7	0.87 (0.39–0.99)	0.99 (0.99–0.99)	0.86 (0.51–0.95)	0.99 (0.60–1.00)	1.00 (0.99–1.00)	0.99 (0.58–1.00)	
8	0.87 (0.53–0.99)	0.99 (0.99–0.99)	0.89 (0.67–0.98)	0.99 (0.60–1.00)	0.99 (0.99–1.00)	0.98 (0.75–1.00)	

Abbreviation: AI, artificial intelligence.

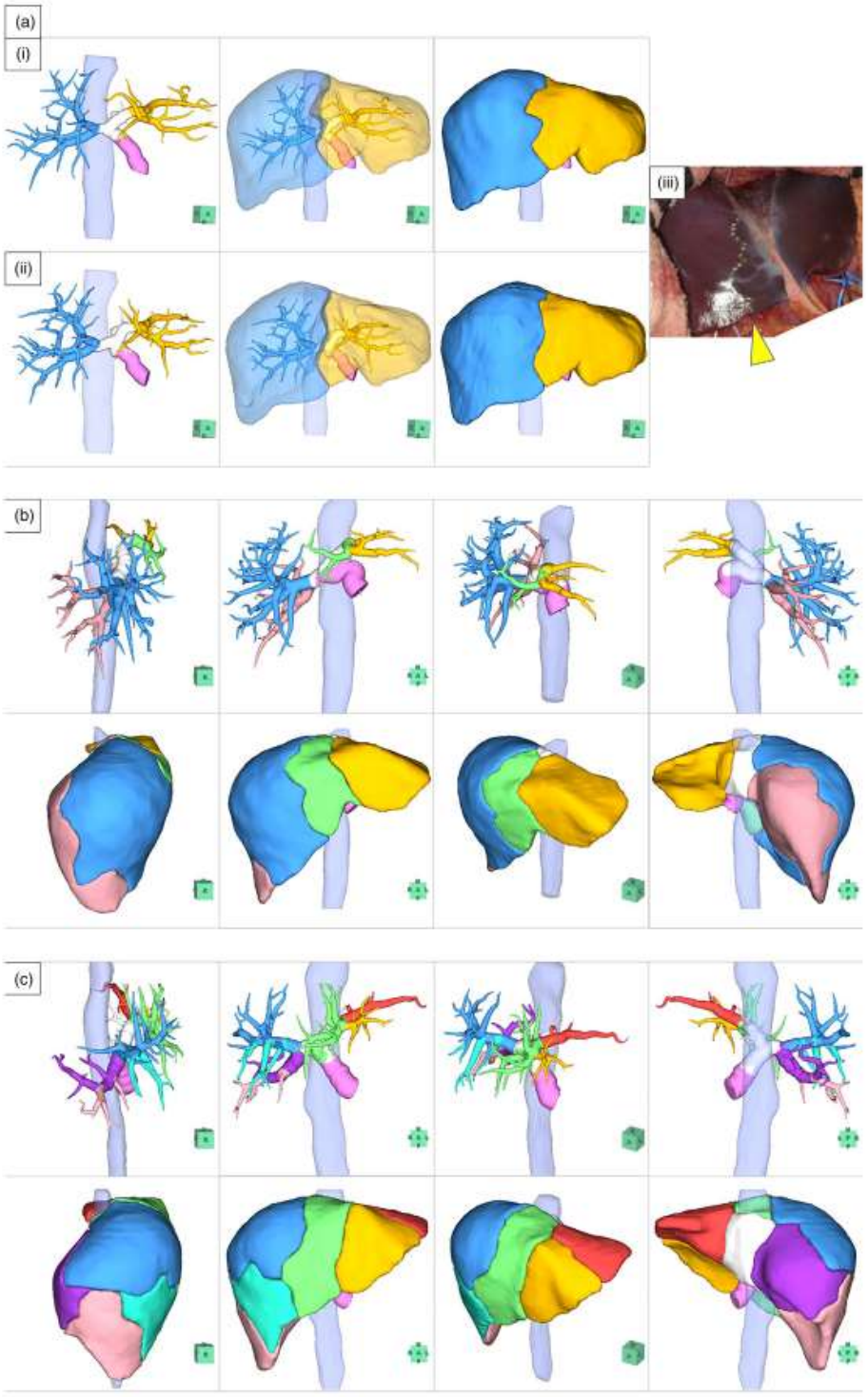

FIGURE 3 Example of liver segmentation. (a) An example of segmentation of hemiliver (left: labeled portal vein branch, middle: with transparent liver parenchyma, right: with opaque liver parenchyma) showed a better similarity demarcation line and its area among Pure-AI, (i) (upper), GT data, (ii) (lower), and an actual photo obtained during living donor liver surgery and the yellow arrowhead in panel a indicates the demarcation line (iii). (b and c) Another example of sector and segment segmentation with a better similarity demarcation line is shown in panels (b) and (c) (upper: labeled portal vein branch, lower: with opaque liver parenchyma; left to right: right anterior oblique, front, left anterior oblique, back). Right, deep blue; left, golden yellow; posterior, light pink; anterior, deep blue; medial, pale green; lateral, golden yellow; segment 1, white; segment 2, orange red; segment 3, golden yellow; segment 4, pale green; segment 5, blue-green; segment 6, light pink; segment 7, red-purple; and segment 8, deep blue; inferior vena cava, transparent blue-green.

respectively, whereas in the Semi-AI group, they were 2115492 (range: 1123326–4679390) and 923668 (range: 332994–1566345), respectively. The differences between the groups were not significant ($p = .907$ and .666). The numbers of voxels for the two hemilivers, four sectors and eight segments are shown in Table S2; the differences between the two groups were not significant ($p = .320$ to .976).

In the Pure-AI group, the median Dice coefficients of the right and left hemilivers were 0.95 and 0.92, respectively. The median Dice coefficients for the posterior, anterior, medial, and lateral sectors were 0.92, 0.91, 0.86, and 0.91, respectively. The median Dice coefficients for the Couinaud's segments 1–8 were 0.71, 0.82, 0.85, 0.86, 0.82, 0.84, 0.86, 0.89, respectively. The results for the Semi-AI group exhibited superior accuracy over the those for the Pure-AI group (all, $p < .001$, Table 1).

3.2 | Accuracy of automated portal vein labeling

A trifurcation and a separate and sole right posterior vessel branching off the main trunk of the PV were 12.1%, 8.6% (Training data), 13.7%, 9.8% (Validation data), and there was no significant difference ($p = .75$, $p = .91$), respectively.

For the PV labeling concordance rate, the labeling of the first-order branch as right or left PV fully matched, with 100% of both the Pure- and Semi-AI (102/102) groups matching the GT data (Figure 3a). For the second-order PV branches of sectors, 92.8% of the Pure-AI (437/471, Figure 3b) and 96.2% of the Semi-AI (478/497) groups matched the GT data. For the third-order branches of segments: 91.6% of the Pure-AI (790/862, Figure 3c) and 95.7% of Semi-AI (885/925) groups matched the GT data (Table 2).

3.3 | Comparing automated segmentation volumes

For the hemiliver assignments, the median right hemiliver volume was 744, 737, and 737 mL for the Pure-AI and Semi-AI groups and GT data, respectively ($p = .983$). The left hemiliver volume was 328, 332, and 333 mL, respectively ($p = .819$). The volumes of the posterior, anterior, medial, and lateral sectors were 134–454 mL in the Pure-AI group, 140–454 mL in the Semi-AI group, 140–457 mL in the GT data. The differences among the groups were not significant ($p = .865$ to .986). The median volumes of segments 1–8 ranged from 48 to 281 mL in the Pure-AI group. The differences in volumes among the groups were not significant ($p = .343$ to .865; Table 3).

Pearson's correlation coefficient of the segmented liver volume revealed a strong positive correlation between the Pure-AI and GT data for the hemiliver (right, 0.993; left, 0.974), sectors (posterior, anterior, medial, and lateral; 0.906 to 0.958), and two of the segments (segment 4, 0.906 and segment 8, 0.934), and a positive correlation for the remaining segments (segments 1, 2, 3, 5, 6, and 7; 0.602 to 0.827). The correlations were all statistically significant ($p < .001$; Figure 4a).

Bland–Altman plots analysis revealed that the mean differences in the right and left hemiliver volumes obtained with the automated segmentation between the Pure-AI group and GT data were -3.2 ± 22.8 and -4.0 ± 18.4 mL, respectively. The 95% limits of agreement were −47.9 to 41.5 and −40.0 to 32.0 mL. For the sector assignments, the mean differences in the volumes of the posterior, anterior, medial, and lateral sectors in automated segmentation between the Pure-AI group and GT data ranged from −7.9 to 4.7 mL, with 95% limits of agreement ranging from −85.5 to 69.7 mL. For automated segmentation of the 8 segments, the mean difference in the volumes between the Pure-AI group and GT data ranged from −21.7 to 14.5 mL, with the 95% limits of agreement ranging from −92.4 to 106.1 mL (Figure 4b). Pearson's correlation coefficient of segmented liver volume and Bland–Altman plot analysis of Semi-AI is shown in Figure S2.

3.4 | Correction time

The Pure-AI took a median of 1.4 min (range: 1.1–1.9 min) on a personal computer (Intel Corp., US, Core i7 with 16 gigabyte random access memory) for full automated liver segmentation. In the Semi-AI and GT data group, the median correction time was 10.2 min (range: 4.5–37.2 min) and 14.9 min

TABLE 2 Concordance rate of portal vein labeling.

	Pure-AI			Semi-AI			
	Detected (*n*)	Correct (*n*)	%	Detected and corrected	Correct (*n*)	%	*p*-value
Hemiliver							
Right	51	51	100	51	51	100	1.000
Left	51	51	100	51	51	100	1.000
All hemi	102	102	100	102	102	100	1.000
Sector							
Posterior	63	56	88.9	63	62	98.4	.029
Anterior	61	59	96.7	64	63	98.4	.552
Medial	199	186	93.5	217	215	99.1	.013
Lateral	148	136	91.9	153	138	90.2	.878
All sections	471	437	92.8	497	478	96.2	.020
Segment							
1	88	78	88.6	95	94	98.9	.026
2	56	56	100	58	57	98.3	.317
3	92	80	87.0	95	81	85.3	.913
4	199	186	93.5	217	215	99.1	.013
5	137	116	84.7	144	135	93.8	.007
6	82	73	89.0	91	83	91.2	.983
7	69	66	95.7	74	72	97.3	.325
8	139	135	97.1	151	148	98.0	.697
All segments	862	790	91.6	925	885	95.7	<.001

Abbreviation: AI, artificial intelligence.

TABLE 3 Volume comparison.

	Pure-AI (median)	Range	Semi-AI (median)	Range	GT data (median)	Range	*p*-value
Hemiliver							
Right	744	511–1407	737	534–1443	737	533–1429	.983
Left	328	184–559	332	174–573	333	173–571	.819
Sector							
Posterior	297	147–631	300	171–645	300	115–631	.953
Anterior	454	247–776	454	309–798	457	307–798	.901
Medial	134	37–284	140	68–286	140	67–282	.865
Lateral	197	109–343	197	106–367	197	106–367	.986
Segment							
1	48	10–126	39	14–114	41	14–124	.511
2	90	8–163	86	41–176	81	39–177	.483
3	105	34–209	104	34–208	108	50–218	.844
4	134	37–284	140	68–286	140	67–282	.865
5	132	40–406	119	34–248	121	43–242	.730
6	124	0–404	132	29–342	125	24–332	.536
7	168	76–277	171	101–303	176	69–360	.545
8	281	164–679	296	200–638	317	198–678	.343

Abbreviations: AI, artificial intelligence; GT, ground truth.

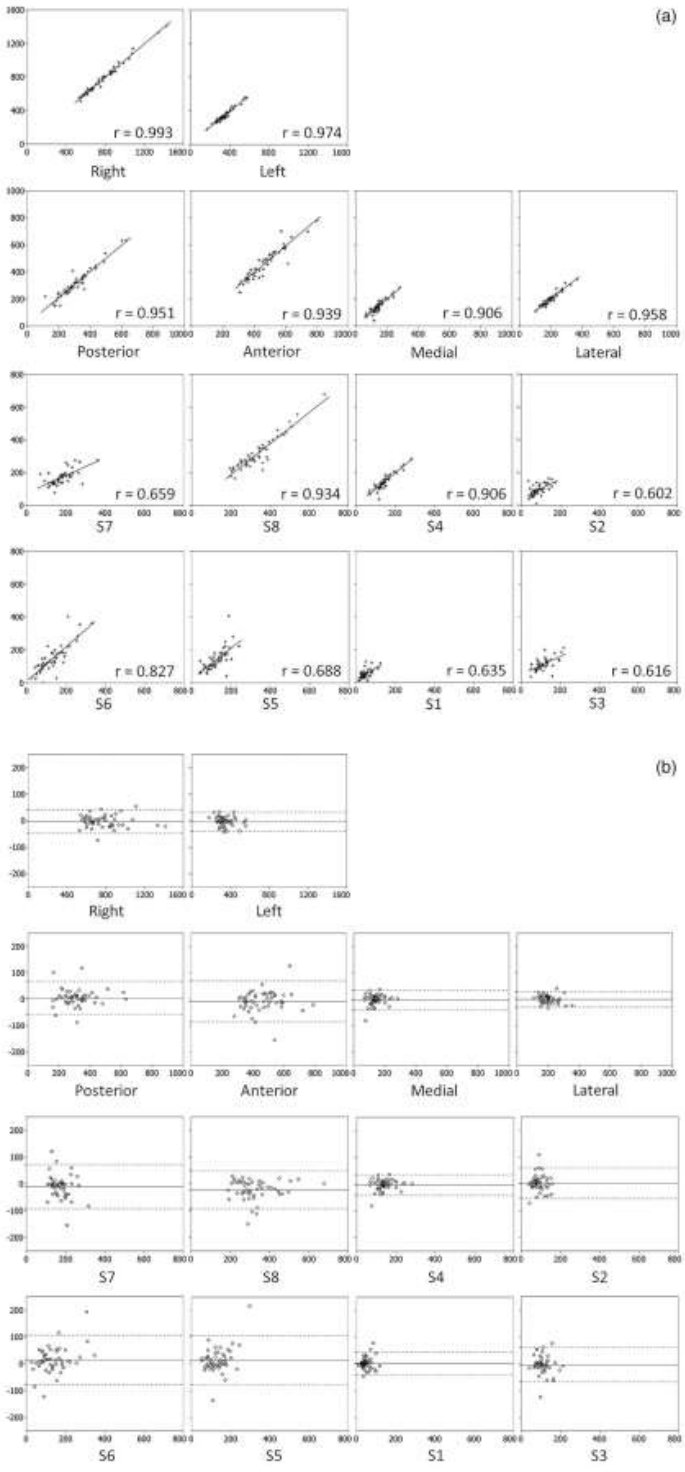

FIGURE 4 Pearson's correlation coefficient of segmented liver volume and Bland–Altman plot analysis of Pure-AI. (a) Pearson's correlation coefficient of the segmented liver volume revealed a strong positive correlation between Pure-AI and GT data in the hemiliver (right 0.993, left 0.974), sectors (posterior, anterior, medial, lateral; 0.906 to 0.958), segment (4, 8; 0.906, 0.934), and a positive correlation in the remaining segments (1, 2, 3, 5, 6, and 7; 0.602 to 0.827). All correlations were statistically significant ($p < .001$). (b) Bland–Altman plot analysis showed that the mean differences in the volumes of the right and left hemiliver in the automated segmentation between the Pure-AI group and GT data were -3.2 ± 22.8 and -4.0 ± 18.4 mL, respectively. The 95% limits of agreement were −47.9 to 41.5 and −40.0 to 32.0 mL, respectively. The mean differences in the volumes of the posterior, anterior, medial, lateral in the sectors by automated segmentation between the Pure-AI group and GT data were −7.9 to 4.7 mL. The 95% limits of agreement were −85.5 to 69.7 mL. The mean differences in the volumes of segments 1 to 8 by automated segmentation between the Pure-AI group and GT data were −21.7 to 14.5 mL. The 95% limits of agreement were −92.4 to 106.1 mL.

(range: 7.8–41.3 min). The Pure-AI required significantly less time for full automated liver segmentation than the Semi-AI and GT data with full correction (each, $p < .001$).

3.5 | Preliminary clinical data

The operation time, blood loss, estimated liver volume, and actual graft liver weight were not significantly different between the No-AI and Pure-AI groups. The difference between the estimated liver volume and the actual graft liver weight tended to be smaller in the Pure-AI group than the No-AI group (19 vs. 49, respectively, Table S3), but the difference was not significant.

4 | DISCUSSION

The present study is the first report of a two-step AI-based algorithm for automated liver segmentation, and we developed a new evaluation method to improve the accuracy and quality of liver segmentation, which will benefit an advance of the AI algorithm. In the noncorrected data (no human intervention, i.e., the Pure-AI group), the AI algorithm correctly assigned 100% of hemilivers into the right and left, 92.8% of the sectors, and 91.6% of the eight segments on the basis of matching to the GT data. Although the Dice coefficient of the Semi-AI group was superior to that of the Pure-AI group, the volumes were not significantly different among the Semi-AI and Pure-AI groups, and the GT data.

Since Hashimoto and colleagues reported the first simulation for estimating liver volume in 1991 from CT data,[19] 3D simulation of a virtual hepatectomy has become the standard for planning liver surgery.[4] Briefly, an expert, the surgeon or radiologist, confirms the PV and HV vascular trees extracted by the software, and then manually selects 1 or several PV branches, so-called "clipping," to determine the areas and volumes of the hemilivers, sectors, and or resecting area to predict the volume of the future liver remnant. These processes are based on the concept of anatomic resection[7] to maximize the remnant functional liver volume. Here, we demonstrated that an AI-based algorithm can help improve the efficiency of the software, and the AI-based algorithm requires significantly less correction time than the GT data without requiring an expert's supervision, based on the present method of evaluating the accuracy of automated liver segmentation.

In the present study, liver segmentation required a two-step AI algorithm, detailed extraction of the PV and HV vascular trees and precise PV labeling into hemiliver, sector, and segment categories. We previously reported that AI enhances the accuracy of PV and HV extraction on CT for virtual hepatectomy as the first step of the AI algorithm. In that report, the sensitivity, specificity, and Dice coefficient for the PV were 0.84, 0.97, and 0.90, respectively.[11] In the present study, we attempted to fully automate liver segmentation by developing a second step for the AI algorithm. With this two-step AI-based algorithm, precise liver segmentation for virtual hepatectomy was achieved and may contribute to more rapid surgical decision-making in the clinical setting.

A feature of second step of the AI algorithm is that segment 1 is given additional weight for differentiating the right and left hemilivers. Generally, the thickness and weight of the PV branches of segment 1 decrease abruptly, directly branching off the thick main trunk or first-order, right or left PV branches compared with the other branches in which the thickness and width gradually taper.[20] As PV branches in segment 1 have different features, we designed various 3D-FCNs to work on the five branch clusters: posterior, anterior, medial, and lateral sectors, and segment 1, as described in *Methods*. This increased the accuracy of the AI algorithm. Further studies are needed to determine the best algorithm for virtual hepatectomy. Additionally, although there are previous reports of liver segmentation based on the HV tree,[9,21] weighing the balance between the PV and HV was another key of the second step of the AI algorithm. The Rex-Cantlie line with the middle HV is a crucial landmark for dividing the liver into the right and left hemilivers.[22] Segmentation focusing on the PV tree rather than the HV tree may still be helpful because some reports describe that the peripheral branches of the right and left HVs do not always run in the plane between the posterior and anterior sectors, that is, segments 2 and 3.[23,24]

As previously reported,[11] the first step of the AI process remains somewhat inaccurate. The missing (failing to extract the PV), and misclassifying (successful extraction of the PV but unable to label it correctly) rates were 6.7% and 4.4%, respectively, for the third-order PV branches. In the present study, the volume did not completely match among the Pure-AI and Semi-AI groups and the GT data. One reason for this may have been a missing and/or misclassified PV in the first AI step. Another reason is that the inaccuracy of the AI algorithm for the fourth-order branches. In our previous study regarding the first AI step, 9.8% and 4.4% of the fourth-order PV branches were missing and misclassified, respectively. These values may be clinically insignificant because fourth-order PV branches have relatively small perfusion area. On the other hand, there was a discrepancy between the low concordance rate and the lack of a significant volume difference (e.g., the posterior and medial sector, and segments 1, 4, and 5). This discrepancy may have been due to the fact that the AI algorithm continued to search for another branch of the PV to create enough volume. Further studies are needed to clarify the clinical impact of the inaccuracy.

The most challenging part of the non-AI algorithm is that there was no clear definition or rule and no consensus among experts for determining the four sectors and segment 1–8, because there are many interindividual variations. We demonstrated that AI addresses and simplifies this challenging task, but some differences existed among the Pure- and Semi-AI groups, and GT data. We also demonstrated that the AI -based algorithm still requires an expert's supervision during the final step, or after the first step of AI in the Semi-AI group. For example, as described above, the volume of Couinaud's segments or labeling of the third-order PV branch level was somewhat inconsistent with the GT data. The AI-based algorithm may have utilized different properties to assess the liver anatomy. Further studies are needed to elucidate the precise boundaries among the sectors and segments.

There were some limitations to the present study. We did not evaluate Pure or Semi-AI in diseased liver. AI was trained in only healthy donor livers, which may affect the accuracy and quality of virtual hepatectomy of diseased liver. A large tumor or liver cirrhosis may deform the intrahepatic PV or HV vascular structure. Thus, further studies with a cohort of diseased livers are needed.

In conclusion, the two-step AI algorithm for liver segmentation automates anatomic virtual hepatectomy. Liver segmentation without human intervention (i.e., the Pure-AI group) correctly divided 100% of the hemilivers, 92.8% of the sectors, and 91.6% of the segments.

AUTHOR CONTRIBUTIONS

Conception and Design Yu. Ka., and J.K. Writing Python code D.K., and Yo.Ki. Acquisition of data Yu. Ka., R.T., and Y.M. Analysis and interpretation of data J.K., Yo.Ka., and N.A. Draft and revision of the manuscript A.I., and K.H. All authors gave their approval for the final version of the article.

FUNDING INFORMATION

This study was funded by Fujifilm Corporation, Tokyo, Japan., and the work was supported by grant no. 19K09191 (Kaneko) from the Ministry of Education, Culture, Sports, Science, and Technology of Japan, as an academic-industrial collaboration.

CONFLICT OF INTEREST STATEMENT

Hepato-Biliary-Pancreatic Surgery Division of the Tokyo University received a research grant from Fujifilm on a collaboration agreement.

SHARING PYTHON CODE

To share python code that was developed in the present study, we uploaded it on Github website following uniform resource locator. https://github.com/FujifilmMedicalSystemsJapan/LiverSegmentation.

ORCID

Junichi Kaneko https://orcid.org/0000-0002-1284-5639
Yoshikuni Kawaguchi https://orcid.org/0000-0003-2986-3224
Nobuhisa Akamatsu https://orcid.org/0000-0003-1603-5147
Kiyoshi Hasegawa https://orcid.org/0000-0001-8734-740X

REFERENCES

1. Sung H, Ferlay J, Siegel RL, Laversanne M, Soerjomataram I, Jemal A, et al. Global cancer statistics 2020: GLOBOCAN estimates of incidence and mortality worldwide for 36 cancers in 185 countries. CA Cancer J Clin. 2021;71:209–49.
2. Cherqui D, Laurent A, Mocellin N, Tayar C, Luciani A, van Nhieu JT, et al. Liver resection for transplantable hepatocellular carcinoma: long-term survival and role of secondary liver transplantation. Ann Surg. 2009;250:738–46.
3. Zeyara A, Torén W, Søreide K, Andersson R. The liver-first approach for synchronous colorectal liver metastases: a systematic review and meta-analysis of completion rates and effects on survival. Scand J Surg. 2021;111:14574969211030131.
4. Mise Y, Hasegawa K, Satou S, Shindoh J, Miki K, Akamatsu N, et al. How has virtual hepatectomy changed the practice of liver surgery?: experience of 1194 virtual hepatectomy before liver resection and living donor liver transplantation. Ann Surg. 2018;268:127–33.
5. Wigmore SJ, Redhead DN, Yan XJ, Casey J, Madhavan K, Dejong CH, et al. Virtual hepatic resection using three-dimensional reconstruction of helical computed tomography angioportograms. Ann Surg. 2001;233:221–6.
6. Strasberg SM, Belghiti J, Clavien PA, Gadzijev E, Garden JO, Lau WY, et al. The Brisbane 2000 terminology of liver anatomy and resections. HPB. 2000;2:333–9.
7. Hasegawa K, Kokudo N, Imamura H, Matsuyama Y, Aoki T, Minagawa M, et al. Prognostic impact of anatomic resection for hepatocellular carcinoma. Ann Surg. 2005;242:252–9.
8. Shindoh J, Makuuchi M, Matsuyama Y, Mise Y, Arita J, Sakamoto Y, et al. Complete removal of the tumor-bearing portal territory decreases local tumor recurrence and improves disease-specific survival of patients with hepatocellular carcinoma. J Hepatol. 2016;64:594–600.
9. Lebre MA, Vacavant A, Grand-Brochier M, Rositi H, Abergel A, Chabrot P, et al. Automatic segmentation methods for liver and hepatic vessels from CT and MRI volumes, applied to the Couinaud scheme. Comput Biol Med. 2019;110:42–51.
10. Alirr OI, Abd Rahni AA. Automatic atlas-based liver segmental anatomy identification for hepatic surgical planning. Int J Comput Assist Radiol Surg. 2020;15:239–48.
11. Kazami Y, Kaneko J, Keshwani D, Takahashi R, Kawaguchi Y, Ichida A, et al. Artificial intelligence enhances the accuracy of portal and hepatic vein extraction in computed tomography for virtual hepatectomy. J Hepatobiliary Pancreat Sci. 2021;29:359–68.

12. Wakabayashi G, Cherqui D, Geller DA, Abu Hilal M, Berardi G, Ciria R, et al. The Tokyo 2020 terminology of liver anatomy and resections: updates of the Brisbane 2000 system. J Hepatobiliary Pancreat Sci. 2021;29:6–15.
13. Bismuth H. Revisiting liver anatomy and terminology of hepatectomies. Ann Surg. 2013;257:383–6.
14. Le Foie CC. Etudes anatomiques et chirugicales. Paris: Masson & Cie; 1957.
15. Rumelhart DE, Hinton GE, Williams RJ. Learning representations by back-propagating errors. Nature. 1986;323:533–6.
16. Dice LR. Measures of the amount of ecologic between species. Ecology. 1945;26:297–302.
17. Klyuzhin I, Chausse G, Bloise I, Lavista Ferres J, Uribe C, Rahmim A. Automated deep segmentation of healthy organs in PSMA PET/CT images. J Nucl Med. 2021;62:1410.
18. Bland JM, Altman DG. Comparing methods of measurement: why plotting difference against standard method is misleading. The Lancet. 1995;346:1085–7.
19. Hashimoto D, Dohi T, Tsuzuki M, Horiuchi T, Ohta Y, Chinzei K, et al. Development of a computer-aided surgery system: three-dimensional graphic reconstruction for treatment of liver cancer. Surgery. 1991;109:589–96.
20. Kumon M. Anatomical study of the caudate lobe with special reference to portal venous and biliary branches using corrosion liver casts and clinical application. Liver Cancer. 2017;6:161–70.
21. Yoon JH, Lee JM, Jun JH, Suh KS, Coulon P, Han JK, et al. Feasibility of three-dimensional virtual surgical planning in living liver donors. Abdom Imaging. 2015;40:510–20.
22. Shindoh J, Mise Y, Satou S, Sugawara Y, Kokudo N. The intersegmental plane of the liver is not always flat—tricks for anatomical liver resection. Ann Surg. 2010;251:917–22.
23. Ishibashi Y, Sato TJ, Hirai I, Murakami G, Hata F, Hirata K. Ramification pattern and topographical relationship between the portal and hepatic veins in the left anatomical lobe of the human liver. Okajimas Folia Anat Jpn. 2001;78:75–82.
24. Sato F, Igami T, Ebata T, Yokoyama Y, Sugawara G, Mizuno T, et al. A study of the right intersectional plane (right portal scissura) of the liver based on virtual left hepatic trisectionectomy. World J Surg. 2014;38:3181–5.

SUPPORTING INFORMATION

Additional supporting information can be found online in the Supporting Information section at the end of this article.

How to cite this article: Kazami Y, Kaneko J, Keshwani D, Kitamura Y, Takahashi R, Mihara Y, et al. Two-step artificial intelligence algorithm for liver segmentation automates anatomic virtual hepatectomy. J Hepatobiliary Pancreat Sci. 2023;30:1205–1217. https://doi.org/10.1002/jhbp.1357